EFFECT OF FUNCTIONALIZED MULTI-WALLED CARBON NANOTUBES ON A POLYSULFONE ULTRAFILTRATION MEMBRANE

Sendango Landry Omalanga

A dissertation submitted to the Faculty of Engineering, University of the Witwatersrand, Johannesburg, in fulfilment for the degree of Master of Science Engineering.

Johannesburg, 2015

DECLARATION

I declare that the dissertation, which I hereby submit for the degree of Master of Science in Engineering at the Faculty of Engineering, University of the Witwatersrand, Johannesburg, is my own work and has not previously been submitted by me to any institution.

The thesis has been prepared maintaining the Rules of Good Scientific Practice.

Sendango Landry Omalanga

26 October, 2015

ABSTRACT

Polysulfone (PSF) membranes were produced by the phase inversion method using three different solvents: N, N-dimethylformamide (DMF), chloroform (CHCL3), and tetrahydrofurane (THF). The produced membranes were used for treatments of oil – water samples supplied by Oil skip/ South Africa. Furthermore Polysulfone (PSF) was blended to different composition of functionalized multi–walled carbon nanotubes MWCNTs by the classical phase inversion method. Multi–walled carbon nanotubes (MWCNTs) functionalized by acid treatment were synthesized using chemical vapour deposition. Scanning Electron Microscope (SEM) and Transmission Electron Microscope (TEM) were used to view the morphology of the blended membrane and MWCNTs. The Raman spectroscope was used to confirm the functionalization of the MWCNTs by comparing the defects on the MWCNTS introduced by acid treatment. It was found that the chemical, physical and mechanical properties improve with the content of functionalized MWCNTs composition in the polymeric membrane. The membrane with the MWCNTs composition of 0.4% w/w demonstrated the highest flux of 117 L/m^2.h and solute (oil) rejection. The selectivity and permeate flux were increased with functionalized MWCNTs content for the membranes produced with the three different solvents.

DEDICATED TO

My parents Pascal Omalanga Pele and Anne –Yvette Mulanga.

My siblings, Armel Omalanga, Paola Omalanga and Israel Omalanga.

ACKNOWLEDGEMENTS

I am grateful to my supervisors Prof. Sunny Iyuke and Dr. Bavon Nkazi for the great contributions to the success of this research study.

The African Materials Science and Engineering Network (AMSEN) / University of the Witwatersrand for financial support.

To Prof Viness Pillay from Wits University/ Medical School for his assistance with the mechanical testing of the membranes.

To Dr Sabelo Mhlanga from the University of Johannesburg for his assistance with the contact angle (hydrophilicity) tests.

To my whole family, for the good advice and love.

Finally, to the Almighty God for the love, inspiration and breath of life.

PRESENTATIONS AND PUBLICATIONS

PRESENTATIONS AT CONFERENCES

- Landry Omalanga, Sunny Iyuke, Bavon Nkazi, Production of a blended membrane for waste water (oil-water) ultrafiltration. **Poster presentation**. 13th International Conference on Inorganic Membranes (ICIM), Brisbane, Australia, 6-9 July 2014.

- Landry Omalanga, Sunny Iyuke, Bavon Nkazi, Functionalized carbon nanotubes on a polysulfone membrane for oil-water treatment. **Poster presentation**. ICC/ SAICHE International Conference, Durban, KZN, 30 August 2014.

- Landry Omalanga, Sunny Iyuke, Bavon Nkazi, Effect of hydrophilicly functionalized carbon nanotubes on a polysulfone membrane for oil-water treatment. **Poster presentation.** Wits University, Workshop, Johannesburg, Gauteng, 16 April 2014.

PUBLICATIONS

- Landry Omalanga, Sunny Iyuke, Bavon Nkazi, Production of a blended membrane for oil-water treatment, **submitted**. Journal of Separation and Purification Technology.

- Landry Omalanga, Sunny Iyuke, Bavon Nkazi, Functionalized carbon nanotubes on a polysulfone membrane for oil-water Ultrafiltration, **Submitted**, South Africa Journal of Chemical Engineering (SAICHE).

TABLE OF CONTENTS

LIST OF FIGURES

LIST OF TABLES

LIST OF ABBREVIATIONS

A	Area
BET	Brunner Emmett Teller
CHCL3	Chloroform
CMC	Critical micelle concentration
CNTs	Carbon nanotubes
CVD	Chemical Vapour Deposition
DAF	Dissolved air floatation
DMF	Dimethylformamide
H	Hour
H NMR	Hydrogen-1 Nuclear magnetic Resonance
IR	Infra red
L	Litre
MMMs	Mixed matrix membrane
MPS	Membrane Separation Process
MWCNTs	Multi –walled carbon Nanotubes
MWF	Metal working Fluid
P	Pressure
PSF	Polysulfone
SEM	Scanning Electron Microscope
SRT	Sludge retention time
SWCNTs	Single – walled carbon nanotubes

T	Time
TEM	Transmission Electron Microscope
TGA	Thermogravimetric analysis
THF	Tetrahydrofuran

Chapter1. Introduction

1.1 Background

Oil wastewater has been identified as one of the most serious pollution sources. This form of wastewater originates from different sources such as crude oil production, oil refineries, metal processing, the petrochemical industry and others [1]. With industrial development, there is an increase in the amount of oil used, but due to various technical factors and inadequate management behind these developments, a lot of oil is found in the water system, causing increasingly serious pollution.

South Africa itself generates approximately 120 million litres of waste oil per annum [2]. Therefore, oil recycling initiatives were encouraged by the Recycle Oil Saves Environment (ROSE) foundation from as early as 1994 when the government removed support for refining used oil as lubricating oil. The major lubricant companies in South Africa then took it upon themselves to provide a means to collect and recycle used lubrication oil. Forming the ROSE foundation, various mechanisms were used to ensure effective protection of the environment [2]. Since the early years, there were other initiatives to protect the environment by ensuring that used oil was collected and safely disposed of or recycled to prevent water pollution. Used oil can contaminate water and groundwater resources if not managed correctly, but is an often illegally dumped or discharged into storm water drain [3, 4].

Oily wastewater is declared to be hazardous industrial wastewater because it contains toxic substances such as petroleum hydrocarbons, polyaromatic hydrocarbons, etc; which are inhibitory to plant and animal growth and also mutagenic and carcinogenic to human beings [5]. Research has showed that physical treatment (eg. Gravity separator, dissolved air floatation) do not completely remove the undesired compounds (pollutants) but just transfers them to a more concentrated waste [6]. Therefore, it is necessary to develop a more efficient separation technique based on a membrane separation process to treat the oily wastewater [7].

The membrane separation process (MSP) has been identified as a novel efficient technology in oil wastewater treatment in recent years. It is an improvement of the conventional activated sludge process in which oily wastewater separation is achieved by MSP instead of using a secondary sedimentation tank [8]. Membrane fouling and concentration polarization are the main factors limiting the efficient of the membrane separation process [9]. According to

Kuzmenko et al, [10] membrane fouling is define as the decrease of the permeate flux of the membrane due to the accumulation of substances on the surface of the membrane or within the membrane pores. Several attempts to solve the problems caused by fouling have been undertaken [10]. A considerable research effort has focused on the addition of inorganic materials such as multi-walled carbon nanotubes (MWCNTs) in the matrix of the polymeric membranes [11]. This so called blended membrane (BM) contains an inorganic material which leads to the improvement of the physical, chemical and mechanical properties of the polymer [12].

However, the effective incorporation of MWCNTs in the BM, it has been found that there is poor interfacial compatibility between the CNT and the polymer, leading to a decrease of the selectivity and permeability of the membrane [13;14]. Attempts to improve the compatibility between MWCNTs and the polysulfone (PSF) membrane, by introducing the use of nanoparticles in the membrane matrix in order to improve the permeate flux and the membrane fouling resistance has shown that MWCNTs improve the mechanical and chemical properties of the polymeric membrane. [15].

Several researchers confirmed that there is the need to modify or functionalize the surface of the inorganic material in order to increase the polymer compatibility without blocking the membrane pores [16]. Polymer blends and modification of backbone and side chains of conventional polymers have been reported for the improvement of wastewater separation [17]. The trends to improve membrane separation have also led to the emergence of an important membrane class, known as mixed matrix membranes (MMMs) [19].

MSP is advantageous in comparison to the normal activated sludge process because it operates at higher solute retention time. This allows degradation of low growing micro-organisms and toxic substances such as petroleum hydrocarbons due to the favourable conditions created [20]. However, membrane fouling and concentration polarization which leads to high-energy consumption and high cleaning chemical requirements have limited performance of the MSP due to high operation cost [21]. Research has been conducted to discover the different causes leading to membrane fouling and concentration polarization [22]. Accumulation of solid particles on the top surface and inside the pores of the polymeric membrane is among the factors affecting the MSP [22].

1.2 Aims and objectives of the project

The main purpose of this study is to assess the effect of acid functionalized MWCNTs on a polysulfone membrane in order to construct highly permeable and selective membranes; which is containing CNTs inside a polymer matrix that could easily be scaled-up.

The objectives of the research are as follows:

- To synthesize MWCNTs using the chemical vapour deposition (CVD) method.
- Pre - treatment of the oily waste water sample using raw MWCNTs
- To functionalize MWCNTs with acid treatment.
- To prepare polysulfone (PFS) membrane and bended membrane (PSF+MWCNTs) by the phase inversion method.
- To characterize the nanostructured materials using a range of techniques: transmission electron microscopy (TEM), scanning electron microscopy (SEM), infra-red spectroscopy (IR), thermogravimetric analysis (TGA), Brunauer-Emmett-Teller (BET), tensile strength, a cross-flow filtration system and the contact angle analyser. This will be undertaken in order to see any structural and performance changes upon modification of the membranes.
- To test the membrane filtration system for the removal of oil from the water solution.
- To study the capability of the new system in fouling resistance.

1.3 Outline of the dissertation

Chapter 1: This chapter provides a brief introduction to problems relating to oily wastewater and membrane separation technology. Furthermore, the chapter addresses the aim of the study and the steps undertaken to achieve the work.

Chapter 2: This chapter provides a general approach in the use of membrane separation technology, the use of CNTs and CNTs/PSF blend membrane composites for oily wastewater treatment, the influence of the solvent in the phase inversion method, and the pre-treatment of oily wastewater.

Chapter 3: This chapter provides a detailed description of the procedures employed for preparation of MWCNTs, functionalization of MWCNTs using acid treatment, production of polysulfone (PSF), and pre-treatment (coagulation and flocculation) of oily wastewater using raw MWCNTs. The characterisation techniques used in this research study are also discussed in this chapter.

Chapter 4: This chapter presents the results obtained from the synthesis and functionalization of MWCNTs, the incorporation of these nanotubes into membrane systems (CNT/PSF) blend membranes, the pre-treatment of oily wastewater, the effect of functionalized MWCNTs and solvent on the performance of the filtration tests.

Chapter 5: This chapter provides a summary and the conclusion of the study. In addition, it provides recommendations for future work.

1.4 References

1. Kajitvichyanukul, P., Hung, Y.-T. & Wang, L. K. (2011). Oil water separation. Handbook of Environmental Engineering, 13: Membrane and Desalination The Humana Press Inc., New York, USA.
2. Oilskip, Eco parteners. (2012). Environmental Scoping report. Report NR: OI040000A31103A. 3-9
3. Rose report. (2014)..Recycling oil saves the environment. 1- 5
4. Nathanael Greene. (2004). How biofuels can help end American's oil dependence. Natural resources defence council. (NRDC).
5. Abass O. Alade, Ahmed T. Jameel, Suleymana A. Muyubi, Mohamed I. Abdul Karim, Zahanga Alam. (2011). Removal of oil and grease as emerging pollutants of concern (EPC) in wastewater stream, IIUM Engineering Journal, 12,4, 161-169.
6. Awaleh M.O., Soubaneh Y.D. (2014). Waste Water Treatment in Chemical Industries: The concept and Current Technologies. Hydrology Current Research 5, 1647.
7. Yuzhang Zhu, dong Wang, Lei Jiang, Jian Jin (2014). Recent progress in developing advanced membranes for emulsified oil/water separation. NPG Asia materials 6, 1884-4057.
8. Hai, F. I. & Yamamoto, K. (2011). Membrane Biological Reactors. In P. Wilderer (Eds.), treatise on Water Science pp. 571-613.
9. Zhao Y.J., Wu K.F., Wang Z.J., Zhao Liang, Li S.S.,(2000). Fouling and Cleaning of membrane.Membrane technology. 12, 241-251.
10. Denis K., Elizabeth A. Sophia B., Viatcheshav F., Vitaly G. (2005). Chemical cleaning of UF membranes fouled by BSa, Journal of desalination, 179, 323-333.
11. Rodríguez-Calvo A. , Silva-Castro G.A., Osorio F., González-López J., Calvo C. (2014) Novel Membrane Materials for Reverse Osmosis Desalination. Hydrology Current Research. 5,167.
12. Asim M., Hilmi B.M., Azmi M.S., Hafiz A.M.(2013). A review: Development of polymeric blend membrane for removal of CO_2 from natural gaz. International journal of Engineering and Technology, 13, 53.
13. Sangil K., Liang C., Karil J., Eva M. (2007). Polysulfone and functionalized carbon

nanotube mixed matrix membrane for gaz separation. Journal of Membrane science. 249, 147-158.

14. Huiqing W., Beibei T., Peiyi W. (2010), Novel ultrafiltration membranes prepared from a multi walled Carbon nanotubes / polymer composite. Journal of membrane Science. 362, 374 – 383.

15. Valid V., Sayed S.M., Rostam M., Sins Z., Bandar A., (2011). Fabrication and Characterization of novel antifouling nanofiltration membrane prepared from oxidized multiwalled Carbon nanotube / polyethersulfone nanocomposite. Journal of Membrane Science 375, 284 -294.

16. Tai S., Lan Y., Yi L., Santi K. (2007). Mixed matrix membranes (MMMs) comprising organic polymers with dispersed inorganic fillers for gas separation. Polymer. Science. 32 483–507.

17. Chettiyapan V., Amila A., (2012). Developments and future potentials of anaerobic membrane bioreactors (AnMBRs). Membrane water treatment, 3, 1-23.

18. Thomas M., Norredine G., Abdulah H., Rinaldi R., Robert G., Gary A.(2013), Subsurface intake for seawater reverse osmosis facilities: Capacity limitation, water quality improvement and Economics, desalination ,322, 37-51.

19. Phan Thanh Tri (2002), Oily wastewater treatment by membrane bioreactor process coupled with biological activated carbon process.Thesis, Asian.

.20. Michelle C.W., Frank L., Ellen A., Bill B., Kim L., The desalting and water treatment membrane manual : A guide to membranes for municipal water treatment (2 nd Edition), Water treatment technology program report 29, Denver Colorado, USA.

Chapter 2. Literature review

2.1 Membranes

A membrane is barrier which allows the transport of the same kind or sized molecules (permeate) and stopping the passage of others (retentate) (Figure 2.1). The membrane definition is quite similar to a normal filter; however, by convention the term filter is used for separation involving the particular suspensions containing particles larger than 1-10 μm [1]. The transport of the molecules is driven using driving forces such as: temperature, pressure, concentration, etc. The membranes can be natural or synthetic by their origin [2].

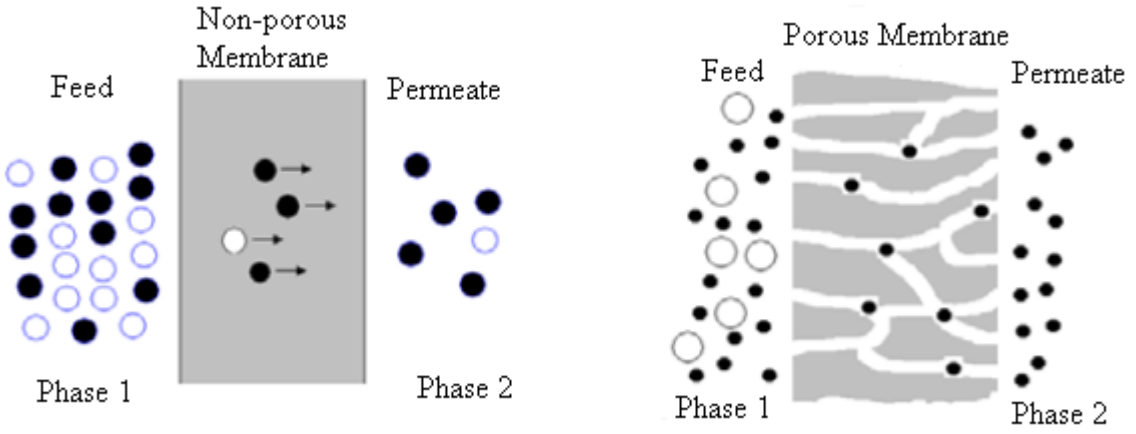

Figure 2.1: Schematic diagram representing the separation of two phases by non-porous and porous membranes

Synthetic membranes can be classified into two main categories depending on the constituents of the membranes i.e. inorganic and organic membranes. Inorganic membrane materials include ceramic, metal and glass etc. and organic membrane materials mainly arise from all kind of polymers [2]. The separation mechanism of the membranes depends on their structure. According to their morphology or structure, the synthetic membranes can be classified as symmetric (or isotropic) and asymmetric (or anisotropic). The classification of the membranes according to their structure is given in Figure 2.2.

2.1.1 Isotropic membranes

Isotropic membranes show a uniform composition structure throughout and can be porous or dense. The resistance to mass transfer in these membranes is determined by the total membrane thickness. A decrease in membrane thickness results in an increased permeation rate. Microporous, non-porous or dense, and electrically charged membranes are categorized under isotropic membranes [1].

2.1.1.1 Microporous membranes

Microporous membranes are similar to the conventional filter in their structure and function. They possess highly voided structures along with interconnected and randomly distributed pores [1]. The separation of the particles takes place by sieving effect mechanism where the particles larger than the membrane pores are rejected while the smaller particles pass through the membrane pores [1]. This type of membrane is used for microfiltration and ultrafiltration membrane processes which find application in breweries, the pharmaceutical industry and waste water treatment from chemical industries. [2].

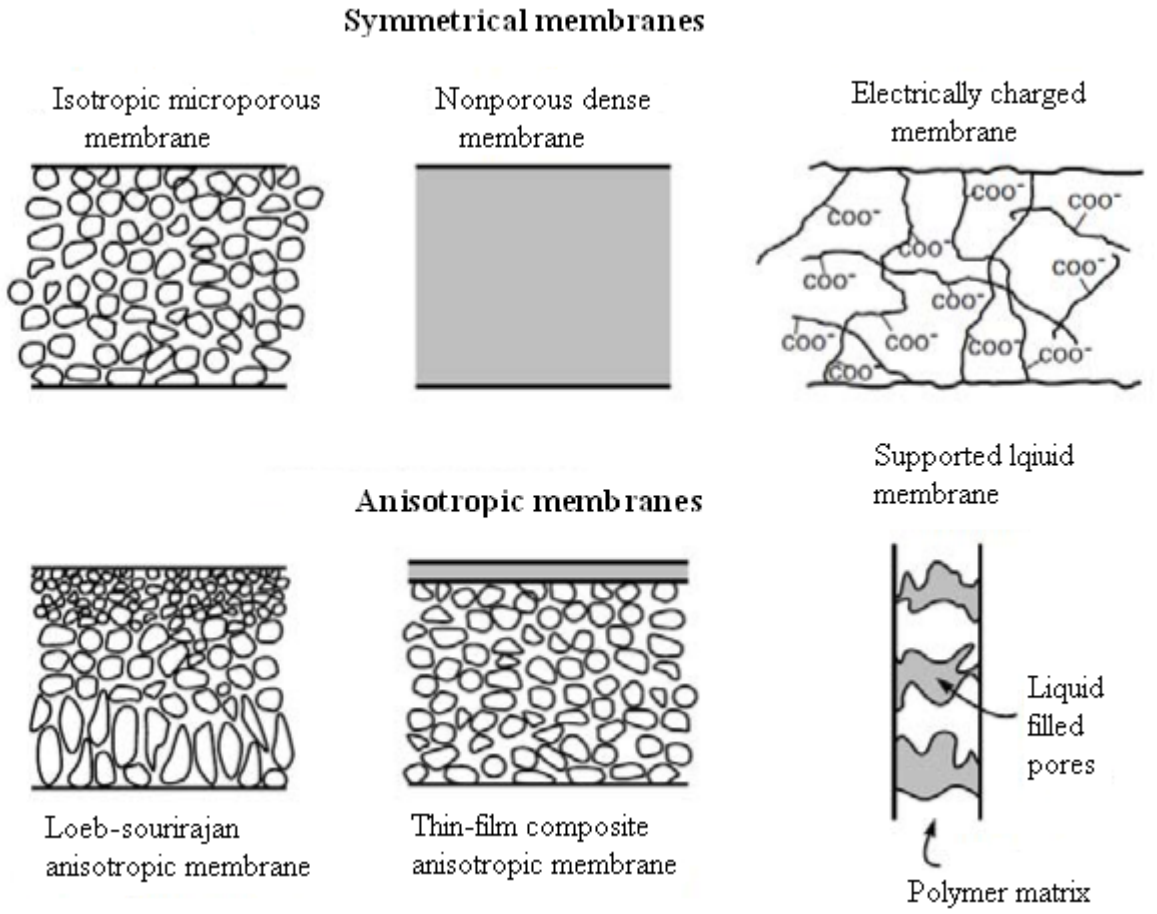

Figure 2.2: Schematics of main types of the membranes (reproduced from [1])

2.1.1.2 Dense membranes

The dense membranes are comprised of non-porous films through which the transportation of permeate (gas or liquid) takes place under the driving force of pressure, concentration, or electrical potential gradient [1]. The transport rate of separating species through the non-porous membranes is determined by their diffusion and solubility in the membrane material [2]. Processes such as gas separation, pervaporation and reverse osmosis are carried out using dense membranes. The permeation of the separating mixtures is usually very slow through dense films, so in commercial applications the dense membranes are usually used in the form at composite anisotropic membranes for the enhancement of the flux [3].

2.1.1.3 Electrically charged membranes

Electrically charged membranes can be dense or microporous. Usually they possess a fine microporous structure where the pore walls contain electrically positive or negative charges [3]. The membranes fixed with positively charged ions (cations) bind negatively charged ions (anions) and are hence, known as anion exchange membranes. The membranes fixed with negatively charged ions bind positively charged ions and termed as cation exchange membranes. These membranes are applied for the processing of electrolyte solutions through the electrodialysis [1].

2.1.2 Anisotropic membranes

The flux of permeate species through the membranes is inversely proportional to their thickness [1]. For economic reasons, higher transport rate of the permeate species is desirable. As such the membranes should be as thin as possible. Loeb and Sourirajan (1963) prepared the first anisotropic membrane with a dense layer supported by a porous asymmetric structure via the so-called “phase inversion” method for water desalination. The anisotropic membrane with a thin dense selective layer ensures high flux of the permeate which is economic because of low energy consumption [3]. The composite membranes also come under the category of anisotrpic membranes where a thin dense selective layer is cast on a porous membrane support [3]. Presently the composite membranes are being used commercially for membrane processes like gas separation, reverse osmosis, nanofiltration and pervaporation [2].

2.1.3 Liquid membranes

Liquid membranes can be purely liquid or they can be in the form of liquid immobilized within the pores of porous membranes. The liquid can be a suitable organic solvent and may contain some carrier molecules [4]. The carrier molecules enhance the transport of those molecular species having affinity with carrier molecules. These membranes are used only in some specific applications owing to their low selectivity [1, 2].

2.1.4 Membrane separation processes

Membrane separation processes are very efficient and useful separation techniques of our century because it has several advantages compared to classical (liquid-liquid extraction, distillation, absorption) processes, such as simple and compact set-up [4], easy operation at ambient temperature and pressure [5], simple up- and downscaling [6], better energy efficiency [7], high purity products [8] and much lower environmental impact [9].

The most common membrane separation processes include microfiltration, ultrafiltration, dialysis, nanofiltration, pervaporation, gas separation and reverse osmosis [2]. Microfiltration is widely used in the food industry for the clarification of fruit juice, wine, beer, waste water treatment and separation of oil and water emulsions [3]. Ultrafiltraion processes are used in the pharmaceutical industry for the processing of enzymes, antibiotics and pyrogens, in diaries for cheese making and processing of milk proteins and in wastewater treatment [10]. Nanofiltration is used in separation of bivalent ions, in rejection of micro pollutants like pesticides, herbicides etc. and in textile industries for the retention of dyes [9]. Reverse osmosis is applied in desalination of sea and brackish water, concentration of fruit juices and sugars in food industry and concentration of milk in diary industries [4]. Pervaporation is mainly used for the dehydration of organic solvents, removal of organic components from water and separation of saturated and unsaturated compounds (e.g. cyclohexane and benzene mixture). Important gas separation processes include hydrogen recovery, organic vapours from the air, nitrogen generation and oxygen enrichment etc. [1; 3]. The membrane itself is the most important element of membrane separation processes. The membrane is a permselective barrier between the two different phases [10]. It separates the (feed) stream into two effluent sides, known as the permeate side and the retentate side as [11] shown in Figure 2.3.

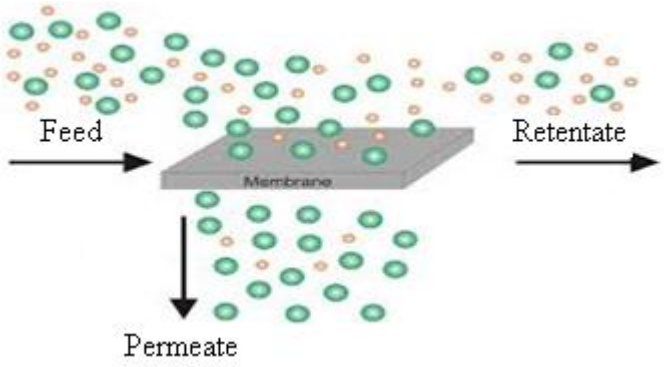

Figure 2.3: Theoretical illustration of a membrane process.

The separation occurs through the difference between the rates of passive transport of the influent molecules. The passive transport happens as a consequence of driving force, which is defined as the difference in chemical potential through the membrane [12]. It may be be the difference in temperature, concentration, pressure or electric potential [13].
Figure 2.4. shows the solution diffusion mechanism which occur when the separation process takes place using a non-porous solid and liquid membrane.

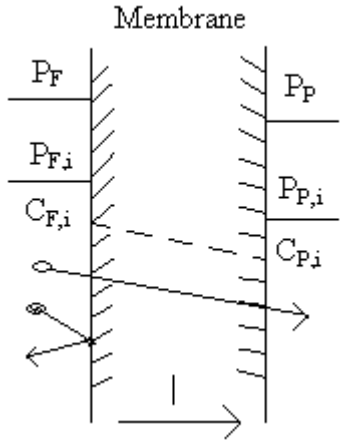

Figure 2.4 Schematic of the solution diffusion mechanism.

Where:

P_F: Pressure on the feed side of the membrane
$P_{F,i}$: Pressure of component i on the feed side of the membrane
$C_{F,i}$: Concentration of component i on the feed side of the membrane
P_p: Pressure on the permeate side of the membrane
$P_{p,i}$: Pressure of component i on the permeate side of the membrane
$C_{p,i}$: Concentration of component i on the permeate side of the membrane

When working on a non porous solid and liquid membrane, the separation process may be demonstrate by the solution diffusion mechanism (Figure 2.4):

1. Molecules dissolve through the membrane material at the high pressure side
2. Molecules diffuse through the membrane according to Fick's law of diffusion
3. Molecules leave the membrane material at the low pressure side [14].

The rate limiting second step can be described by equation (2.1):

$$Ji=DiSi(pi,F-pi,P)/l=Pi(pi,F-pi,P)/l \quad (2.1)$$

Where:
Ji is the diffusive flux; *Di* is the diffusion coefficient; *Si* is the solubility coefficient; *pi,F* is the pressure of the component i on the feed side of the membrane; *pi,P* is the pressure of the component i on the permeate side of the membrane; *l* is the membrane thickness; and *Pi=DiSi* is the permeability of the membrane [15].

The capability of the membranes to separate components can be efficiently described by the permeability and the selectivity of the membrane. In a simple component process, the ideal selectivity (α*) can be given by equation (2.2) [15]:

$$\alpha*i/j=Pi/Pj=(Di/Dj)(Si/Sj) \quad (2.2)$$

If consider two different component mixtures, *i* and *j* the selectivity (α) may be described by the following equation (2.3):

$$\alpha\ i/j=(CP,i/CP,j)/(CF,i/CF,j) \quad (2.3)$$

Where: *CP,i* and *CP,j* : the concentrations of the components in permeate;
CF,i and *CF,j* : the concentrations of the components in retentate [16]

Generally, it has been reported that liquid membrane, which is produced from a porous membrane phase and an organic liquid phase in the pores by capillary forces, show higher selectivity properties than the non-porous solid membranes due to higher liquid phase diffusivities [17]. Due to the incorporation of some carrier (*C*), which reacts reversibly and selectively with a specific permeate in the liquid membrane, further increase in mass flux and

selectivity can be achieved [18] . This phenomenon is known as an agent helps to facilitate transport [19].

2.1.5 Fabrication of the membranes

There are two main geometries which may be used to produce membranes:

- Flat sheet membranes and
- Cylindrical (Hollow fibre membranes)

Membranes may be produced using both polymeric and ceramic materials [20]. Ceramic materials show higher thermal and chemical stability than the polymer ones. However, with respect to market share polymeric membranes are far more accessible, less expensive and easier to process than the ceramic ones [19]. Polymers are used as membrane materials for 95% of several practical applications [20]. Polymeric materials that are used to produce filtration membranes are generally organic compounds.

2.1.5.1 Membranes with symmetric structure

Generally, asymmetric membranes are the most useful membranes in separation technology applications; They may be produced by track etching or precipitation from the vapour phase [21].

2.1.5.2 Membranes with asymmetric Structure

Membranes with asymmetric structure are used in industrial membrane processes. Figure 2.5 shows a cross-sectional view of an asymmetric membrane [21]. It contains two different layers: the top layer is a very thin dense layer which is called the top skin layer and the bottom one is a porous sublayer. The top dense layer leads the performance permeate and selectivity properties of the membrane; the porous sublayer provides the mechanical strength to the membrane. The membranes of symmetric structures do not have a top dense layer [19]. The integrally skinned asymmetric membrane is observed when the material of the top layer and porous sublayer are similar in the asymmetric membrane. The composite membrane may be described when the top skin layer polymer is different from the porous sublayer one. The composite membrane is advantageous over the integrally skinned asymmetric membrane

because can choose separately the material of the top skin layer and the porous sublayer to optimize overall performance.

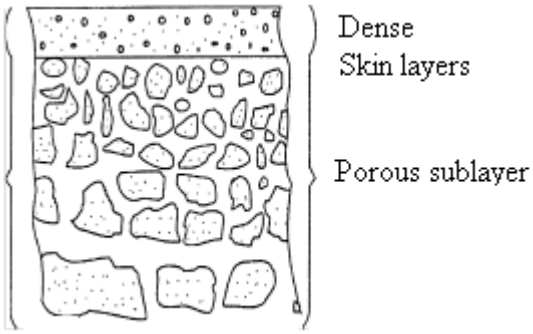

Figure. 2.5: Cross-sectional surface of an asymmetric membrane (Integrally skinned structure) . (reprinted from [21]).

2.1.5.3 Production of integrally skinned asymmetric membranes by phase inversion method

Phase inversion method by Dry wet technique: Phase inversion method can be done by using several methods [19]. Generally, membrane manufacturing uses commonly the dry–wet phase inversion technique and thermally induced phase separation. The dry–wet phase inversion technique (Loeb-Sourirajan technique). Loeb and Sourirajan (1963) produced the first cellulose acetate membrane for desalination and treatment of seawater [22]. In this technique, the polymer and solvent are mixed to produce the membranes (sometimes a non-solvent may be used). The solution is then cast on a glass support using a Doctor blade to a pre-determined membrane thickness. After allowing the evaporation of the solvent, the cast film is immersed in a non-solvent system (water bath). Solidification of the polymer happens after evaporation of the solvent and the exchange with the non-solvent in the gelation bath. It may be advantageous to choose a solvent which has a high volatility and dissolving power [23]. The exchange process of the solvent–non solvent causes the change in the composition of the polymer solution film. This is usually called the "composition path" and is illustrated schematically in Fig.2.6 (lines *A, B,* and *C* each represent a composition path). [23].

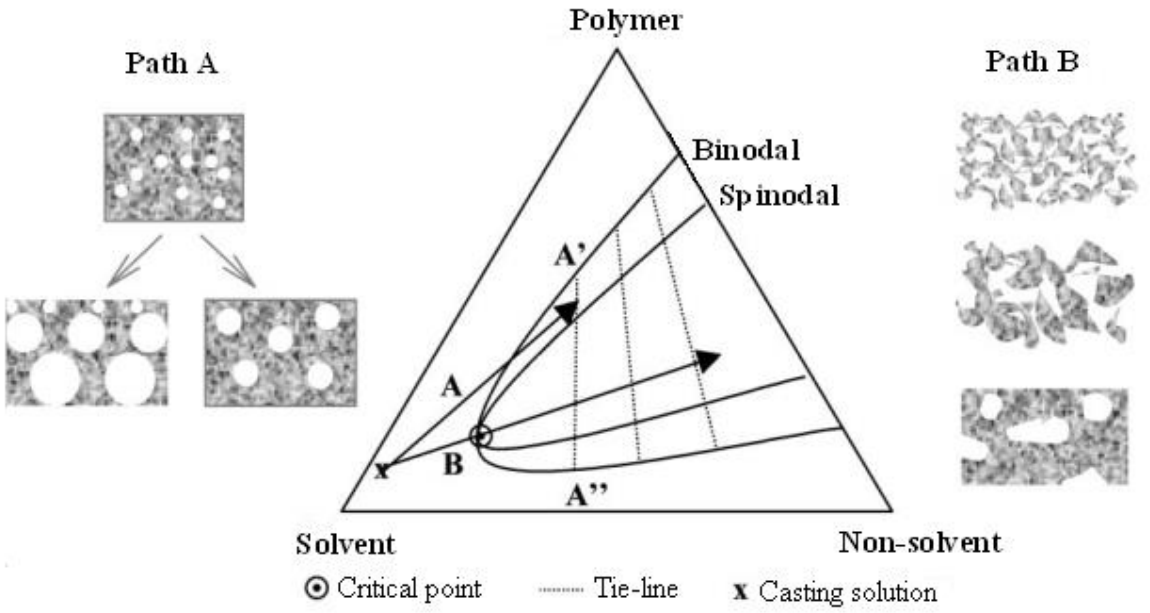

Figure. 2.6: Illustration of the triangular diagram of solvent (s), polymer (p), and non-solvent (n) (Reproduced from [21]).

Phase inversion method by "Thermally induced technique" In this method, the polymer solution temperature is reduced in order to introduce the phase inversion [24]. A polymer is blended with a substance which may act as a solvent at a higher temperature then the polymer solution may be cast into a film. After casting the solution, get an immiscible region because the solvent power has been lost [25].

2.1.6 Preparation of composite membranes

The composite membranes can be produced using two main methods:

- **Dip coating method:** Use the phase inversion method to produce the integrally skinned asymmetric membrane with a porous skin [21].
- **Interfacial polymerization method:** This method is mostly used to prepare high performance reverse osmosis and nanofiltration membranes. It was developed by Cadotte and co-workers in the 1970s [24]. The interfacial in situ polycondansation is used to place the thin selective layer on top of a porous substrate membrane. The choice of monomer may distinguish the kind of method used [25]. However, for simplicity, the polycondensation may be simply described by a pair of diamine and diacid chloride monomers [21].

After producing a diacid chloride solution in hexane and diamine solution in water. A porous membrane is then dipped into the aqueous diamine solution [25]. In this process, the aqueous solution fills the pores at the top of the porous substrate membrane. The membrane is immersed in the diacid chloride solution in hexane. It may happen that the interface is formed at the boundary of the two different phases because water and hexane are not miscible. It happens at the interface a poly condensation of diacid chloride and diamine, resulting in a very thin layer of polyamide. Figure 2.7**.** is schematically presented the preparation of composite membranes by interfacial in situ poly condensation [21].

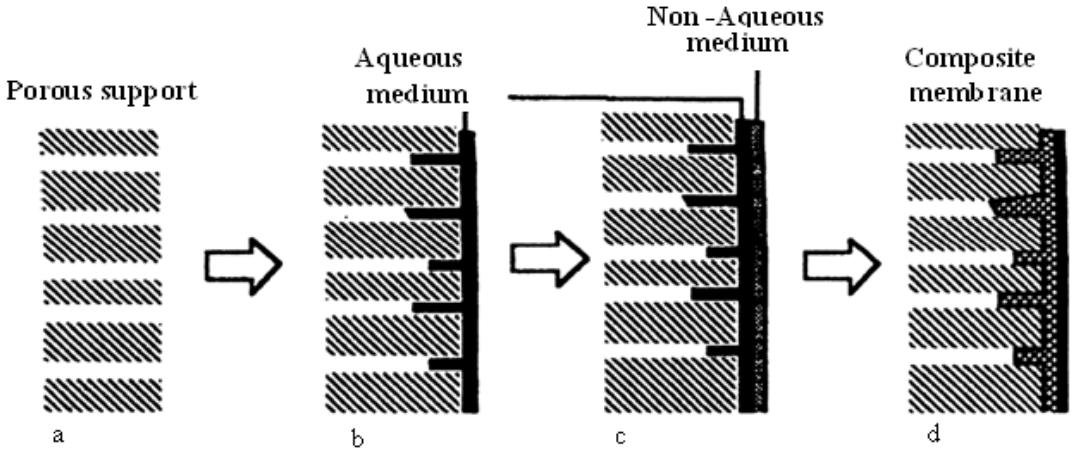

Figure 2.7: Illustration of the proceedings of the formation of a composite membrane using the interfacial polymerization method. (reprinted from [21]).

2.1.6.1 Membrane surface modification

As discussed above, the separation membrane performance is controlled by the top skin layer. The surface properties of the membrane influence the surface deposition of contaminants from solutions or from gas mixtures. This is particularly important when contaminant deposition causes a decrease in the membrane flux when a prolonged process time is observed [21]. Hence, many attempts have been made to modify the membrane surface [25]. Different surface modification methods are discussed below.

Chemical modification: Chemical reactions may lead to the modification of the surface of a membrane. For example, when the surface of a polymeric composite membrane is brought

into contact with functionalized MWCNTs, the top polymeric layer becomes slightly thinner by a chemical reaction. As a result, the mebrane flux improves considerably [26].

Plasma polymerization: The substrate surface is chemically active and introduced to the surface and upon contact with organic compounds, an irregular polymerization may occur at the surface of the substrate. This is called plasma polymerization [27].

Graft polymerization: γ-rays is used to irradiate the surface of a porous substrate membrane, which leads to radicals generation on the surface of the membrane. The membrane is then immersed into a solution of monomer [27]. Basically, the surface of the membrane is the part where the graft polymerization of the monomers begins. The choice of a very hydrophilic monomer leads to a considerable increase in hydrophilicity of the surface of the membrane [28].

Surface modification (by surface modifying macromolecule**):** A polymer is blended, the demixing of polymers occurs due to the thermodynamic incompatibility between different polymers. If the polymer is equilibrated in air, there will be a concentration of the hydrophobic polymer at the air interface which leads to the reduction tension of the interfacial system [29]. Several researchers have confirmed and announced for the miscible blending of two different polymers, that a polymer with lower surface tension shows optimum adsorption [29]. Poly(ether sulfone) (PES) was used to produce and characterize surface- active additives (surface modifying macromolecules) (PES). Depending on the hydrophobic [28;29] or hydrophilic [30] nature of the MMMs, the membrane surface becomes either more hydrophobic or more hydrophilic than the base polymeric material.

2.1.6.2 Membrane drying

Gas separation process may be allowed by using the dried wet cellulose acetate membranes which were produced for reverse osmosis purposes [30]. It is impossible to evaporate in air the water in the cellulose acetate membrane however, because the membrane (with asymmetric structure) may collapse. It is better to apply evaporation and multi-stage solvent exchange method [31]. A water-miscible solvent such as ethanol takes place first instead of the water in the membrane. The first solvent will then be replaced by a second volatile one such as hexane. The second solvent is thereafter air-evaporated, which leads to a dry membrane [31; 32]. The capillary force inside the pores is reduced by replacing water with hexane so that the collapse will be avoided during the drying process.

2.1.7 Membranes for separation processes

2.1.7.1 Membranes for the separation of solutions and solvent mixtures

Pore sizes are used to distinguish membranes for the separation of solutions:
Reverse osmosis (RO): pores size below 1 nm, Ultrafiltration (UF): 2–100 nm, and microfiltration (MF) 100 nm to 2 μm. Pore sizes of nanofiltration (NF) membranes may be range between RO and UF membranes.

2.1.7.2 Reverse osmosis membranes

A Ro membrane is a semi permeable membrane which acts as barrier to flow, allowing selective passage of a particular species (permeate) while other species (retentate) are retained. Retentate separation and permeate solution (water in most cases) flux depend on the selectivity and permeability of the membrane, the preparation procedures, and the structure of the membrane barrier layer [23; 33]. In this method, a higher pressure is applied to overcome the osmotic pressure.

2.1.7.3 Nanofiltration membranes

Mostly, nanofiltration membranes contain pores size in the range of 0.5 – 2 nm. They are most used for multivalent ion and organic molecule removal. One of the particular methods of preparing nanofiltration membranes is to dip-coat a thin layer of sulfonated poly (phenylene oxide) (SPPO) [35], sulfonated polysulfone (SPS) [36], or carboxylated polysulfone [37] on a porous substrate membrane. The sulfonic acid groups in SPPO and SPS also become negatively charged with $–SO_3$ groups upon dissociation.

2.1.7.4 Ultrafiltration membranes

Ultrafiltration is a pressure-driven membrane filtration process. UF membranes generally have pore sizes in the range of 2–100 nm and retain species in the molecular range from 3000 to 500 000 Da [38]. UF membranes have smaller pores than microfiltration membranes. They are mainly use for the removal of colloids and macromolecules [38].

2.1.7.5 Microfiltration membranes

Microfiltration membranes have the largest pore sizes relative to the others and therefore, thus use less pressure. Mainly produced for the removal of biological and chemical compounds with diameters ranging between 100 to 10000 nm.

2.1.7.6 Membrane applications

The use of synthetic membranes (mainly synthetic polymeric membranes) in engineering, biology and medecine is the result of advances in membrane technology research. For instance, the separation of light olefin and paraffin in the petrochemical industry was studied and reported by Faiz and Li [39]. Choi et.al studied the improvement of the physical and transport properties of the membrane by modifying the Nafion membranes with grapheme oxide, which can be efficient for the application of fuel cells [40]. Budd and Mc Keown researched the application of polymeric membranes for gas separation. They developed their use in carbon dioxide removal, nitrogen generation, hydrogen recovery etc [41]. Generally, the applications of membranes have been for desalination. However, other options have been detected with variety of membrane structures developed [42]. These include removal of organic, inorganic and microbial contaminants from wastewater. Other applications of polymeric membranes can be found in the food industry [43; 44], pharmaceutical industry [45], electrodes [46], biomedicine [47], and beverages [48-50].

2.1.7.7 Membrane fouling and its control

Membrane fouling can be defined as an accumulation of solid substances on the top surface of the membrane and inside the membrane pores [51]. Fouling mechanisms are very complex and interconnected. The most common categories of membrane fouling mechanisms are:

(i) Formation of a cake layer on the top surface of the membrane. Adsorption of solid matter on the surface and within the pores of the membrane.

(ii) Accumulation of solid substances within the membrane pores.

(iii) Accumulation of rejected solutes within the membrane.

(iv) Bio - fouling phenomena because of the presence of micro-organisms.

Membrane fouling can decrease the permeate flux and selectivity of the membrane and therefore increase energy consumption and cost [51; 52].

2.2. Carbon nanotubes

Carbon nanotubes (CNTs) were re-discovered and characterized in 1991 by Iijima as was made possible by the use of transmission electron microscopy [53]. CNTs are cylinder-shaped tubes, with diameters as small as a few nanometers and length varying from a few microns to centimeters, hence making them high aspect ratio nanoparticles [54; 55]. These cylindrical shaped tubes are comprised of rolled graphene sheets and can be classified according to the number of graphene layers. A rolled up single graphene layer leads to single-walled carbon nanotubes (SWCNTs) and several concentric layers to multi-walled carbon nanotubes (MWCNTs) [56]. The first identified CNTs were comprised of 2 to 50 concentric cylindrical like shells. These shells were regularly spaced by a distance of 0.34 nm as in conventional graphite materials [57]. SWCNTs were synthesized in 1993 after the identification of MWCNTs [58].

2.2.1 Structure of carbon nanotubes:

The structure of CNTs depends on the rolling pattern of the graphene sheet. The rolling of the graphene layer can be described by a chiral vector C_h which connects two crystallographically equivalent sites (A and A´ in Fig. 2.8) on the sheet [59].

The chiral vector C_h can be defined as:

$$C_h = n\vec{a}_1 + m\vec{a}_2 \qquad (4)$$

Where $\vec{a}_1$ and $\vec{a}_2$ are unit vectors of the hexagonal honey comb lattice and ‘n’ and ‘m’ are integers denoting the relative position of a pair of atoms on the graphene sheet.

The chiral vector C_h defines the circumference of the tube and the diameter of the nanotube (d_t) can be estimated by equation (2.5).

$$dt = \frac{a}{\pi}\sqrt{n^2 + nm + m^2} \qquad (2.5)$$

Where *a* is the lattice constant of the honeycomb network

$$x = \sqrt{3}\,.\,a_{cc} \qquad (2.6)$$

Where a_{cc} ~ 0.142 nm, the C-C bond length.

The chiral vector C_h defines a particular (n,m) tube, as well as its chiral angle θ which is the angle between C_h and 1 $_a$. The chiral angle can be calculated using equation (2.7)

$$\text{Cos}\,\theta = \frac{2n+m}{2\sqrt{n^2+nm+m^2}} \qquad (7)$$

Because of the hexagonal symmetry of the graphene lattice, θ value lies in the range $0 \le \theta \le 30$. The chiral angle θ represents the tilt angle of the hexagons with respect to the direction of CNTs axis. CNTs of the type (n,0) (θ=0°) are classified as zigzag tubes because they exhibit a zigzag pattern along the circumference. C-C bonds in these tubes exist parallel to the tube axis. CNTs of type (n,m=n) (θ=30°) are categorized as armchair tubes because they exhibit an armchair pattern along the circumference. These tubes display C-C bonds perpendicular to the tube axis [58]. Both zigzag and armchair CNTs are grouped together under achiral tubes in contrast with general chiral tubes (n, m≠n≠0) (Figure 2.9). For double walled CNTs (DWCNTs) and MWCNTs, the control of chirality along the grapheme layers is complicated. Hence, it is difficult to classify them according to their chirality [57; 59].

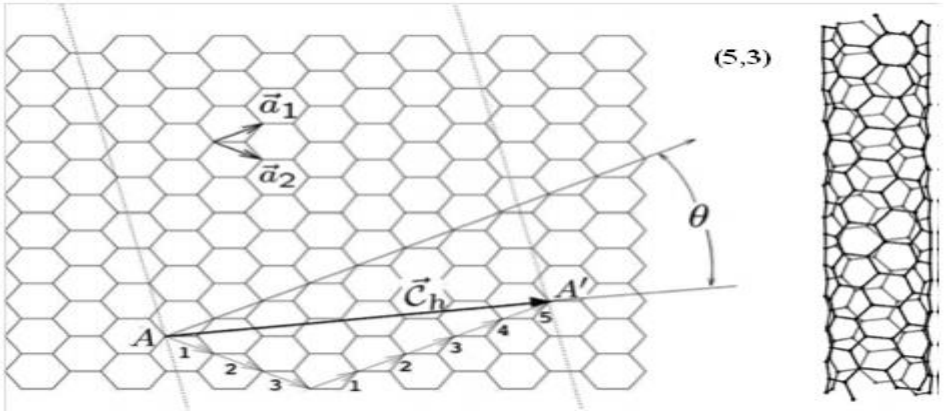

Figure 2.8: Graphene sheet with lattice vectors a_1 and a_2, The chiral vector Ch=$3a_1$+$5a_2$ □ represents a possible wrapping of the two dimensional (2D) graphene sheet into a tube form. The resulting (5,3) nanotube is shown on the right side having chiral character. (reproduced from [59]).

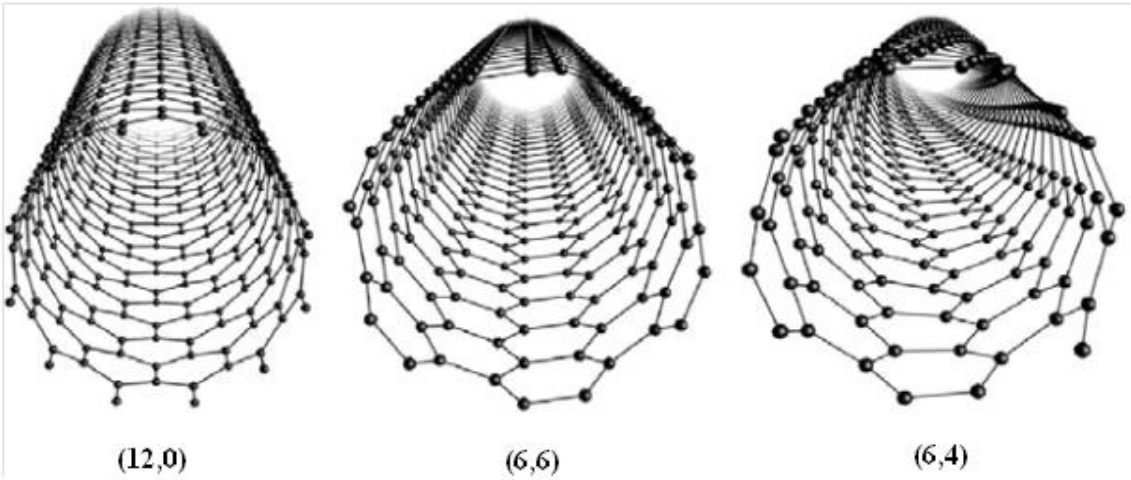

Figure 2.9: Illustration of the atomic structures of (12,0) zigzag, (6,6) armchair and (6,4) chiral nanotubes (reproduced from [59]).

2.2.2 Synthesis of CNTs

Mostly, CNTs are prepared using three different main methods: arc discharge, laser ablation and chemical vapour deposition [53].

2.2.2.1 Arc Discharge Method

Iijima used the arc discharge method to synthesize MWCNTs in 1991 [53]. This method involves the evaporation of carbon atoms from the anode when DC arc plasma is generated between graphite anode and cathode under an inert atmosphere. The anode is consumed by the evaporation of carbon atoms and filamentous deposit containing CNTs and other by-products are collected on the cathode (Fig. 2.10 (a)). MWCNTs produced by the arc discharge method are very straight which is indicative of their high crystallinity. There exist a few defects such as pentagons or heptagons on the side walls of arc produced CNTs [60]. By-products of this process are multilayered graphitic particles with polyhedron shapes. For the growth of SWCNTs, a metal catalyst is needed in one arc discharge system. The first success of SWCNTS synthesis was achieved by Bethune et al [57]. in 1993. Used carbon anode with small percentage of cobalt catalyst in the discharge experiment and found abundance of SWCNTs in the soot material [58; 60].

2.2.2.2 Laser Ablation Method

Smalley and co-workers used this method for the synthesis of SWCNTs [61]. In this method intense laser pulses are used to ablate a carbon precursor containing 0.5 atomic percent of

nickel and cobalt at 1200°C with continuous inert gas flow. The flow of inert gas leads to a collection of CNTs on a cold finger (Fig. 2.10 (b)) [60]. This method is not suitable for mass production; nevertheless CNTs with good quality, controlled diameter, and diameter distribution are possible by this technique. SWCNTs samples prepared by this method have been used extensively for fundamental studies [61].

2.2.2.3 Chemical Vapor Deposition

Walker et al. [62] reported the catalytic chemical vapor deposition of carbon in 1959; however, it was used in 1993 for the production of CNTs [63]. This method is used for the production of CNTs on an industrial scale. It involves the decomposition of hydrocarbon gas for a period of time through a tube reactor containing catalyst material at higher temperatures (Figure 2.10 (c)). CNTs grown over the catalyst are collected upon cooling of the system to room temperature. The key parameters and components for CVD growth of CNTs include the type of hydrocarbons, catalysts and temperatures. In most CVD methods, ethylene or acetylene are used as carbon feedstock. The temperature range for the CVD process is 550-750°C and iron, nickel or cobalt nanoparticles are employed as catalyst precursors [59; 63].

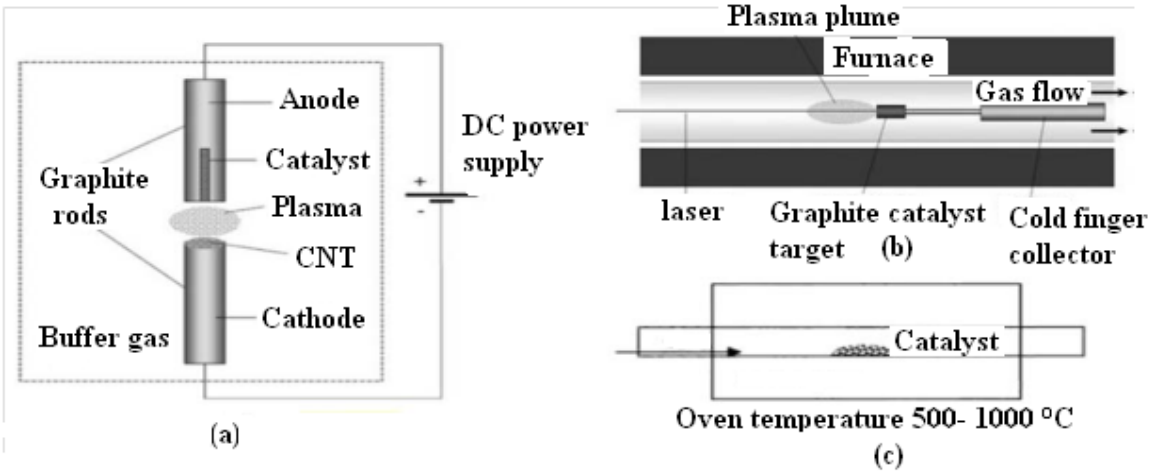

Figure 2.10: Illustration of the diagrams of (a) Arc discharge method, (b) Laser ablation method and (c) CVD reactor, for carbon nanotube growth. (a) and (b) reproduced from [61] and (c) reproduced from [59].

2.2.3 Mechanical Properties of CNTs

Like graphite, MWCNTs possess sp^2 hybrid bonding among carbon atoms and the grapheme layers are 0.34 nm spaced [53]. It is known that graphite has an in plane modulus of 1.06 TPa and MWCNTs expected to display similar stiffness [64]. Computer based simulation studies also forecasted their extraordinary mechanical properties [65]. The first actual mechanical measurements were performed on MWCNTs by Treacy et al.[66] in 1996. Calculated Young's moduli (0.41-4.15 TPa) using the measurement of the amplitude of intrinsic thermal vibrations by transmission electron microscopy (TEM). Wong et al.[66] conducted the first direct measurement of the mechanical properties of arc-grown MWCNTs using atomic force microscopy (AFM) in 1997. Reported Young's modulus of 1.28 TPa and bending strength of 14 GPa [67]. Salvetat et al. [69] measured an average modulus value of 810 GPa for arc-MWCNTs using AFM. Measured a modulus of ~1TPa for small diameter SWCNTs bundles using the same method [69]. The mechanical properties of CNTs strongly depend upon the concentration of defect sites and type [70]. Xie et al. [71] synthesized MWCNTs via CVD method and the values of Young's modulus and tensile strength were found to be 0.45 TPa and 3.6 GPa, respectively. The modulus and strength values were much lower compared to arc grown CNTs. The defects in the tubes and the interwall slides of MWCNTs may be responsible for the depression of mechanical properties of the tubes [71]. The mechanical properties of CNTs make them valuable candidates for application in composite materials.

2.2.4 Electrical Properties of CNTs

A SWCNT possesses metallic or semiconducting behavior depending on its structure i.e., rolling pattern of the graphene sheet which is driven by chiral vector with n and m as integers (Figure 2.7) [58]. A SWCNT (n,m) is metal like, if n=m i.e., an armchair SWCNT. A CNT with n-m=3*l*, where *l* is an integer, behaves like a semi metal [72]. With n-m≠3*l*, other results in a SWCNT are semiconductor. The average abundance of metallic SWCNTs is one third of total, and the rest of SWCNTs are semiconductors [73]. MWCNTs have also been reported to have quite good electrical conductivity. Ebbesen et al. [74] measured the conductivities of individual MWCNTs that ranged between 20 and 2×107 S/m. Reported that MWCNTs can carry current densities of values as high as 6×106 $A \cdot cm^{-2}$ (without damaging the sample) [74]. Electrical conductivity of CNTs is greatly influenced with the introduction of defects created during production and by functionalization on their surface. The extraordinary electrical properties of CNTs make them fillers to introduce electrical conductivity in synthetic plastics which are mostly insulators [73].

2.2.5 Functionalization of CNTs

CNTs are produced in the form of bundles where the individual CNTs are stacked together in the form of aggregates via van-der-Waals and π –π stacking interactions. Modification of their surface chemistry is an important tool for better dispersion in solvents and polymer matrices [74]. Surface functionalization involves the introduction of various functional groups or reacting sites on the side walls of CNTs [75]. Surface functionalization of CNTs can be divided into two main categories; covalent and non-covalent functionalization.

2.2.5.1 Covalent Functionalization

Covalent functionalization creates defects on the side walls of CNTs to incorporate various functional groups. It changes the hybridization of carbon atoms on the walls of CNTs from sp^2 to sp^3, resulting in a loss of conjugation [76]. Covalent functionalization of CNTs has been reported by oxidation [77, 78], halogenation [79, 80], radical addition [81 and electrophilic or neucleophilic addition [82, 83] etc. The attached functional groups can be small functional groups like – COOH, –OH, –F, –NH2 etc. depending upon the functionalization pathway followed. These primary functional groups can be used for the attachment of various chemical species and polymers on the surface of CNTs. Covalent binding of the polymer functionalities on CNTs takes place via "grafting from" or "grafting onto" approaches [84].

2.2.5.1.1 "Grafting From"

"Grafting from" means that polymerization of monomers from the active functional groups present on side walls of CNTs [77, 78]. This approach may be carried out by employing different polymerization mechanisms i.e. free radical polymerization, anionic polymerization, reversible addition-fragment chain transfer (RAFT) polymerization and atom transfer radical polymerization (ATRP) [78]. ATRP is the most commonly used technique for this approach. Yao et al. [85] incorporated phenol end groups on SWCNTs using a 1, 3 dipolar cycloaddition reaction [85]. The phenol groups were further derived with 2-bromoisobutyryl bromide resulting in an ATRP initiator on the nanotube side walls. Finally, methyl methacrylate (MMA) and *tert*-butyl acrylate (*t*BA) were grafted from the initiator modified SWCNTs via ATRP. Yan et al. [78] modified MWCNTs with carboxyl groups using nitric acid and carboxyl groups and were further activated with thionyl chloride to create carbonyl chloride end groups [78]. Carbonyl chloride end groups were modified by ethylene glycol to

introduce –OH end groups. –OH functionalized MWCNTs were then reacted with 2-bromoisobutyryl bromide to bind ATRP initiator on the side walls of MWCNTs. Finally, the ATRP technique was used to graft Poly (methyl methacrylate) PMMA from the initiating sites present on the MWCNTs. The polymer thickness was controlled by varying the weight ratio between monomer and initiator modified MWCNTs. Polymer modified nanotubes showed good solubility in non polar solvents and weakly polar solvents like chloroform and tetrahydrofuran (THF) etc [85].

The above mentioned examples describe multiple reaction steps for modification of CNTs with polymer. The production of polymer functionalized CNTs via ‘’grafting from’’ technique can be performed on hydroxyl and amine functionalized CNTs produced industrially by special thermal oxidation methods [78]. The immobilization of ATRP initiator on CNTs follows the grafting of polymers from the initiator fractions. In this study, polystyrene and poly (methyl methacrylate) were grafted from industrially supplied pre-functionalized MWCNTs i.e MWCNTs containing amine functional groups by applying ATRP [85].

2.2.5.1.2 “Grafting Onto”

In the “grafting onto” approach, the polymers with reactive end functional groups are attached with functional groups present on the CNTs. Polymer chains can be attached to the carboxyl functionalized MWCNTs by amidation and esterification reactions [86; 87]. Lin et al. [88] grafted poly (vinyl alcohol) (PVA) onto carboxyl functionalized CNTs by carbodiimide activated esterification reactions. PVA functionalized CNTs showed stable dispersion in water, dimethyl sulfoxide (DMSO) and PVA matrix [88]. Sano et al. [86] performed $SOCl_2$ reaction with carboxyl functionalized SWCNTs to create carbonyl chloride end functional groups. Grafted amino terminated polyethylene oxide onto carbonyl chloride functional groups via amidation reaction. The modified SWCNTs showed better dispersion in water and *N*, *N*-dimethylformamide (DMF) [86]. Lou et al. [89] reported the grafting of polystyrene (PS), poly (ε-caprolactone) (PCL), and their block copolymers, end capped with (2,2,6,6-Tetramethylpiperidin-1-yl)oxyl (TEMPO), onto MWCNTs by the radical addition mechanism [89]. PS and PCL modified MWCNTs showed stable dispersion in toluene and tetrahydrofuran (THF). The grafting density of polymer chains is lower for “grafting onto” technique compared to “grafting from” technique.

2.2.5.2 Non-covalent Functionalization

In comparison to covalent functionalization, non-covalent functionalization preserves the sp^2 configuration of CNTs and thus conserves their electrical and mechanical properties. Organic mediating molecules, ranging from low molecular weight species to polymers, are used for non-covalent functionalization of CNTs [76]. These mediating molecules change the surface characteristics of CNTs by either adsorption or wrapping the CNTs surface [90]. Amphiphilic molecules like surfactants, copolymers and polyaromatic compounds etc. adsorb on the surface of CNTs and lead to better dispersibility without any destruction or defects on the surface of the CNTs. The most commonly used surfactants for dispersing CNTs in aqueous media include sodium dodecyl sulfate (SDS) [90], sodium dodecyl benzene sulfonate (SDBS) [90], Brij, Tween [91; 92], and Triton X 100 [90]. The individual dispersion of CNTs is made possible by their encapsulation inside the micelles having hydrophobic interiors [93]. Islam et al. [90] found that SDBS is more powerful surfactant to disperse SWCNTs compared to SDS in aqueous media. In addition to surfactant interactions, SDBS possess aromatic ring π-π interactions with the graphitic walls of SWCNTs [90].

Polyaromatic compounds also possess π-π interactions with CNTs. Tomonari et al. [94] found that ammonium salts based on pyrene fractions led to better and stable dispersions of SWCNTs in aqueous solution compared to phenyl and naphtyl based ammonium salts [94]. The strong adsorption capability of the pyrene fraction on the surface of CNTs provides the opportunity to attach derivatives containing different functionalities on CNTs. Chen et al. [95] attached proteins on SWCNTs surfaces using 1-pyrenebutanoic acid, succinimidyl ester [95]. Ji et al. [96] reported surfactants based on polysiloxane derivatives of pyrene and porphyrin [96].

The surfactant containing the pyrene moiety led to dispersed SWCNTs and MWCNTs in non polar solvent like petroleum ether. However, found that the surfactant with porphyrin moiety gave rise to a better dispersion of only SWCNTs. Liu et al. [31] functionalized MWCNTs in water using poly (ethylene glycol) (PEG) derivative of pyrene [97]. Proved the adsorption of pyrene-PEG on MWCNTs by analyzing the dispersion of MWCNTs, obtained after different cycles of dialysis by UV-Vis spectroscopy. Adsorption of pyrene-PEG was also confirmed by thermogravimetric analysis (TGA). Various research groups have attached pyrene with different polymers and subsequently functionalized CNTs using pyrene modified polymers by non covalent functionalization [97; 98].

Polymer wrapping on CNTs surface also improves their dispersion in organic and aqueous medium. Conjugated polymers like poly(m-phenylene vinylene) (PmPV) [99] or poly(3-hexylthiophene) (P3HT) [100] interact with CNTs via strong π-π interactions which drives the wrapping of polymers around CNTs. Zou et al. [101] reported the π-π interaction of a conjugated block copolymer, poly(3- hexylthiophene)-block-polystyrene (P3HT-b-PS) with CNTs [101]. The conjugated block interacts with CNTs while the PS block improves the dispersion of CNTs in chloroform. The wrapping of the conjugated polymer weakens the inter-tube van-der-Waals interactions and the PS block improves the dispersion of CNTs. Other polymers like poly (vinyl pyrrolidone) [102], polystyrene-block-poly(acrylic acid) [103] or poly(styrene sulfonate) [102] display week π-π interaction with CNTs but can be used to wrap CNTs.

2.3 References

1. Baker. R.W. (2014). Membrane Technology and Applications, 2nd edition, Wiley-VCH.
2. Mulder M., (1996). Basic Principles of Membrane Technology, 2nd edition, Kluwar Publishers.
3. Nunes S. P., Peinemann K. V. (2006). Membrane Technology in the Chemical Industry, 2nd edition, Wiley-VCH.
4. Stern S.A. (1994). Polymers for Gas Separations**,** the Next Decade. Journal of Membrane Science., 94, 1-65.
5. Porter, M.C. (1990). Handbook of Industrial Membrane Technology, William Andrew Publishing/Noyes, New Jersey, USA.
6. Atchariyawut S., Feng C., Wang R., Jiraratananon R., Liang D.T. (2006). Effect of membrane structure on mass-transfer in the membrane gas–liquid contacting process using microporous PVDF hollow fibers. Journal of Membrane Science.
7. Acharya N.K., Kulshrestha V., Awasthia K., Jain A.K., Singh, M., Vijay, Y.K. (2008). Hydrogen separation in doped and blend polymer membranes. International Journal of Hydrogen Energy, 33, 1, 327-331.
8. Jönsson J.Å., Mathiasson L. (1999). Liquid membrane extraction in analytical sample preparation I. Principles. Trends in Analytical Chemistry, 18, 5, 318-325.
9. Soni, V., Abildskov, J., Jonsson, G., Gani, R. (2009). A general model for membrane-based separation processes. Computers and Chemical Engineering, 33, 3. 644-659.
10. Koops, G.H. (1995). Nomenclature and symbols in membrane sand technology. University of Twente, Membrane Technology Group, Netherlands.
11. Strathmann, H., Giorno, L., Drioli, E. (2006), An introduction to membrane science and technology, Roma, Italia.
12. Ulbricht, M. (2006). Advanced functional polymer membranes. Polymer, 47, 7, 2217-2262.
13. Mulder, M. (1996). Basic principles of membrane technology, Kluwer Academic Publishers, Dordrecht, the Netherlands.
14. Lashkari, S., Tran, A., Kruczek, B. (2008). Effect of back diffusion and back permeation of air on membrane characterization in constant pressure system. Journal of Membrane Science, 324, 1-2, 162-172, 03767388.

15. Baker, R.W. (2004). Membrane technology and applications, John Wiley & Sons, ISBN: 0-470-85445-6, Chichester, England.
16. Koros, W.J., Fleming, G.K. (1993). Membrane-based gas separation, Journal of Membrane Science, 83, 1, 1-80. 03767388.
17. Chakma, A. (1995). Separation of CO_2 and SO_2 from flue gas streams by liquid membranes. Energy Conversion and Management, 36, 6-9., 405-410.
18. Ravanchi, M.T., Kaghazchi, T., Kargari, A. (2010). Supported liquid membrane separation of propylene propane mixtures using a metal ion carrier. Desalination, 250, 1, 130- 135.
19. Kocherginsky N.M., Yang Q., Seelam L. (2007). Recent advances in supported liquid membrane technology. Separation and Purification Technology, 53, 2, 171-177.,13835 866.
20. Peinemann, K. (2004). Next generation membrane materials. In: Abstracts of the 15th annual meeting of the NAMS, Honolulu, 26–30.
21. Matsuura T. (1994) Synthetic membranes and membrane separation processes. CRC, Boca Raton.15.
22. Loeb S., Sourirajan S. (1963). Sea water demineralization by means of an osmotic membrane. Advances in Chemistry Series 38, 117–132.
23. Sourirajan S., Matsuura T. (1985). Reverse osmosis / ultrafiltration process principles. National Research Council of Canada.
24. Rozelle L.T., Cadotte J.E., Cobian K.E., Kopp C.V. Jr (1977) .Nonpolysaccharide membrane for reverse osmosis: NS-100 membranes. In: Sourirajan S (ed) Reverse osmosis and synthetic membranes: theory, technology, engineering. National Research Council of Canada.
25. Peterson R.J. (1993). Composite reverse osmosis and nanofiltration membranes Journal of membrane science 83:81.
26. Kulkarni A., Mukherjee D., Gill W.N. (1994). Reprocessing hydrofluoric acid etching solutions by reverse osmosis.Chemical Engineering Communications, 129, 53-68
27. Hirotsu T. (1987). Graftpolymerized membranes of methacrylic acid by plasma for water ethanol permseparation. Journal of Industrial and Engineering Chemical Research, 26:1287-1290.
28. Suk D.E., Chowdhury G., Narbaitz R.M., Santerre J.P., Matsuura T., Glazier G., Deslandes Y. (2002). Macromolecules 35:3017.

29. Khayet M., Suk D.E., Narbaitz R.M., Santerre J.P., Matsuura T. (2003). Study on surface modification by surface-modifying macromolecules and its applications in membrane-separation processes. Journal applications polymer science 89:2902.
30. Hester J.F., Banerjee P., Won Y.Y., Akthakul A., Acar M.H., Mayes A.M. (2002). Macromolecules 35:7652.
31. Lui A., Talbot F.D.F, Sourirajan S., Fouda A.E., Matsuura T (1998). Separation science technology 23:1839.
32. Gantzel P.K., Merten U. (1970). Gas separations with high flux cellulose acetate membranes. Journal of Industrial and Engineering Chemistry Process Des Dev 9:331.
33. Lloyd D. (1985). Membrane materials science: an overview. In: Lloyd DR (ed) Materials science of synthetic membranes. ACS Symposium Series 269. American Chemical Society, Washington.
34. Hoehn H.H. (1985) .Aromatic polyamide membranes. In: Lloyd DR (ed) Materials science of synthetic membranes. ACS Symposium Series 269. American Chemical Society, Washington.
35. Matsuura T. (2001) Reverse osmosis and nanofiltration by composite polyphenylene oxide membranes. In: Chowdhury G, Kruczek B, Matsuura T (eds) Polyphenylene oxide and modified polyphenylene oxide membranes. Kluwer, Dordrecht.
36. Allegrezza A.E.Jr, Parekh B.S., Parise P.L., Swiniarski E.J., White J.L. (1987). Chlorine resistant polysulfone reverse osmosis modules. Desalination 64:285.
37. Guiver M.D, Tremblay AY, Tam CM (1985) Reverse osmosis membrane from novel hydrophilic polysulfone. In: Sourirajan S, Matsuura T (eds) Advances in reverse osmosis and ultrafiltration. National Research Council of Canada.
38. Kulkarni S.S., Funk E.W., Li N (1992). Ultrafiltration. In: Ho WSW, Sirkar K.K. (eds) Membrane handbook. Van Nostrand, New York, 393.
39. Faiz, R. and Li, K. (2012). Polymeric membranes for light olefin/paraffin separation. Desalination, 82-97.
40. Choi, B.G., Huh, Y.S., Park, Y.C., Jung, D.H., Hong, W.H., and Park, H (2012). Enhanced transport properties in polymer electrolyte composite membranes with graphene oxid sheets. Carbon, 5395-5402.
41. Budd, P.M. and McKeown, N.B. (2010). Highly permeable polymers for gas separation membranes. Polymer Chemistry, 63-68.

42. Geise, G.M., Lee, H.S., Miller, D.J., Freeman, B.D., McGrath, J.E., and Paul, D.R.(2010), Water purification by membranes: The role of polymer science. Journal of Polymer Science Part B: Polymer Physics, 1685-1718.
43. Akin, O., Temelli, F., and Köseoğlu, S. (2012), Membrane Applications in Functional Foods and Nutraceuticals. Critical Reviews in Food Science and Nutrition, 2012. 52(4): 347-371.
44. Gyura, J., Šereš, Z., and Eszterle, M. (2005), Influence of operating parameters on separation of green syrup colored matter from sugar beet by ultra-and nanofiltration. Journal of Food Engineering, 89-96.
45. López-Fernández, R., Martínez, L., and Villaverde, S. (2010), Membrane bioreactor for the treatment of pharmaceutical wastewater containing corticosteroids. Desalination.300: 19-23.
46. Huang, M., Ding, Y., and Li, X.(2012), Improvement of lower detection limit of ion-selective electrodes based on PVC membrane. Progress in Chemistry, 24(8): 1560-1571.
47. Ramakrishna, S., Ma, Z., and Matsuura, T. (2010), Polymer membranes in biotechnology: Preparation, functionalization and application, London: Imperial College Press.
48. Garcia-Castello, E.M. and McCutcheon, J.R.(2011), Dewatering press liquor derived from orange production by forward osmosis. Journal of Membrane Science. 97-101.
49. Grassino, A.N., Milardović, S., Grabarić, Z., and Grabarić, B.S. (2012), Simple and reliable biosensor for determination of glucose in alcoholic beverages. Food Research International, 2012. 47(2): 368-373.
50. Yazdanshenas, M., Nejad, S.A.R.T., Soltanieh, M., Tavakkoli, A., Babaluo, A.A., and Fillaudeau, L. (2010), Dead-end microfiltration of rough nonalcoholic beer by different polymeric membranes. Journal of the American Society of Brewing Chemists, 68(2): 83- 88.
51. Mohanty, K. and Purkait, M.K.(2010), Membrane technologies and applications, Boca Raton FL: CRC Press. USA.
52. Zhang, T.C. (2012), Environmental, Water Resources Institute. Membrane Technology Task, C., and American Society of Civil, E., Membrane technology and environmental applications, Reston, VA: American Society of Civil Engineers.

53. Iijima S. (1991), helical microtubules of graphitic carbon, Nature, 354, 56-58.
54. Balasubramanian K., Burghard M. (2005). Chemically functionalized carbon nanotubes, Small, 1, 180-192.
55. Wang X., Li Q. , Xie J., Jin Z., Wang J. , Li Y., Jiang K., Fan S. (2009). Fabrication of ultralong and electrically uniform single-walled carbon nanotubes on clear substrates. Nanotechnology Letter., 9 3137-3141.
56. Reich S., Thomsen C. , Maultzsch J. (2004). Carbon Nanotubes: Basic Concepts and Physical Properties, Wiley-Vch.
57. Bethune D., Klang C. , De Vries M. , Gorman G., Savoy R., Vazquez J. , Beyers R.(1993). Cobalt – catalysed growth of carbon nanotubes with single atomic layer walls.Nature, 363 (1993) 605-607.
58. Charlier J. C. , Blase X. , Roche S. (2007). Electronic and transport properties of nanotubes. Review of Modern Physics. 79, 677.
59. Dai H. (2001), Carbon Nanotubes: Synthesis, Structure, Properties and Applications. Springer. Account of Chemical Research.1035-1044.
60. Thess A., Lee R. , Nikolaev P. , Dai H., Petit P., Robert J., Xu C. , Lee Y. H., Kim S. G. Rinzler A. G., Colbert D. T., Scuseria G. E., Tomanek D., Fischer J. E. , Smalley R. E. (1996). Crystalline ropes of metallic carbon nanotubes. Journal of Science, 273, 487.
61. Rümmeli M. H., Ayala P., Pichler T.(2010) , Carbon Nanotubes and Related Structures, 1-21.
62. Walker P., Rakszawski J., Imperial G. (1959). Carbon formation from carbon monoxide hydrogen mixtures over iron catalysts. Journal of Physics and Chemistry, 63, 133- 140.
63. Jose-Yacaman M. , Miki-Yoshida M., Rendon L., Santiesteban J. (1993). Catalytic growth of carbon microtubes with fullerene structure. Applied Physics letters. 62, 202-204.
64. Coleman J. N. , Khan U., Gun'ko Y. K. (2006). Mechanical reinforcement of polymers using carbon nanotubes. Advanced Materials, 18, 689-706.
65. Overney G. , Zhong W., Tomanek D. (1993). Structural rigidity and low frequency vibrational modes of long carbon tubules, Molecules and Clusters, 27 ,93-96.
66. Treacy M. , Ebbesen T., Gibson J. (1996). Exceptional high young's modulus observed for individual carbon nanotubes. Nature, 381, 678-680.

67. Wong E. W. , Sheehan P. E., Lieber C. M. (1997). nanobeam mechanics: elasticity, strength and toughnes of naorods and nanotubes. Science, 277, 1971-1975.
68. Salvetat, J. P., Kulik A. J.,. Bonard J. M , Briggs G. D., Stöckli T., Méténier K., Bonnamy S. , Béguin F. , Burnham N. A. , Forró L. (1999). Elastic modulus of ordered and disordered multiwalled carbon nanotubes. Advanced materials, 11, 161-165.
69. Salvetat J. P., Briggs G. a. D. , Bonard J. M., Bacsa R. R., Kulik A. J., Stöckli T., Burnham N. A. , Forró L. (1999). Elastic and shear moduli of single-walled carbon nanotubes ropes. Physics Review Letter, 82 ,944-947.
70. Salvetat J. P.,. Bonard J. M, Thomson N. , Kulik A., Forro L., Benoit W., Zuppiroli L. (1999). Elastic and shear moduli of single-walled carbon nanotubes ropes. Applied physics. Material science processing, 69,255-260.
71. Xie S., Li W., Pan Z. , Chang B., Sun L. (2000). Mechanical and physical properties on carbon nanotubes. Journal of Physics and Chemistry of Solids, 61 ,1153-1158.
72. Dai H., Javey A., Pop E., Mann D., Lu Y. (2006). Ellectrical transport properties and field effect transistors of carbon nanotubes. Nanotechnology, 1, 1-13.
73. Kataura H. , Kumazawa Y. , Maniwa Y., Umezu I. , Suzuki S. , Ohtsuka Y., Achiba, (1999). Optical properties of single-walled carbon nanotubes. Synthetic Metals, 103, 2555-2558.
74. Ebbesen T. , Lezec H., Hiura H. , Bennett J. , Ghaemi H. , Thio T. (1996). Electrical conductivity of individual carbon nanotubes. Nature, 382, 54- 56.
75. Tasis D., Tagmatarchis N. , Bianco A., Prato M. (2006). Chemistry of carbon nanotubes. Chemical Reviews, 106 , 1105-1136.
76. Kim S. W., Kim T. , Kim Y. S. , Choi H. S. , Lim H. J. , Yang S. J., Park C. R.(2012). Chemistry of carbon nanotubes , Chemical review, 50, 3-33.
77. Qin S., Qin D., Ford, W. T., Resasco D. E., Herrera J. E. (2004). Polymer brushes on single-walled carbon nanotubes by atom transfer radical polymerization of n-butyl methacrylate. Journal of the American chemical society., 126, 170-176.
78. Kong H., Gao C., Yan D. (2004). Controlled functionalization of multi-walled carbon nanotubes by atom transfer radical polymerisation. Journal of the American chemical society. 126, 412-413.
79. Mickelson E., Huffman C., Rinzler A., Smalley R., Hauge R., Margrave J.(1998). Fluorination of single-walled carbon nanotubes. Chemical Physics Letters, 296 (1998) 188-194.

80. Khabashesku V. N. , Billups W. E. , Margrave J. L. (2002). Fluorination of single-walled carbon nanotubes and subsequent derivatization reactions. Accounts Chemical research. 35, 1087-1095.
81. Liu J., Zubiri M. R. I. , Dossot M. , Vigolo B., Hauge R. H. , Fort Y. , Ehrhardt J. J., Mcrae E. (2006). Sidewall functionalization of single-walled carbon nanotubes through aryl free radical addition. Chemical Physics Letters, 430, 93-96.
82. Holzinger M. , Vostrowsky O., Hirsch A. , Hennrich F. , Kappes M., Weiss R, Jellen F. (2001). Sidewall functionalization of carbon nanotubes. Angewandte Chemie., 40, 4002-4005.
83. Tagmatarchis N., Georgakilas V. , Prato M., Shinohara H. (2002). Chemical Commununications, 2010-2011.
84. Liu P. (2005). Modification of carbon nanotubes with polymers. Euro Polymers Journal. 41, 2693-2703.
85. Yao Z., Braidy N., Botton G. A., Adronov A. (2003). Polymerization from the surface of single-walled carbon nanotubes- preparation and characterization of nanocomposite. Journal American Chemical Society., 125 ,16015-16024.
86. Sano M. , Kamino A. , Okamura J., Shinkai S., Langmuir, (2001). Self organisation of PEO-graff-single-walled carbon nanotubes in solutions and Langmuir-blodgett films. Langmuir, 7, 5125- 5128.
87. Albuerne J., Boschetti-de-Fierro A., Abetz V. (2010). Modification of multi-walled carbon nanotubes by grafting from controlled polymerization of styrene: Effect of characteristics of the nanotubes. Journal of Polymer Science, 48, 1035-1046.
88. Lin Y. , Zhou B. , Fernando K. a. S., Liu P. , Allard L. F., Sun Y. P .(2003). Polymeric carbon nanocomposites from carbon nanotubes functionalized with matrix polymer. Macromolecules, 36 , 7199-7204.
89. Lou X., Detrembleur C. , Sciannamea V., Pagnoulle C., Jérôme R. (2004). Grafting of alkoxyamine end –capped (Co) polymers onto multi-walled carbon nanotubes, Polymer, 45, 6097-6102.
90. Islam M., Rojas E., Bergey D., Johnson A., Yodh A. (2003). High weight fraction surfactant solubilisation of single-walled carbon nanotubes in water. Nano Letters, 3, 269-273.
91. Wenseleers W., Vlasov I. I, Goovaerts E., Obraztsova E. D., Lobach A. S., Bouwen A. (2004). Efficient isolation and solubilisation of pristine single-walled nanotubes in bile salt micelles. Advanced Functional Materials, 14, 1105-1112.

92. Moore V. C.,. Strano M. S.,Haroz E. H, Hauge R. H., Smalley R. E. , Schmidt J., Talmon Y., (2003). individually suspended single-walled carbon nanotubes in various surfactants. NanoLetters, 3, 1379-1382.
93. Fujigaya T., Nakashima N. (2008). Methodology for homogeneous dispersion of single-walled carbon nanotubes by physical modification. Polymer Journal, 40, 577-589.
94. Tomonari Y. , Murakami H., Nakashima N. (2006). Solubilization of single-walled carbon nanotubes using polycyclic aromatic ammonium amphiphiles in water-strategy fir the design of solubilizers with high performance. Chemical European Journal, 12, 4027-4034.
95. Chen R. J., Zhang Y. , Wang D., Dai H. (2001). Noncovalent sidewall functionalization of single-walled carbon nanotubes for protein immobilization. Journal of the American Chemical Society, 123, 3838-3839.
96. Ji, Y. Y., Huang Y., Tajbakhsh A. R., Terentjev E. M. (2009). Polysiloxane surfactants for the dispersion of carbon nanotubes in nonpolar organic solvents.Langmuir, 25 ,12325-12331.
97. Liu J. , Bibari O. , Mailley P., Dijon J. , Rouvière E., Sauter-Starace F., Caillat P., Vinet F., Marchand G. (2009). Stable non-convalent functionalization of multi-walled carbon nanotubes by pyrene-polyethylene glycol through $\pi - \pi$ stacking. New Journal of Chemistry, 33, 1017-1024.
98. Meuer S., Braun L., Zentel R. (2009). Pyrene containing polymers for the non-covalent functionalization of carbon nanotubes. Macromolecular Chemistry and Physics. 210, 1528- 1535.
99. Star A., Stoddart J. F., Steuerman D., Diehl M., Boukai A., Wong E. W., Yang X., Chung S. W., Choi H. (2001). Preparation and properties of polymer-wrapped single-walled carbon nanotubes, Angewandte Chemie, 40, 1721-1725.
100. Giulianini M., Waclawik E. R. , Bell J. M., De Crescenzi M., Castrucci P., Scarselli M., Motta N. (2009). Regioregular poly (3– hexyl-thiophene) helical self organization on carbon nanotubes. Applied Physics Letters, 95, 013304.
101. Zou J., Liu L., Chen H. , Khondaker S. I., Mccullough R. D., Huo Q., Zhai L. (2008). Dispersion of pristine carbon nanotubes using conjugated block copolymers. Advanced materials, 20, 2055-2060.
102. O'connell M. J., Boul P., Ericson L. M., Huffman C., Wang Y., Haroz E., Kuper C., Tour J., Ausman K. D., Smalley R. E. (2001). Reversible water – solubilisation of

single-walled carbon nanotubes by polymer wrapping. Chemical Physics Letters, 342, 265-271.

103. Kang Y., Taton T. A. (2003). Micelle encapsulated carbon nanotubes: A route to nanotube composites. Journal of the American Chemical Society., 125, 5650-5651.

Chapter 3 Experimental procedure and analysis techniques

3.1. Methodology

3.1.1. Chemicals and materials

Polysulfone (PSF), chloroform, N, N-dimethylformamide, tetrahydrofuran, polyvinyl alcohol, maleic acid, ferrocene, acetylene, argon, sulphuric acid, nitric acid and chloric acid were purchased from Sigma Aldrich (Johannesburg, South Africa). All organic solvents were used as received.

3.1.2 Synthesis of carbon nanotubes

Multi-walled carbon nanotubes (MWCNTs) were synthesized using a vertically orientated chemical vapour deposition (CVD) reactor (Figure 3.1). The CNTs were synthesized at 800 ^{o}C to 850^{o}C with ferrocene which acts as both the catalyst and carbon source [1]. An amount of the catalyst, ferrocene was placed inside the vaporizer and the apparatus was connected as shown in Figure 3.1. Nitrogen was passed through the system to flush out contaminants and ensure there were no leakages. Argon and acetylene which act as carrier gases, was then passed through the system, and the ferrocene (which acts as carbon source) was vaporized and carried to the reactor where the MWCNTs were synthetised. The solid carbon product was collected from the cyclone and characterized using a scanning electron microscope (SEM) and a transmission electron microscope (TEM).

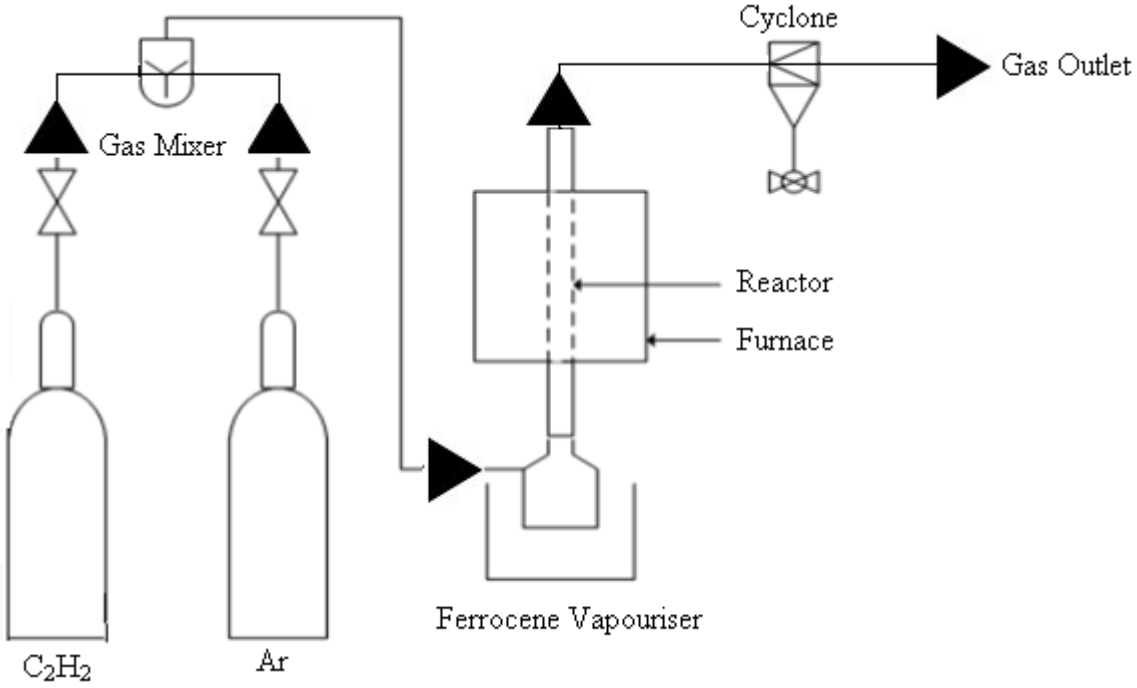

Figure 3.1: Schematic of the chemical vapour deposition reactor [1]

3.1.3 Functionalization of MWCNTs

The MWCNTs were functionalized by adding to a solution of 35% HNO_3 as shown in Figure 3.2, and stirred under reflux for 4 h at 110 °C. The solution was then filtered and the MWCNTs were washed with distilled water until the pH was neutral. MWCNTs were then reduced in an oven at 120 °C for 12 h. The degree of functionalization was studied using Raman spectroscopy. This was important since the degree of functionalization relates to the hydrophilicity of the CNTs, which could have an impact on the hydrophilicity of the polymeric membranes.

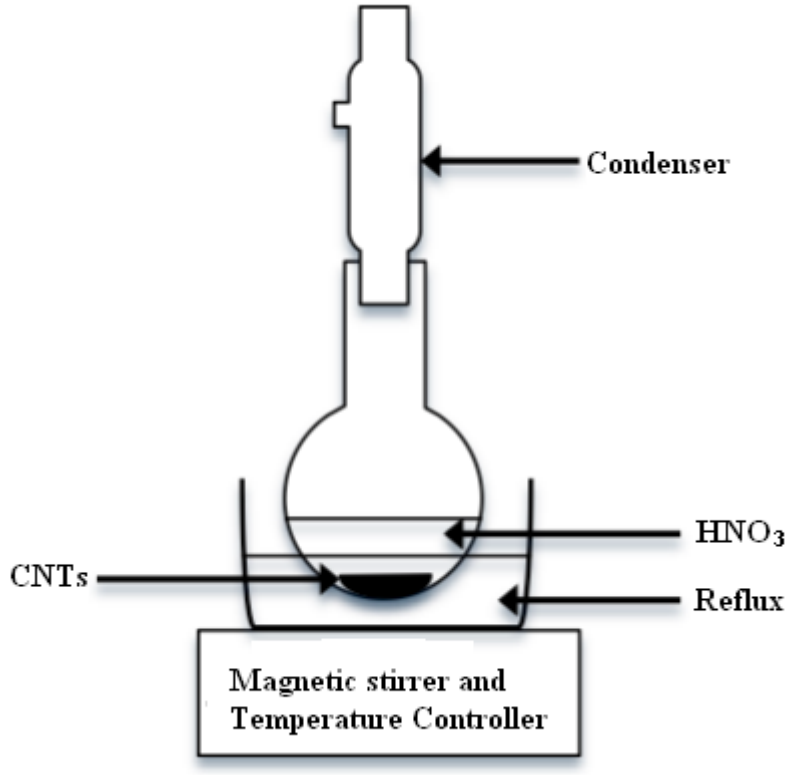

Figure 3.2: Set up for functionalization at CNTs.

3.1.4 Production of the polymeric membrane

Membrane was prepared by using the immersion precipitation phase inversion method [2]. The PSF was dissolved in three different solvents: N-N' dimethylformamide (DMF), chloroform ($CHCl_3$) and tetrahydrofuran (THF) under constant stirring for 24 h. An ultra-sonicator, set to a frequency of 60 % was used to sonicate the solution for 10 min. A casting blade was used to cast the solution onto a glass substrate and left in ambient conditions for 20 to 30 seconds before being immersed in a bath of water. The membrane was then left to air-

dry for another 24 hours. 0.2 wt% (w/v) of Maleic acid (MA) which acts as a cross linker solution was also poured over the membrane. Finally, the membrane was placed in an oven at 125 °C for 30 min.

3.1.5 Production of the functionalized MWCNTs / PES membranes

The MWCNTs/PES blend membranes were produced using the immersion phase inversion method for production of the polymeric membrane. The functionalized CNTs were blended with the polymer solution in varying concentrations: 0, 0.1, 0.2, 0.3, 0.4, 0.5 and 0.6 wt% (during stirring stage).

3.1.6 Pre-treatment of oil water emulsion

The oil wastewater emulsion used in this work was a metal working fluid (MWF) used to cool work - pieces on a lathe provided by Oil Skip of South Africa. Metalworking fluids differ widely in character but it normally consists of water, oil, emulsifier, anti-microbial additives and solid particles. The bulk of the oil used is typically mineral oil. However organic oil may also be present in small quantities since some of its components could assist in emulsification. Therefore, a pre-treatment of the MWF proves necessary before starting the membrane filtration process.

Emulsions stabilized by solid particles have been known for more than a century and were named after S. Pickering, who discovered that coalescence of droplets is suppressed when solid particles are adsorbed at the oil-water interface [3]. It is widely accepted that this suppression in coalescence is a kinetic effect caused by a combination of the formation of a rigid interfacial film and the increase in viscosity of the continuous phase.

Pre-treatment tests were carried out by dispersing raw MWCNTs in oily waste-water. A constant amount of the oil-water mixture (15 ml) containing solid particles was added in six different sample tubes. Different concentrations of raw MWCNTs: 0.0, 0.2, 0.3, 0.4 and 0.5 g were added to each tube. The sample tubes were then left for 21 days. The result of coagulation and flocculation of oil wastewater emulsion using raw MWCNTS was identified by comparing the tubes using natural observation and NMR spectroscopy.

Figure 3.3 shows the oil-water emulsion mixed with raw MWCNTs using an ultrasonicator for 15 min. During this step, a homogeneous emulsion is formed, which remains between the water (bottom) and the organic (top) phases. The interface between the two phases can be

clearly distinguished given that essentially all of the MWCNTs remain suspended in the emulsion fraction.

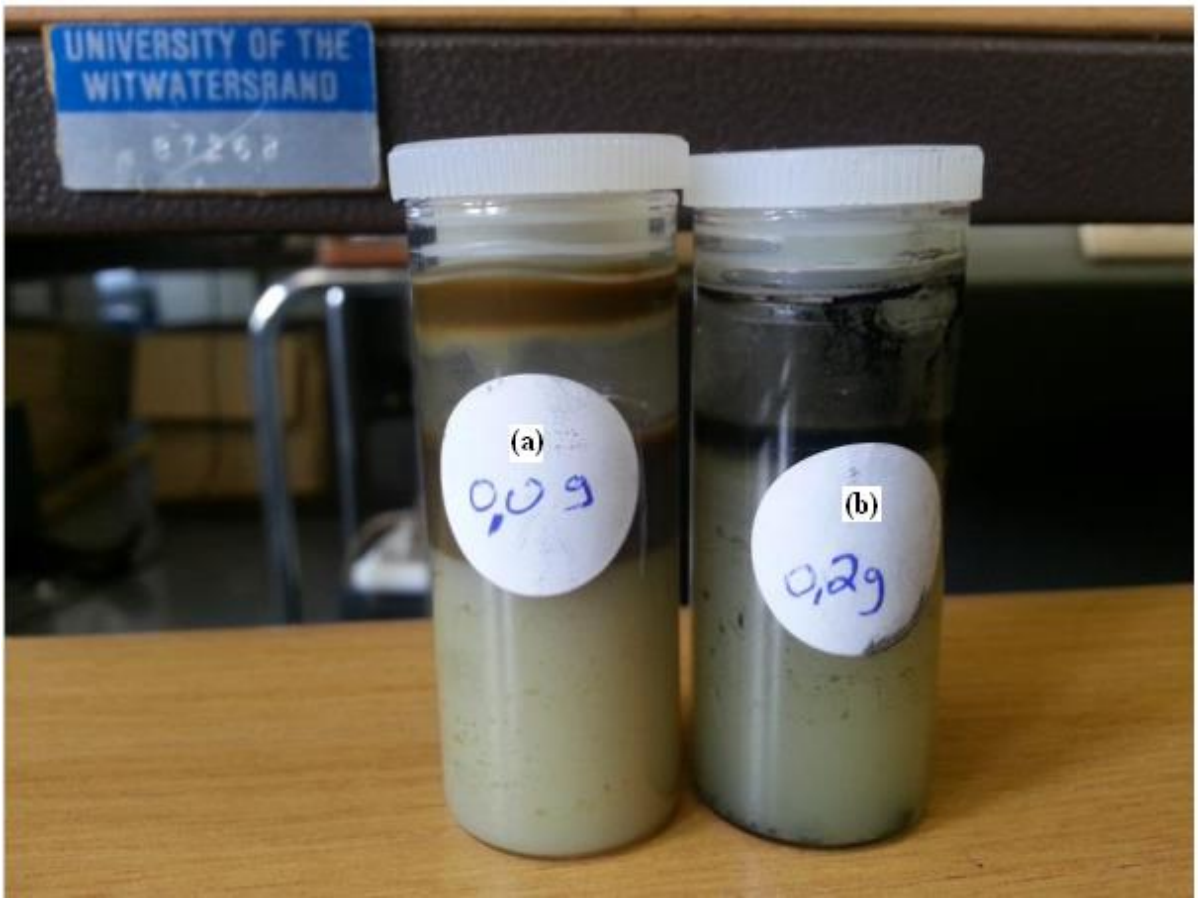

Figure 3.3: Illustration of (a) the initial solution of oily wastewater and (b) oily wastewater emulsion containing 0.2 grams of raw MWCNTs for pre-treatment by flocculation.

3.1.7 Filtration tests

The cross-flow model shown in Figure 3.4 was used for the filtration tests. A 45 cm^2 membrane was used at room temperature. The membranes were first compacted by flushing water through the system. The oil-water emulsions were then passed through the pump at different pressures (2, 2.5, 3, 3.5, 4, 4.5 and 5 bar) and the time required to measure the collected permeate was recorded. The flux through the membrane (F) was then calculated using equation 3.1:

$$F = \frac{V}{A \times t} \quad (3.1)$$

Where:

V= volume of the permeate collected in litres (l),
A= active surface area of the membrane in m^2 and
t= time required to obtain the required volume across the membrane (h).

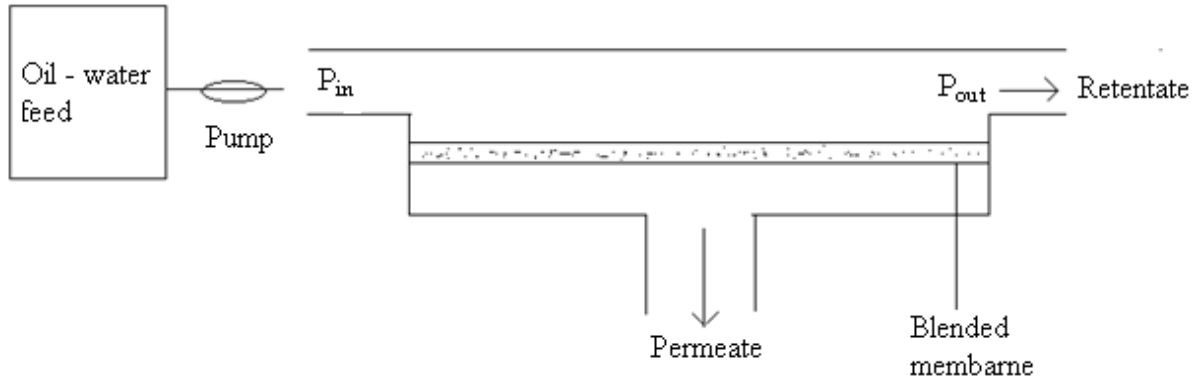

Figure3.4: Schematic of the filtration module design

3.2 Characterization

3.2.1 Scanning electron microscopy (SEM)

A Sigma series FE-SEM in-lens Sigma was used to characterize both the MWCNTs and the PES membrane. The SEM, operating at accelerating velocities of 15kV and 17kV, provided the morphology of the MWCNTs and the membranes, respectively. The polymeric membranes were placed on a carbon tape, stuck to an aluminium stud and coated with gold and palladium to provide a reflective surface for the SEM imaging.

3.2.2 Transmission electron microscope (TEM)

A FEI Tecnai T12 TEM was used to observe the internal structure of the samples. The microscope had accelerating voltage from 80 to 200 kV and standard magnification from 1000 to 800000. Images were acquired using a peltier-cooled CCD camera KeenView. The CCD chip in this camera provides maximum resolution of 1376 x 1032 pixels with a 12 bit dynamic range (4096 gray values)..

3.2.3 Raman spectroscopy

The Raman spectra of raw and functionalized MWCNTs were measured using a Raman microscope (λ = 785 nm, 10 mW) at room temperature.

3.2.4 Contact angle

The wettability and surface hydrophilicity of the PES membrane and MWCNTs were evaluated by the DATA Physics optical contact angle using the sessile drop measurement method. A 2 μl drop of deionised (DI) water was placed on a flat membrane surface using a Gilmont syringe. Using the SCA20 version 4.1.12 build 1019 software, the advancing angle (θ) was measured as the water droplet was placed on the surface. In general, the larger the angle, the lower the hydrophilicity and vice versa. Figure 3.5 illustrates the apparatus used for the contact angle tests

Figure 3.5: SCA20 version 4.1.12 build 1019 software used for contact angle measurements

3.2.5 Porosity measurement

The porosity measurements of membranes were carried out by the dry-wet method using the expression given in equation (3.2):

$$Porosity = \frac{W_2 - W_1}{V.d_{butanol}} \times 100\% \qquad (3.2)$$

where '*w*1' (g) is the weight of dry membrane, '*w*2' (g) is the weight of membrane after dipping into 1-butanol for 2 hours, '*v*' (cm^3) is the volume of the membrane and $d_{butanol}$ (g/cm^3) is the density of 1-butanol at room temperature.

3.2.6 Mechanical characterization

Polymeric nanocomposite membranes were prepared by the phase inversion process without using non-woven polyester to carry out mechanical characterization. A TA.XT Plus Texture Analyzer was used to carry out the analysis. Strips of the membrane (with 5 cm effective length and 1 cm width) were measured to determine the rigidity gradient, strain energy and percentage resilience. Figure 3.6 illustrates the apparatus used for the mechanical tests of membranes.

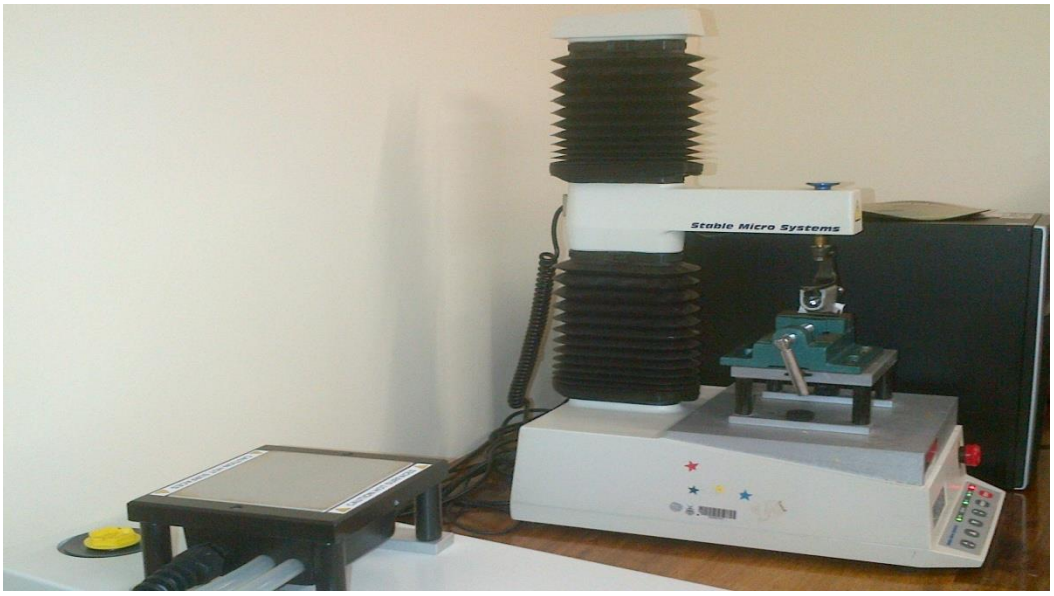

Figure: 3.6 TA.XT Plus Texture Analyzer used for mechanical tests

3.2.7 Analysis of oil water samples with nuclear magnetic resonance (NMR)

An Ultra Shield 500 was used to perform this experiment; (NMR) spectra of organic compounds were recorded on Bruker AV-300 (Bruker Biospin GmbH, Karlsruhe, Germany) at 300 MHz. The samples were dissolved in CDCl3 containing tetramethylsilane (TMS). Figure 3.7 illustrates the apparatus used for the H NMR analysis of the oil water samples.

Figure: 3.7 Ultra Shield 500 used for H NMR analysis

3.2.8 Water flux measurement

Water flux measurements were performed using a cross flow cell where the membranes (with an effective area of 45 cm^2) were analysed at room temperature. The schematic diagram of the cross flow module is shown in Figure 3.8. The water flux was calculated by equation (3.1). The feed flow rate was kept constant and the flux was calculated at different trans-membrane pressures i.e. 2, 2.5, 3, 3.5, 4, 4.5, 5 bar in order to study the membrane compaction behaviour. For the flux measurements, the trans-membrane pressure was maintained at 2 bar for 45 minutes and then water flux was measured. Figure 3.8 illustrates the filtration module used for the membrane filtration tests.

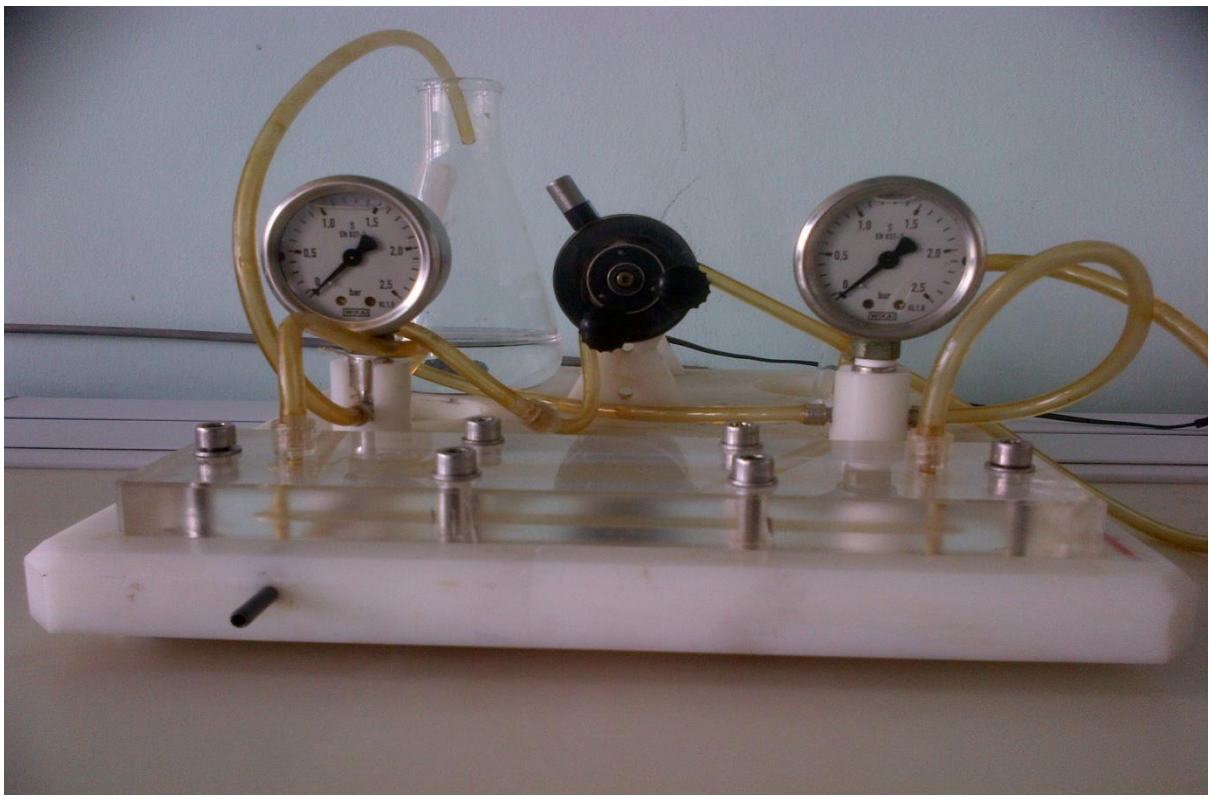

Figure 3.8 Cross flow filtration module used in this work.

3.3 References

1. Iyuke, S.E., Mamvura T.A., Liu K., Sibanda V., Meyyappan M., Varadan V.k. (2009). Process synthesis and optimization for the production of carbon nanostructures. Nanotechnology 20, 375602.

2. Kesting R.E., Lloyd D.R. (1985). Phase inversion membranes. Materials Science of Synthetic Membranes American Chemical Society, Washington, DC ACS Symp. Ser. No. 269.

3. Min S., Daniel E. R. (2009). Emulsions stabilized by carbon nanotubes – silica nanohybrids.American chemical Society. Langnuir 25(18), 10843-10851.

Chapter 4 Results and Discussion

This chapter presents the results obtained in this research study. It includes the characterization of MWCNTs and MWCNT/PES blend membranes using the methods and techniques discussed in Chapter 3. The performance of the membranes using oil–water emulsion for permeation studies, and the effect of functionalized MWCNTs and solvent on the PES membrane is discussed in detail. In addition, results relating to the NMR spectroscopy characterization of the permeate (flux) of the oil –water filtration are discussed.

4.1 MWCNTs characterization

4.1.1 Scanning electron microscope of MWCNTs

A scanning electron microscope with high resolution is a powerful instrument for imaging of fine structures of materials and nanoparticles fabricated by the nanotechnology. For MWCNT observation and morphological analysis the field emission scanning Electron microscope Sigma series FE-SEM in–lens was used at a 15kV and 17kV accelerating voltage. This method gives information mainly about the surface morphology of the sample (Figure 4.1 a, b, c).

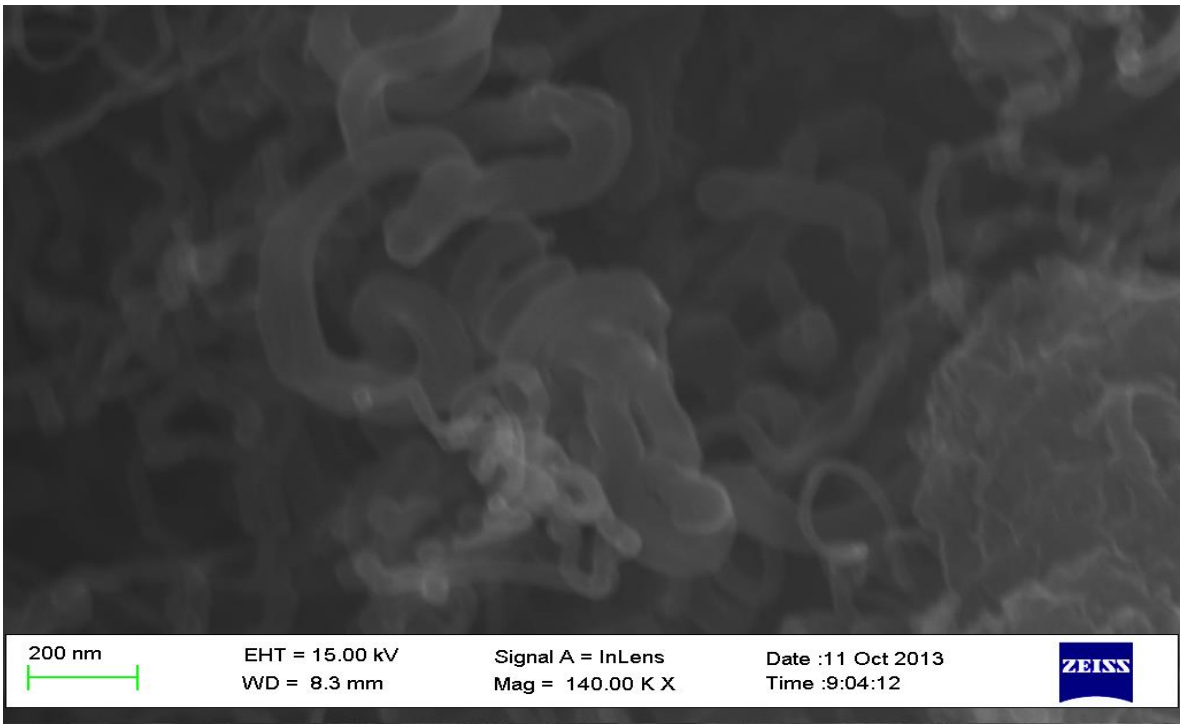

(a)

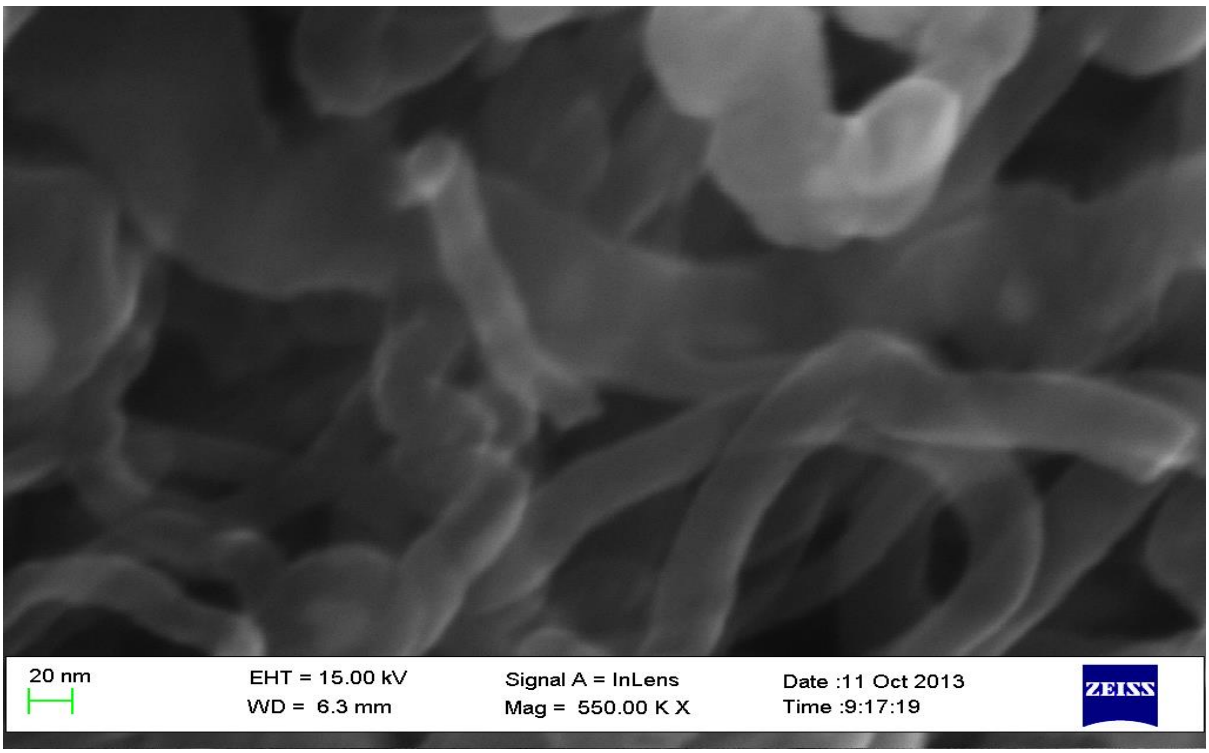

(b)

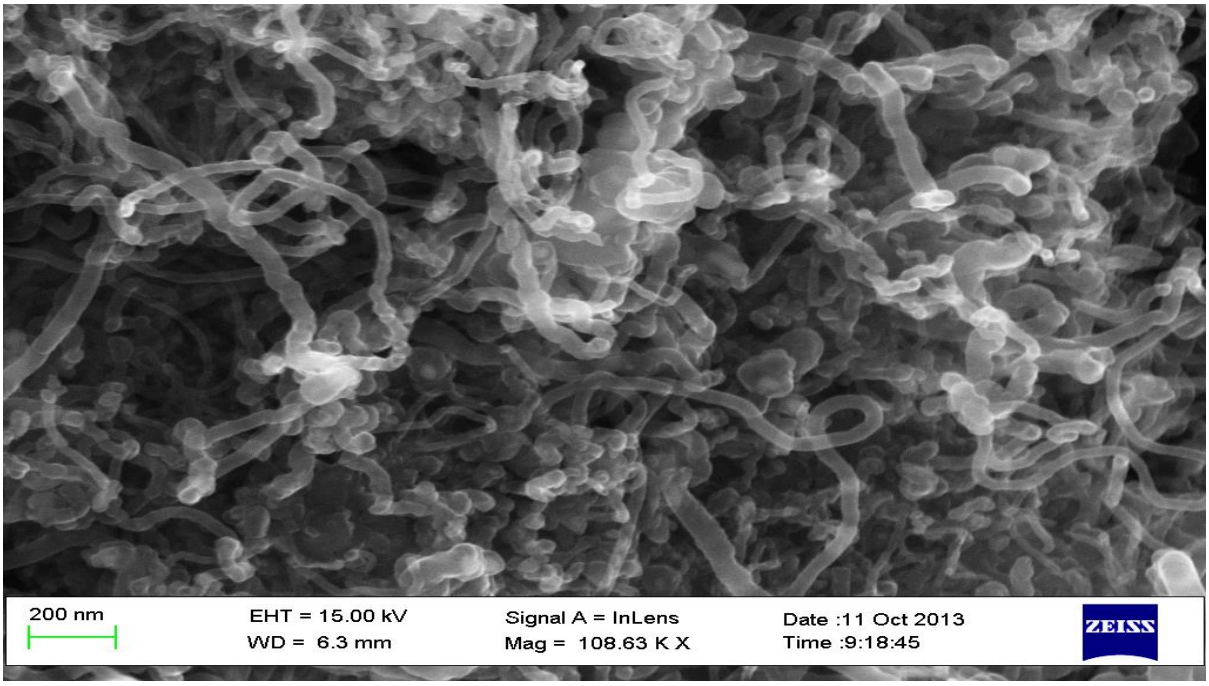

(c)

Figure 4.1: SEM images of (a, b) raw MWCNTs and (c) functionalized MWCNTs

The SEM images from Figure 4.1 show MWCNTs of diameters less than 100 nm. From the scale of the images, the calculation of the outer diameter of the MWCNT is determined to be approximately 50 nm, which falls within the literature ranges for MWCNTS of between 2.4 nm and 100nm. The morphology of CNTs is very similar to that of carbon nano-fibres (CNFs). The difference however between the two is the lack of a hollow tube in carbon nano-fibres. Figure 4.1 (c) confirms that MWCNTs were functionalized because the tubes appear to be hollow. A closer inspection of the image reveals one tube with a blocked end, a characteristic of MWCNTs and not CNFs[35].A Raman spectroscope was used to characterize the functionalized MWCNTs.

SEM gives valuable information on the morphology of MWCNTs, it is not sufficient to establish the ultimate nature of the CNTs. It is easy to confuse only on the basis of SEM observations carbon nanotubes from nanofibres. Thus, one proceeds to TEM analysis of the samples to have deeper information on obtained MWCNTs.

4.1.2 Transmission electronic microscope observation of MWCNTs

Transmission electron microscope FEI Tecnai T12 was used to observe the internal structure of the sample. The microscope had accelerating voltage from 80 to 200 kV. Images were acquired using the peltier-cooled CCD camera KeenView. The CCD chip in this camera provides maximum resolution of 1376x1032 pixels with a 12bit dynamic range (4096 gray values). The KeenView supports frame rates of more than 20 images per second at 2x binning and of 10 images per second at full resolution. This high frame rate is ideal for locating suitable sample segments directly on screen. Accelerating voltage 120 kV and magnification 100000-400000 times were used in this work.

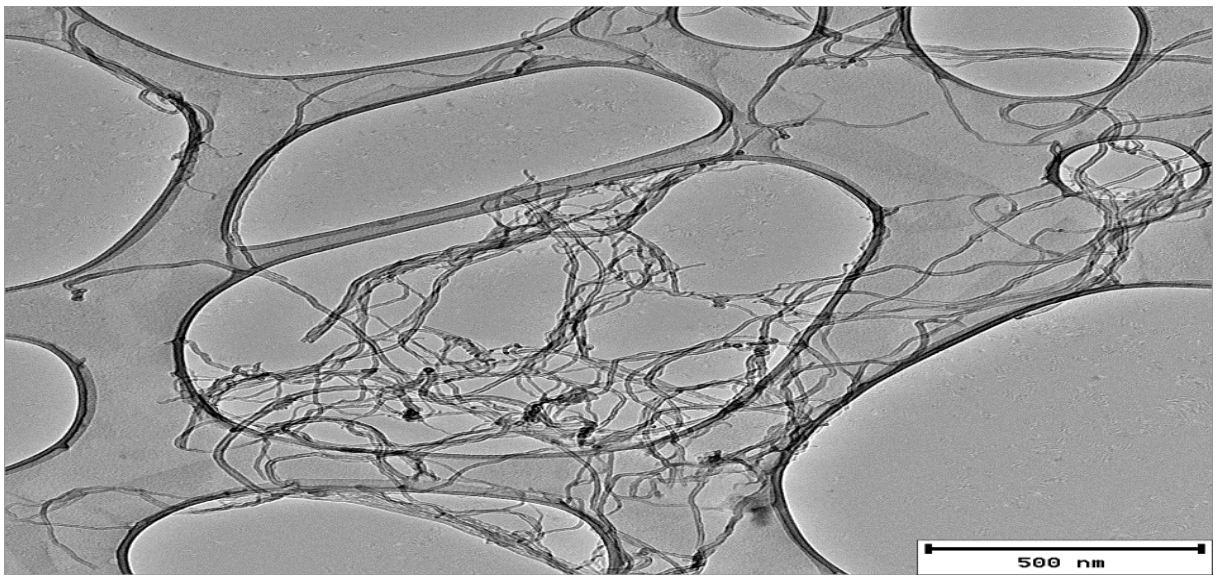

(a)

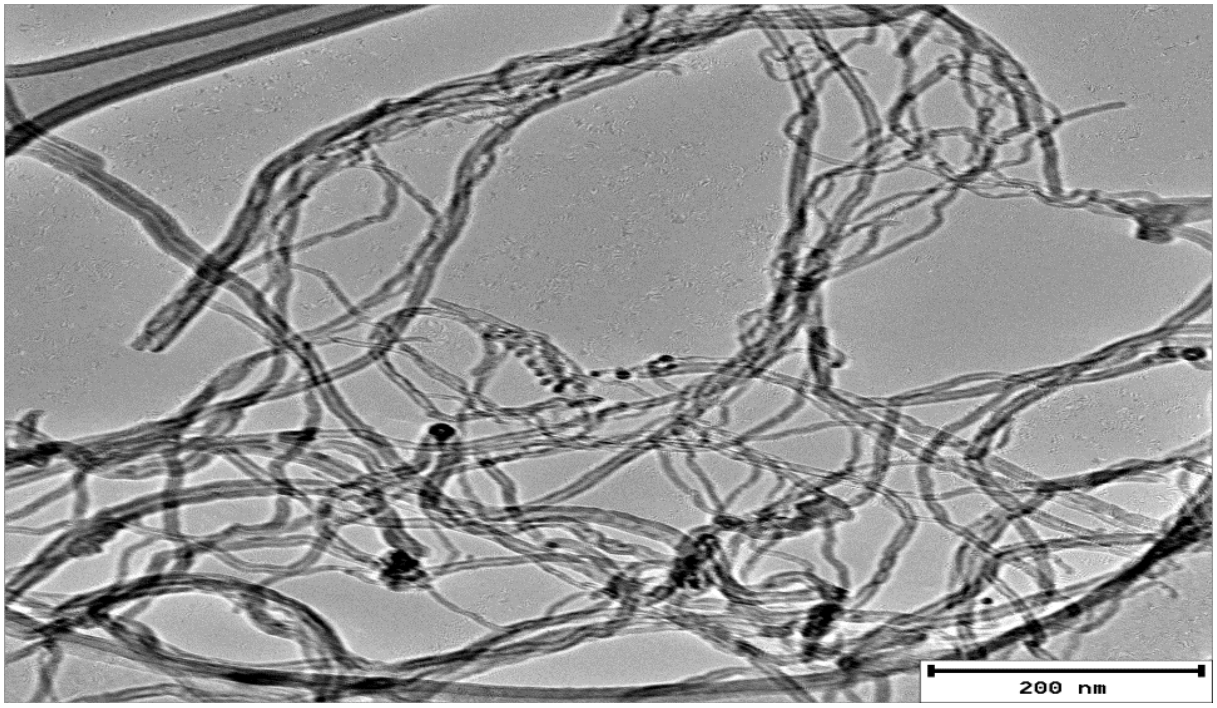

(b)

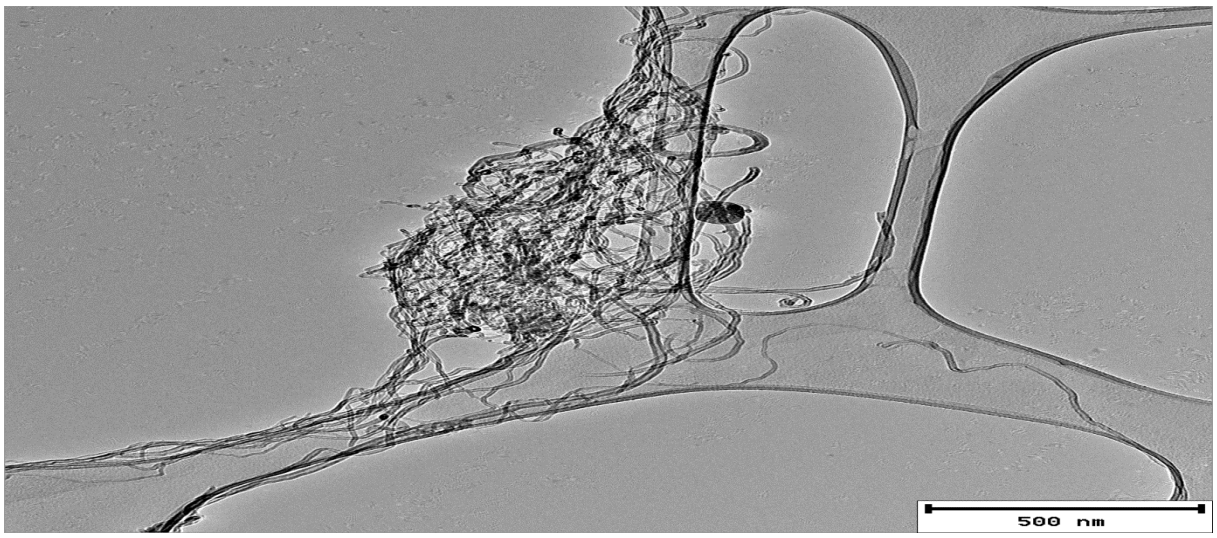

(c)

Figure 4.2 (a, b, c): Three different views of the TEM image of the raw MWCNTs

TEM was used due to its ability to measure nanotube diameter in the bundle. From the TEM images (Figure 4.2) it is possible to determine directly the diameter of one nanotube and bundle diameter. Due to this information, the number of nanotubes in the bundle can be found. Mostly, nanotubes in the sample are not in bundle, so they are alone (Figure.4.2 c).

TEM micrographs clearly illustrate that nanotubes obtained display widely different morphologies according to some variable parameters. It is possible to control the morphology. Within the medium value of the plasma power, as shown with SEM study, carbon nanotubes are already grown. These samples however display different mutual orientations. The highly oriented films are obtained under optimized conditions and poorly and medium oriented films are also obtained, showing more defects.

Although the high resolution of the transmission electron microscope can be used to observe even atomic resolution, the TEM images could not provide the opportunity to determine the exact number of walls of each sample of MWCNTs (Fig. 4.2: a, b, c) This deficiency may be the result of defects. In this way, mutually aligned tubes of different densities are obtained, depending on the nature the reactive gas mixture. TEM images of MWCNTs show that the mean diameter is around 25 nm. From the TEM image it could be observed that MWCNTs are very thin. The TEM images of MWCNTs and CNFs are clearly distinct; however it is quite difficult to know the exact number of walls.

4.1.3 Raman spectroscopy of functionalized and unfunctionalized MWCNTs

Prior to functionalization, it is important to achieve a well dispersed mixture of MWCNTs in the solvents (DMF, CHCl3 and THF) during the phase inversin method. Fig. 4.3 shows the Raman spectroscopy of the functionalized and unfunctionalized MWCNTs. The deviation in the graph confirms an intensification of the defects in the wall matrix of the functionalized MWCNTs. The fact that the graphs have the same shape shows that the functionalization process does not change the material made.

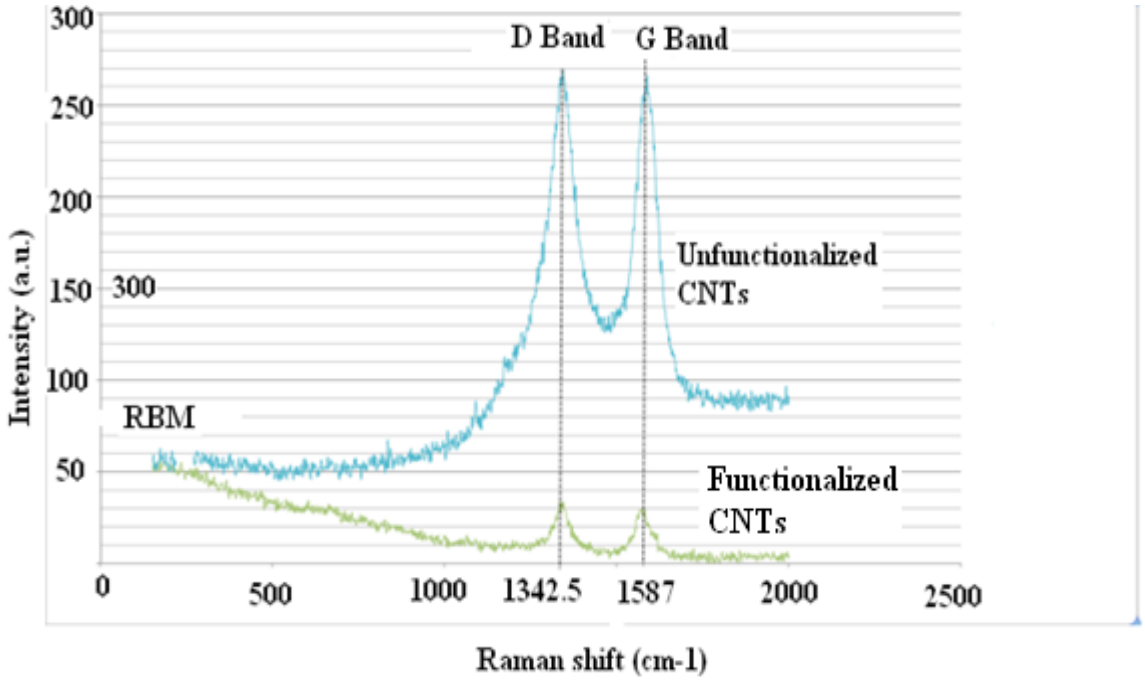

Figure 4.3: Raman spectroscopy for functionalized and unfunctionalized MWCNTs

The D and G band from Figure 4.3 are 1342.5 cm^{-1} and 1587 cm^{-1} respectively. This is a 0.94% and 0.44% deviation from the literature values of 1330 cm^{-1} and 1580 cm^{-1}. These values confirm that graphene sheets were formed and that defects were introduced into the walls of the MWCNTs. Raman spectroscopy is very sensitive and this slightly affects the quality of results obtained. The graph for the unfunctionalized MWCNTs shows how the effect of noise intensified the vibrational frequencies. Figure 4.3 shows an RBM for the lower frequencies of the functionalized MWCNTs but no evident RBM for the unfunctionalized MWCNTs. The lack of RBM for the unfunctionalized indicates that the average diameter of the MWCNTs is greater than 3nm, which agrees with the diameter of 66nm calculated above.

The ratio at I_D/I_G is the intensity of the D band to the G band and indicates the degree to which defects have been introduced into the MWCNTs wall matrix. The values are summarized in Table 4.1, which shows that $I_{D/G}$ increased by 9.98%, confirming the presence of defects in the wall matrix of the MWCNTs. Therefore, it can be concluded that the MWCNTs were successfully functionalized.

Table 1: Intensity ratio for functionalized and unfunctionalized MWCNTs

	Unfunctionalized CNTs		Functionalized CNTs	
	D Band	G Band	D Band	G Band
Raman Shift cm^{-1}	1342.5	1587	1340.50	1572.50
Intensity (a.u.)	268.752	265.692	33.670	30.258
$I_{D/G}$	1.012		1.113	

4.2 Membrane characterization

The membrane surface morphologies were further studied using SEM. An image of the top surface and the cross sectional view of the membrane was taken as shown in Fig.4.4 (a). The top view of the membrane is a plane image as expected for an anisotropic membrane. The PVA layer over the membrane covers the porous layer from view using the SEM. A closer inspection of Figure 4.4 (b) however, shows small pores running across the membrane at a scale of 12 microns.

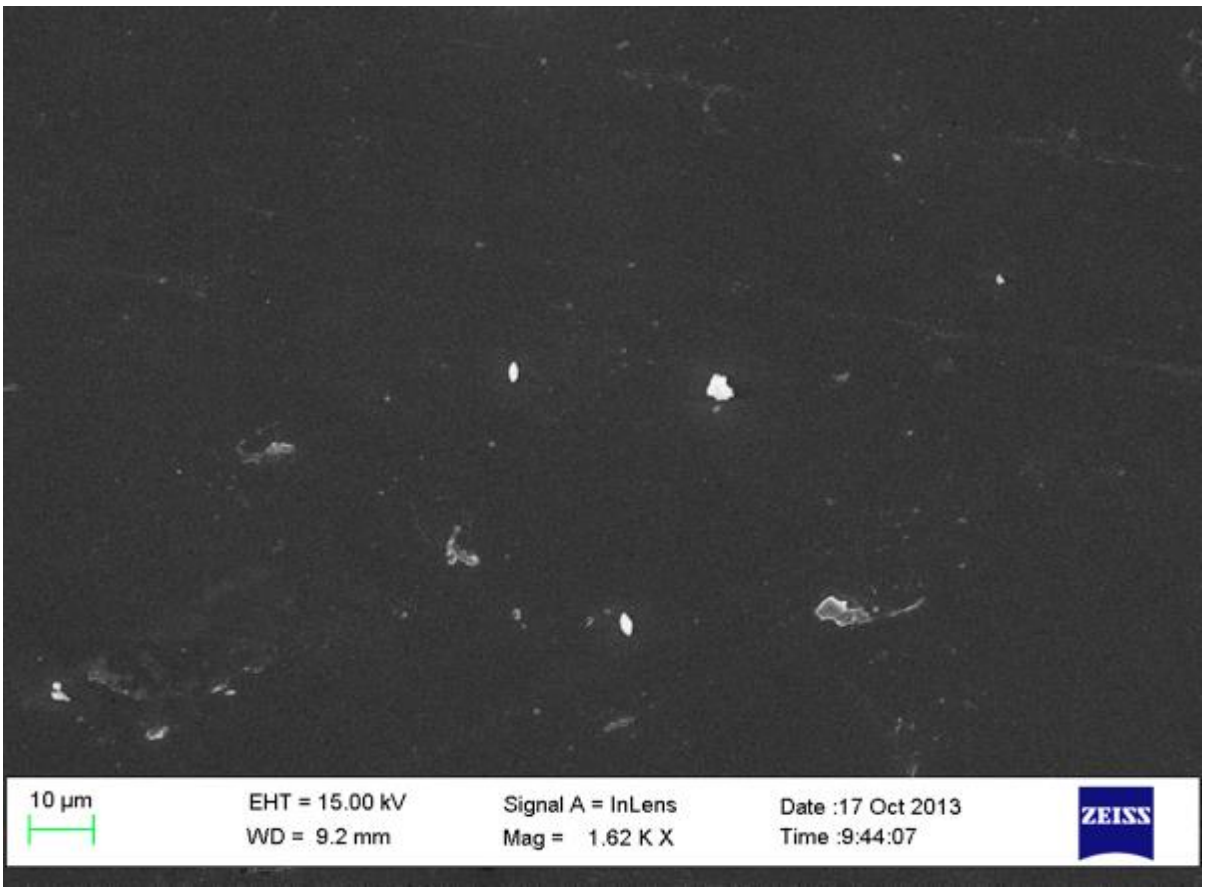

(a) Top surface view of the CNTs/PSF membrane produced with DMF

.

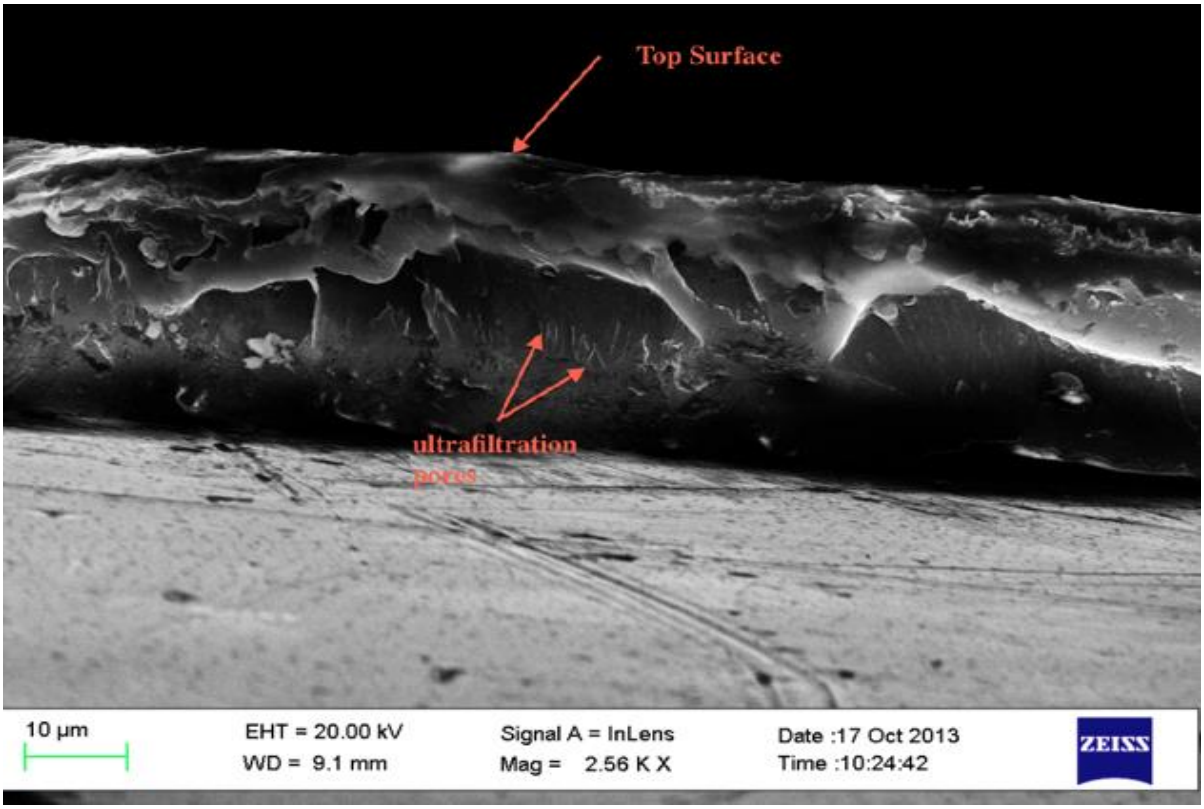

(b) Cross section view of the CNTs/PSF membrane produced with DMF

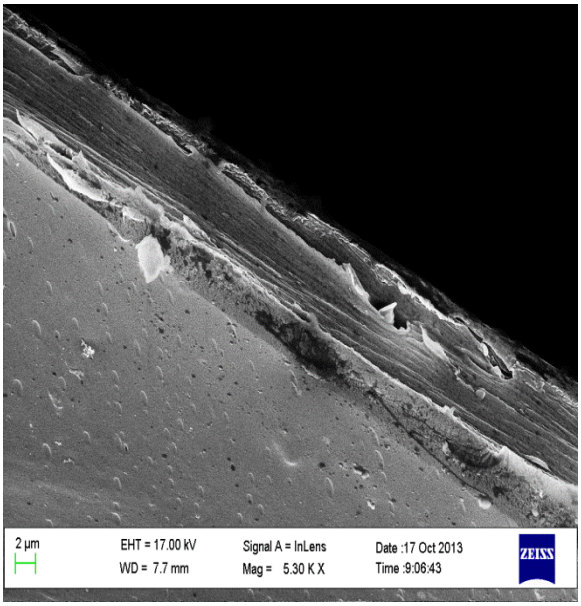

(c) Cross section view of the CNTs/PSF membrane produced with $CHCl_3$

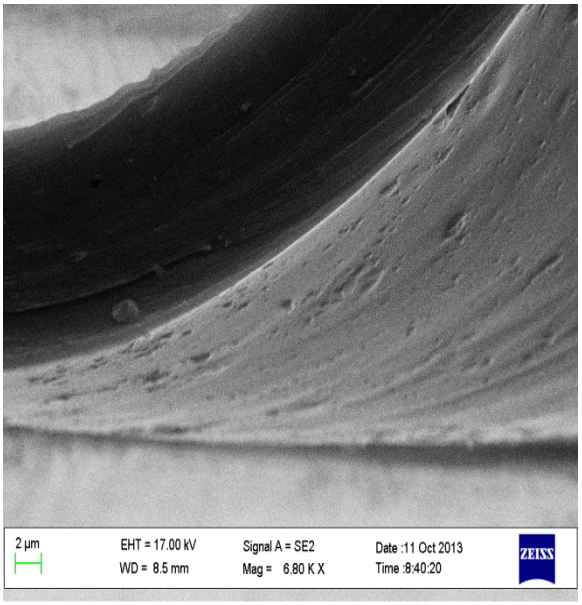

(d) Cross section view of the CNTs/PSF membrane produced with THF

Figure 4.4: SEM images of (a, b), the top surface and cross-sections of the membranes produced with DMF as solvent, and (c, d) the cross-sections of the membranes produced with $CHCl_3$ and THF as solvent, respectively.

Functionalized (and characterized) MWCNTs were blended in to the PSF membrane in varying concentrations from 0.1 to 0.6 wt%. Figure 4.5 (a, b, c,) show the membranes produced with three different solvents at a constant MWCNTs loading of 0.4 wt%. It was observed that the addition of MWCNTs influenced the physical, chemical and mechanical properties of the membrane. From Figure 4.4 the change in the physical appearance of the membrane is evident. A pure polymeric membrane (0 wt. % of MWCNTs) darkens with the addition of MWCNTs.

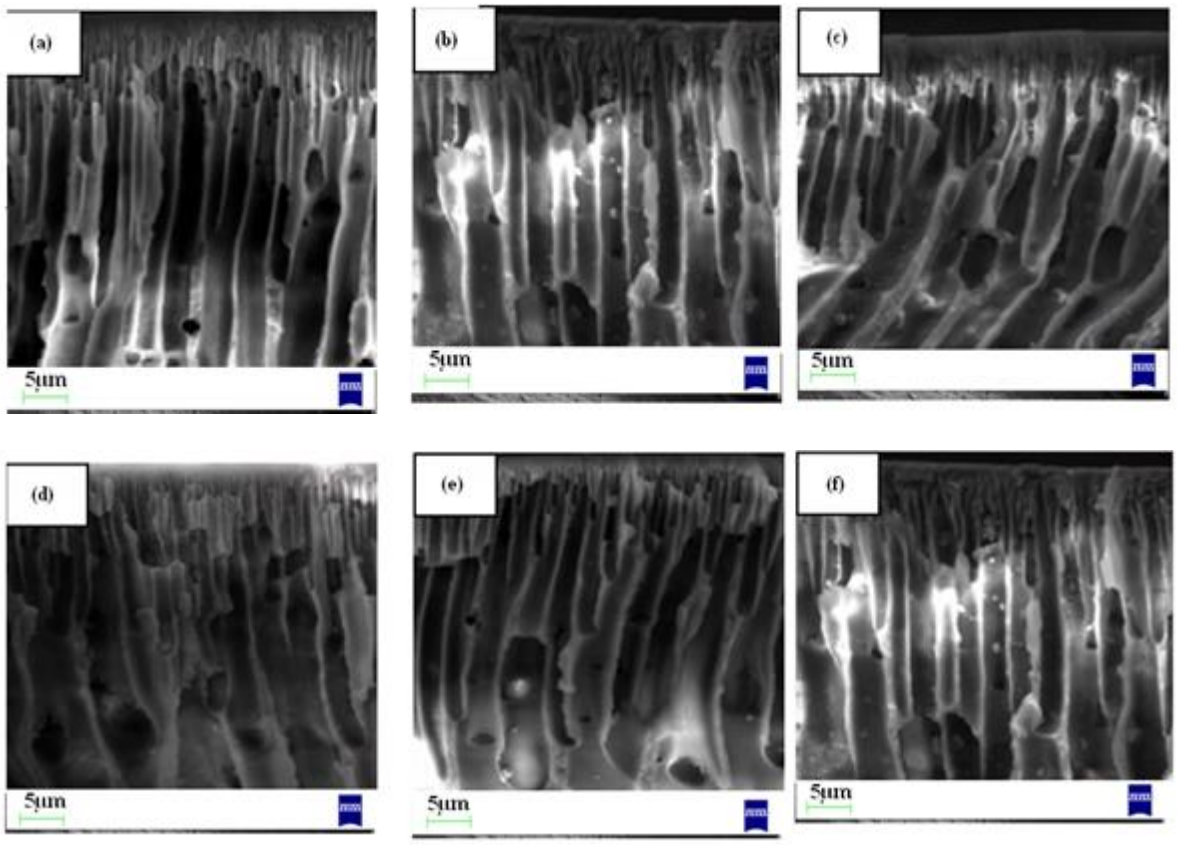

Figure 4.5: SEM images of the (a, b, c, d, e, f) cross-sections of MWCNTs/PSF membrane produced with different concentration of MWCNTs (0.1, 0.2, 0.3, 0.4, 0.5, 0.6 wt %)

To investigate the influence of weight fraction of MWCNTs on the PSF membrane performance, the MWNTs/PSF membranes containing 0.1 wt% MWCNTs to 0.6 wt% MWCNTs were prepared using three different solvents (DMF, $CHCl_3$ and THF). The SEM images of the cross-sections of MWCNTs/PSF membranes with different amounts of MWCNTs are shown in Figure 4.5. It has been found that there is not a pronounced difference in the structures of the cross-sections of the different MWCNTs/ membranes. All the cross-section images have finger-like structures with various pore sizes. Furthermore, as the amount of MWCNTs increases, the surface of the MWCNTs/PSF membrane becomes rougher and the pores of the cross-section become larger. The MWCNTs/PSF membrane with 0.4 wt% MWCNTs has the roughest surface and the largest pore size. For membranes containing more than 0.4 wt% MWCNTs, the surfaces become smoother and the pore sizes of the cross-section are smaller. This is due to agglomeration of MWCNTs inside the matrix of the polymeric membrane.

Figure 4.6: (a, b, c) blended membranes produced with different solvents (THF, DMF and $CHCl_3$ respectively) with a constant MWCNT loading of 0.4 wt%

(a) 0 wt % CNTs DMF membrane

(b) MWCNTs blended DMF membrane

Figure 4.7: (a, b) membranes produced with DMF as solvent containing 0 wt% and 2 wt% MWCNTs.

4.2.1 Hydrophilicity test of the membranes

A Sessile drop experiment was performed using a Goniometer to determine the water contact angles on the membrane surface. Figures 4.8 - 4.10 show that all the polymeric membranes have a contact angle of less than 90^{o}, confirming that they are hydrophilic [1]. It shows an initial decrease in the contact angle from 75^{o} for the pure polymeric membrane to 45^{o} for the 0.4 wt. % DMF membrane. This indicates an increase in the hydrophilicity of the membrane with increasing the concentration of functionalized MWCNTs; however a decrease it observed in hydrophilicity of the membrane was observed for the MWCNTs concentration more than 0.4 wt. % due to the agglomeration of CNTs inside the PSF membrane matrix. A decrease in contact angle from 81^{o} to 49^{o} was observed for the $CHCl_3$ membrane and from 83 ^{o} to 52^{o} for the THF membrane (figures 4.9 and 4.10). This indicates an increase in hydrophilicity of the membranes with increasing concentration of MWCNTs. Contaminants on the surface of the membrane significantly increase the measured contact angles [2]. The 0.4wt. % MWCNTs membranes show the best contact angles for each type of membranes produced. The membranes produced with DMF as solvent give the best hydrophilicity results. Figures.4.8- 4.10 show the results as expected, i.e. an increase in hydrophilicity with the addition of CNTs. The DMF membrane is however more hydrophilic than the $CHCl_3$ and THF membranes. These results suggest that the addition of *f*MWCNTs to the membrane did modify its hydrophilicity.

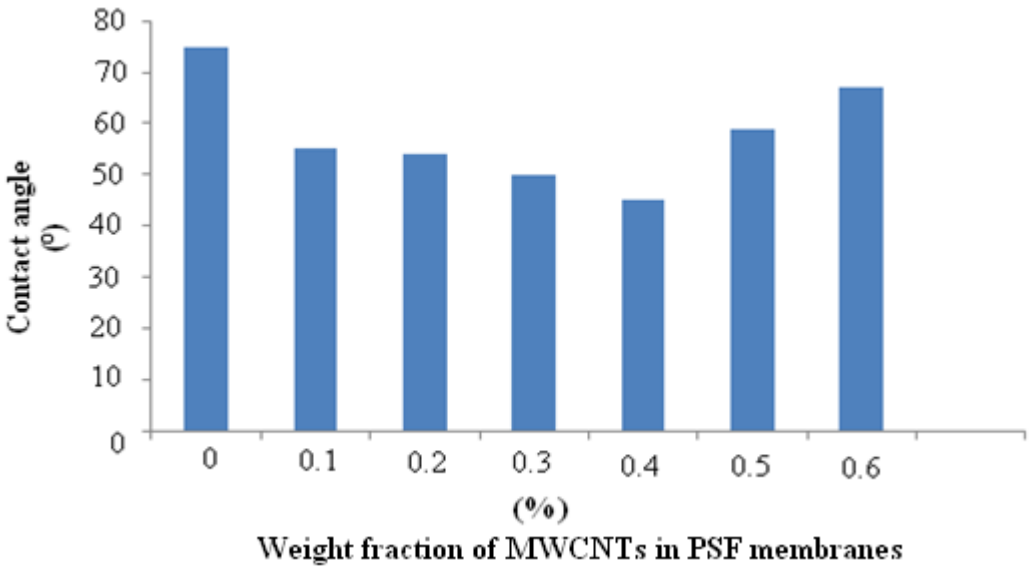

Figure.4.8: Contact angle of the *f*MWCNTs/PSF membranes produced with DMF as solvent and different MWCNTs concentrations.

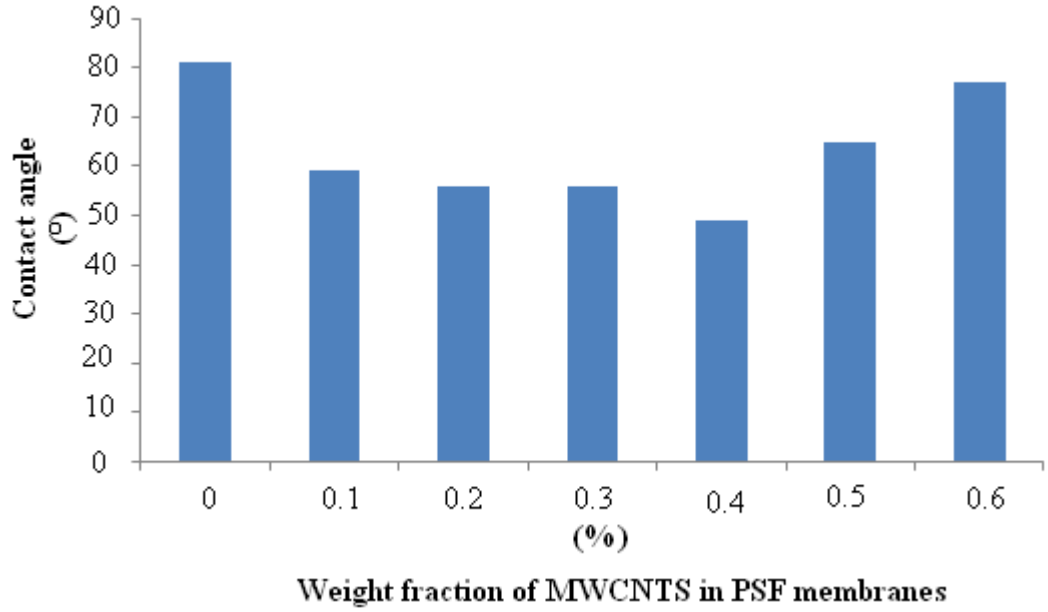

Figure 4.9: Contact angle of the *f*MWCNTs/PSF membranes produced with $CHCl_3$ as solvent and different MWCNTs concentrations

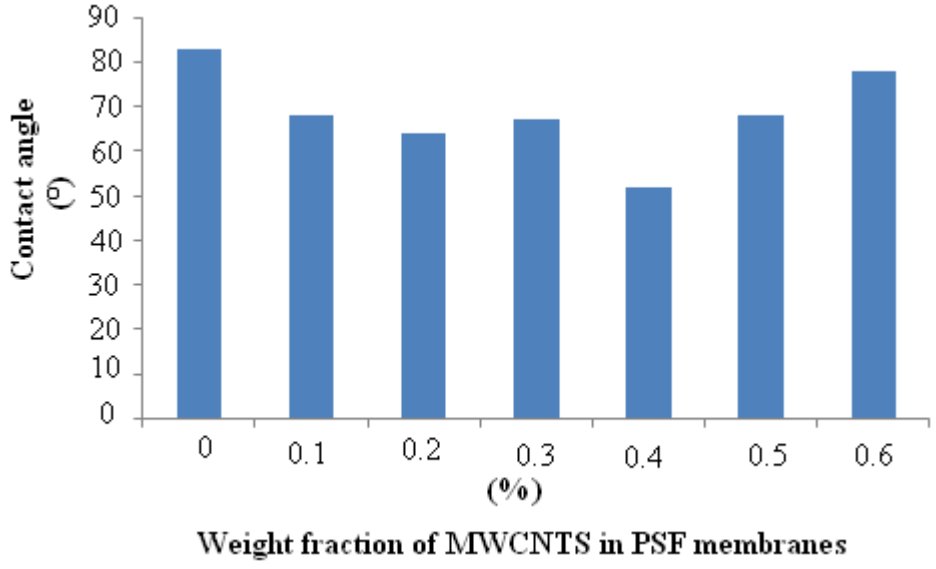

Figure 4.10: Contact angle of the *f*MWCNTs/PSF membranes produced with THF as solvent and different MWCNTs concentrations

4.2.2 Mechanical test results

The rigidity gradient, strain energy and percentage resilience is measured using the TAXT plus Texture Analyzer and is presented in Figures. 4.11 to 4.13. The mechanical property shown in Figures 4.11, 4.12, and 4.13 strongly supports the suggestion of the improvement of resilience, rigidity gradient and tensile strength with addition of MWCNTs in the PSF membrane matrix. The hardness of the DMF, $CHCl_3$ and THF blended membranes increases with increasing MWCNTs composition up to 0.1 wt%. However, Figures 4.11 and 4.12 show flattening behaviour for the $CHCl_3$ and THF blended membranes from 0.4 to 0.6 and from 0 to 0.2 wt% MWCNTs respectively (due to the agglomeration of MWCNTs). The strength of the MWCNTs/PSF membrane increases with increasing volume fraction of MWCNTs, which is comparable to the results of variation of resilience and rigidity gradient with MWCNTs composition. It is concluded that the homogeneous distribution of MWCNTs within the PSF membrane matrix and the formation of strong interfaces between CNTs and PSF enhances the strength, rigidity gradient and resilience of MWCNT/PSF nanocomposites [2].

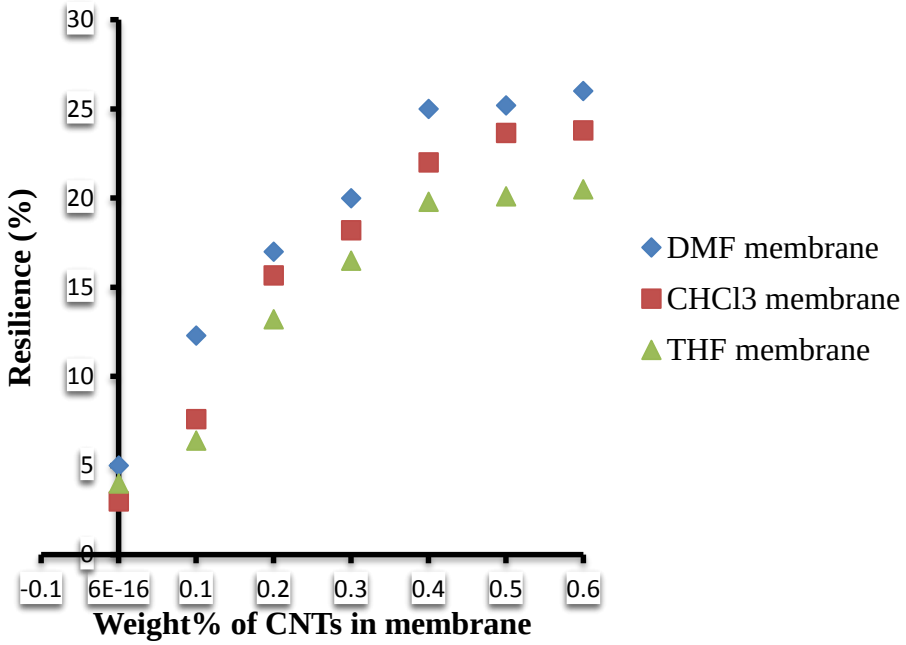

Figure 4.11: Variation of % resilience with CNTs composition

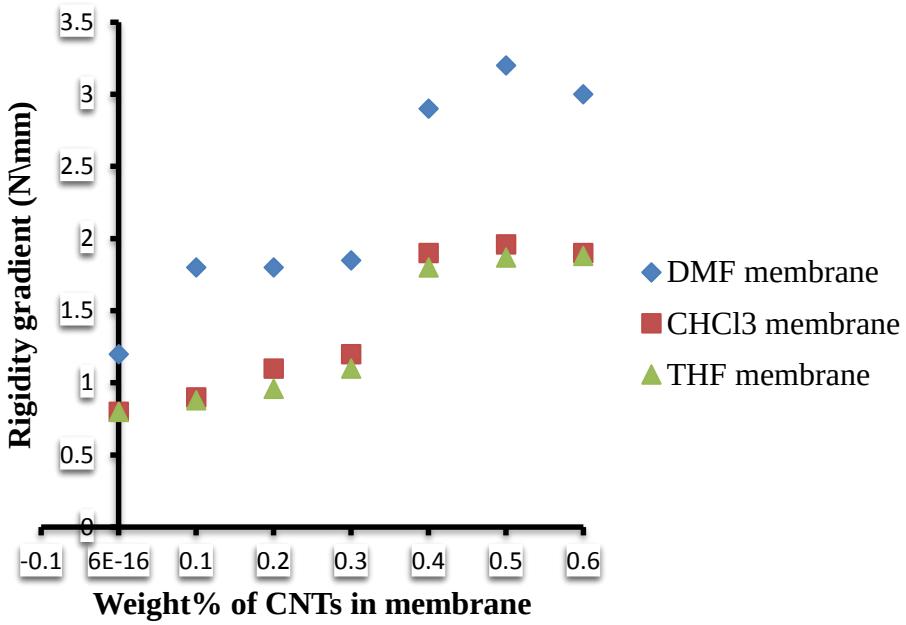

Figure 4. 12: Variation of rigidity gradient with CNTs composition

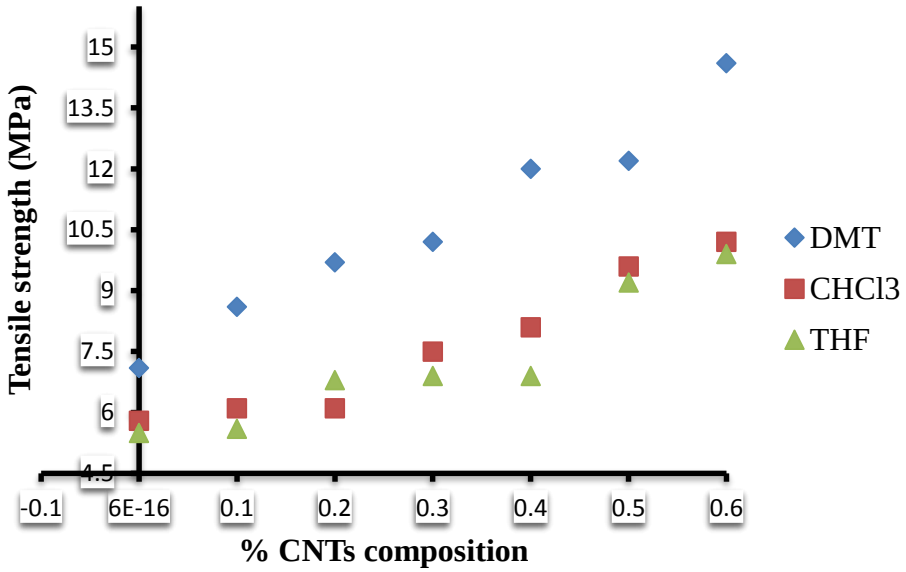

Figure 4.13: Variation of tensile strength with composition of CNTs

In this study, it was proved that multi-walled CNTs could improve the mechanical properties of MWCNTs/PSF nanocomposites. However, the $CHCl_3$ and THF membranes show some irregularities due to the agglomeration of MWCNTs inside the PSF membrane matrix and the low dispersion of MWCNTs in the PSF matrix .Therefore, DMF membrane shows a

homogeneous distribution of MWCNTs in the PSF membrane matrix and strong interfacial bonding between MWCNTs and PSF membrane matrix which are the most important factors in obtaining strengthening and toughening of MWCNTs/PSF membrane.

4.3. NMR characterization of the pre-treated oily wastewater

The metal working fluid (MWF) provided contained several solid particles and unknown impurities and compounds. Therefore, pre-treatment of the MWF was necessary before starting the membrane filtration process. The MWCNTs used in this study were produced from ferrocene by the chemical vapour deposition (CVD) method as described before.

The pre-treatment test was carried out by dispersing raw MWCNTs in oil waste-water as described in chapter 3. A constant amount of the oily wastewater (15 ml) containing solid particles and impurities was added in five different sample tubes. Different concentrations of raw MWCNTs: 0.0, 0.2, 0.3, 0.4 and 0.5 g were added in each respective tube. Raw MWCNTs lack dispersion and solubility properties [3]. It was necessary to use the ultrasonicator to improve the dispersion of MWCNTs in the oily wastewater. (the sample tubes were then left for 21 days). ^{1}H NMR and ^{13}C NMR spectra were recorded on a Bruker AVANCE III 500 at 500.13 MHz for ^{1}H and 125.75 MHz for^{13}C. Spectra were recorded in deuterated water unless otherwise stated. The chemical shift values for all spectra obtained are reported in parts per million and referenced against the internal standard, TMS, which occurs at zero parts per million for ^{1}H NMR and relative to the central solvent signal taken as δ77.00 for ^{13}C NMR spectra. Coupling constants quoted are given in Hertz.

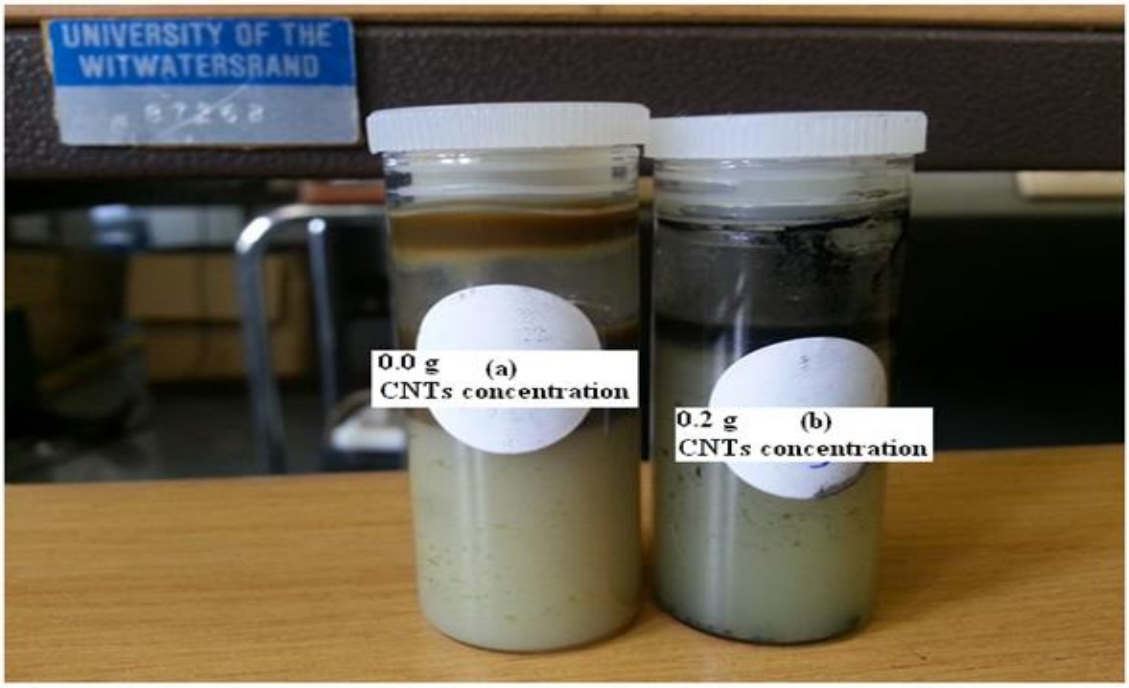

Figure 4.14: (a) initial solution of oil waste-water and (b) oil waste-water containing 0.2 g of raw MWCNTS for pre-treatment by flocculation.

Figure 4.15 shows the spectra of the initial oily waste water emulsion as provided by Oil skip (South Africa). This H NMR spectra was used as reference for the rest of the experiments. Since the oil waste- water sample was provided without any information relating to its composition, it became quite difficult to identify the compounds that are present in the emulsion.

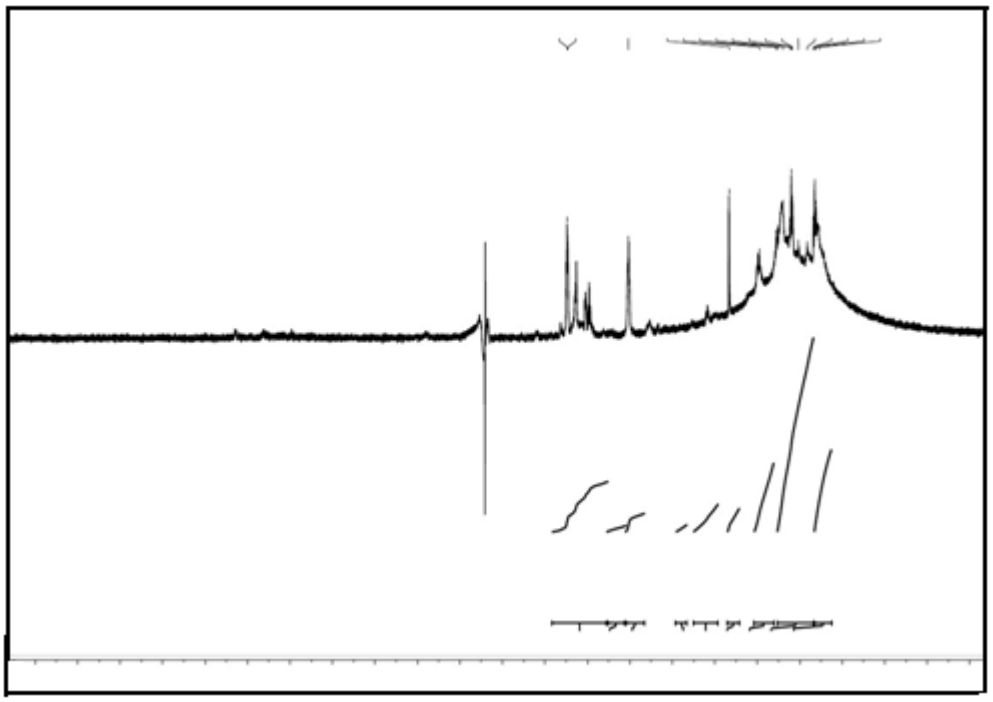

Figure 4.15: H NMR spectra of the initial emulsion of oil waste-water before any pre-treatment

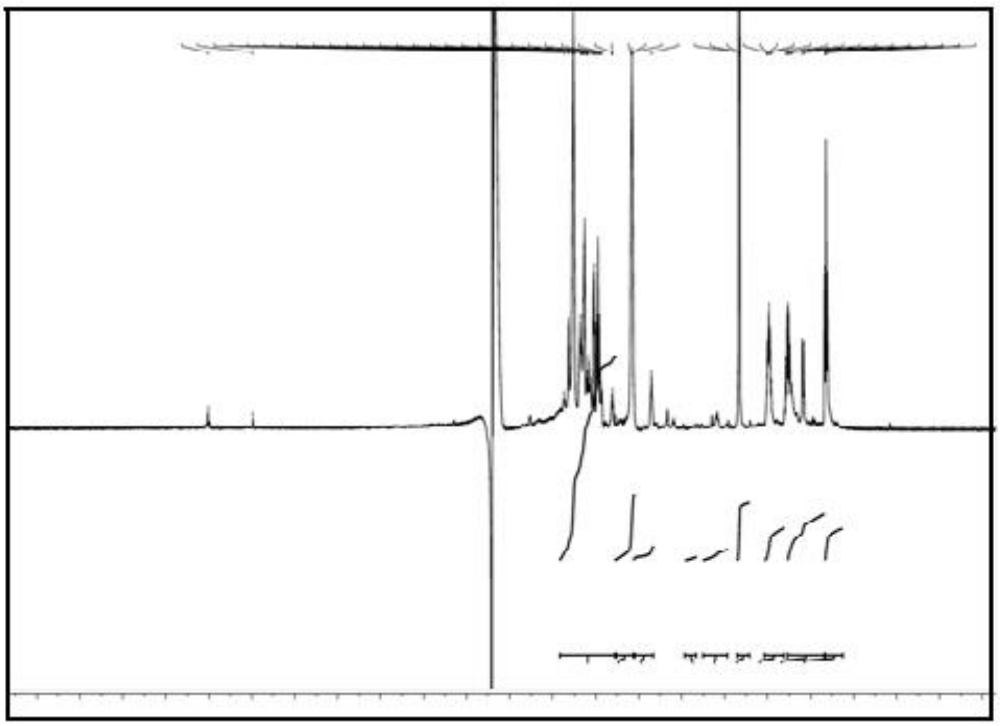

Figure 4.16: H NMR spectra of the emulsion after the pre-treatment (coagulation and flocculation) with 0.2 raw MWCNTs

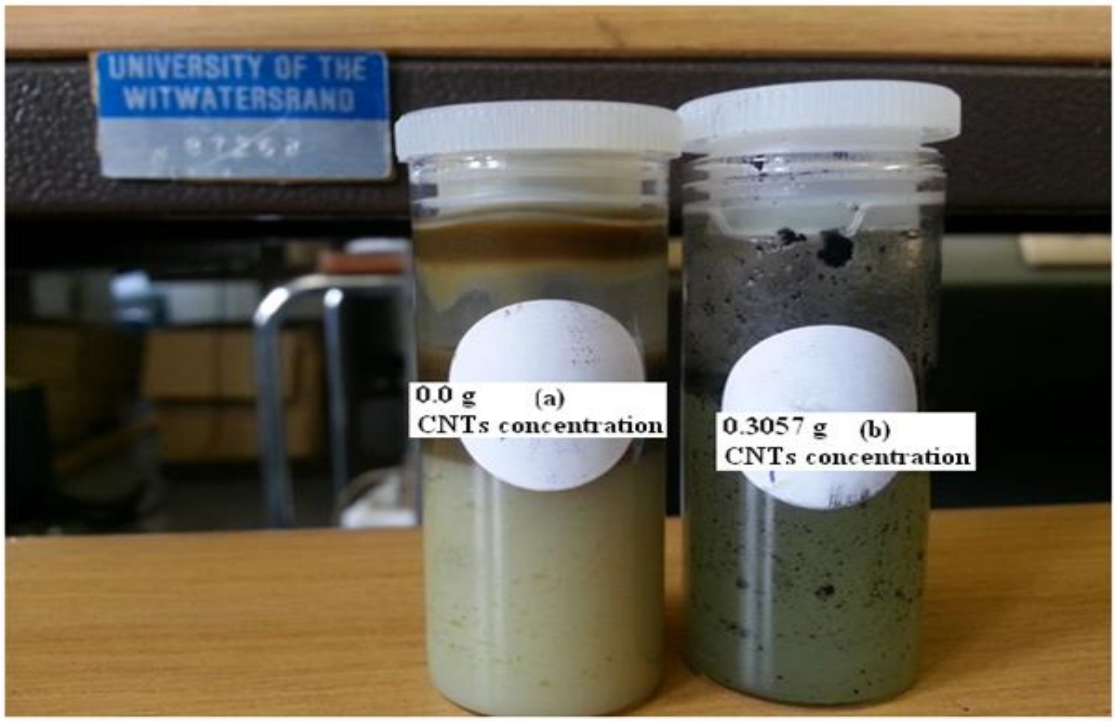

Figure 4.17: (a) initial solution of oil waste-water and (b) oily waste water containing 0.3 g of raw MWCNTS for pre-treatment by flocculation.

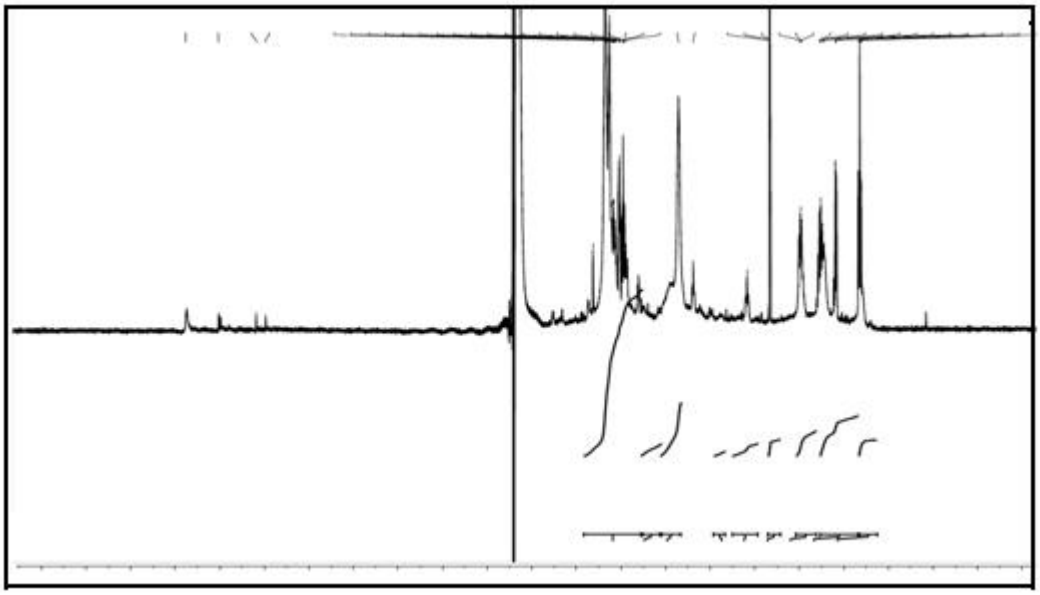

Figure 4.18: H NMR spectra of the emulsion after the pre-treatment (coagulation and flocculation) with 0.3 grams of raw MWCNTs

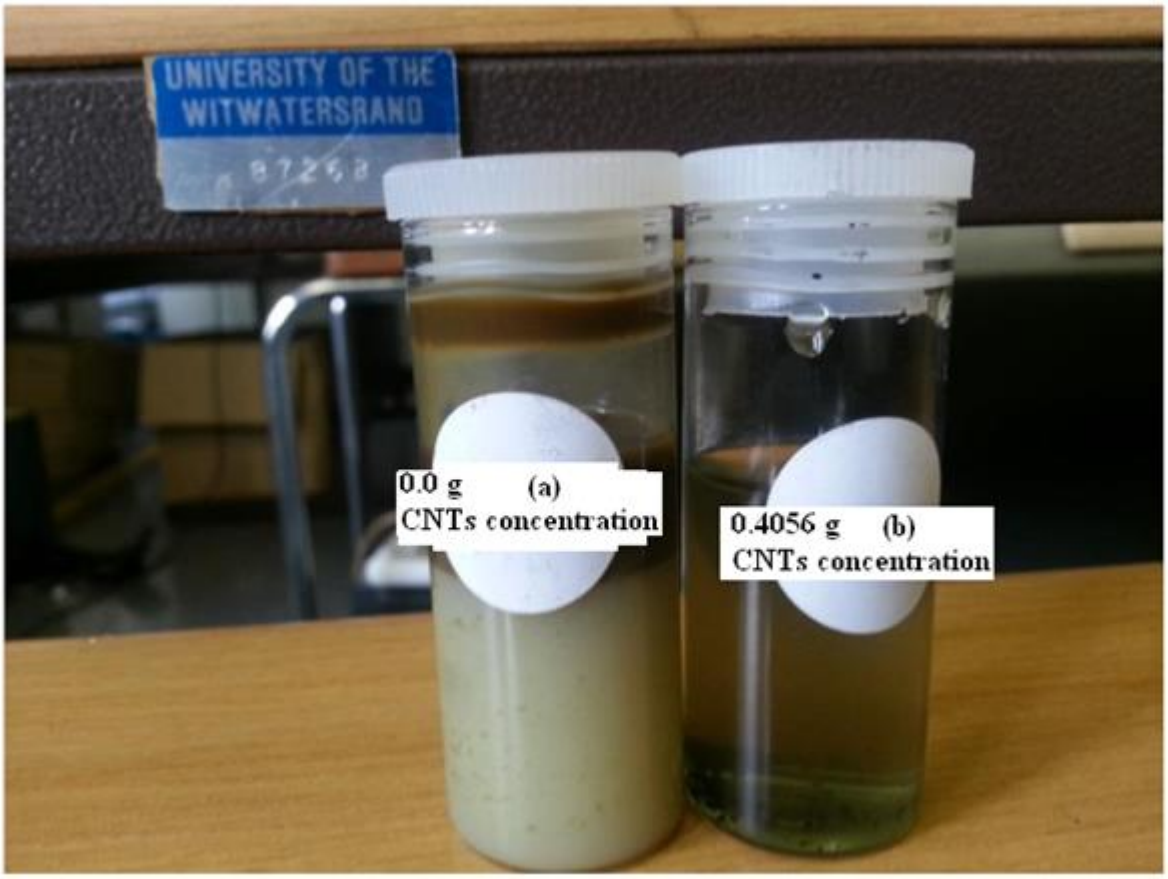

Figure 4.19: (a) initial solution of oil waste-water and (b) oily waste water containing 0.4 g of raw MWCNTS for pre-treatment by flocculation

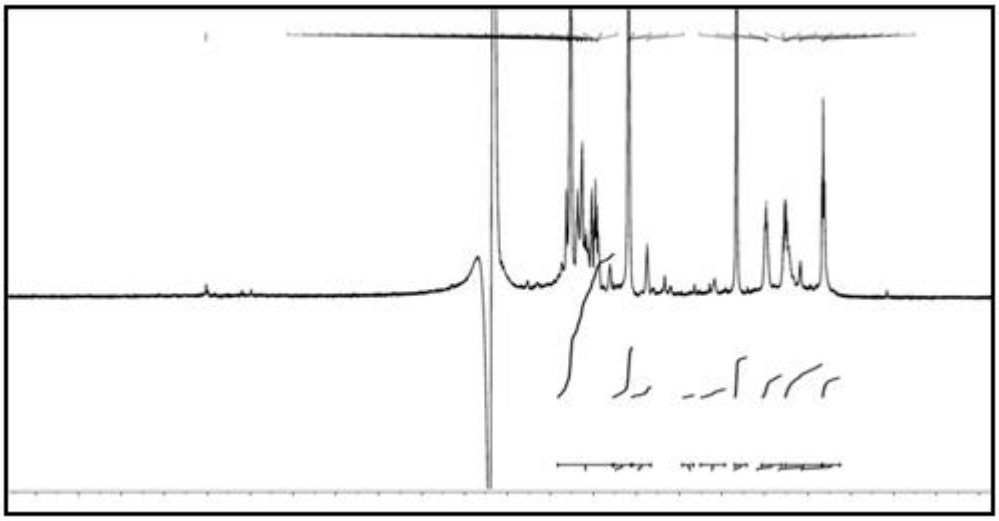

Figure 4.20: H NMR spectra of the emulsion after the pre-treatment (coagulation and flocculation) with 0.4 grams of raw MWCNTs

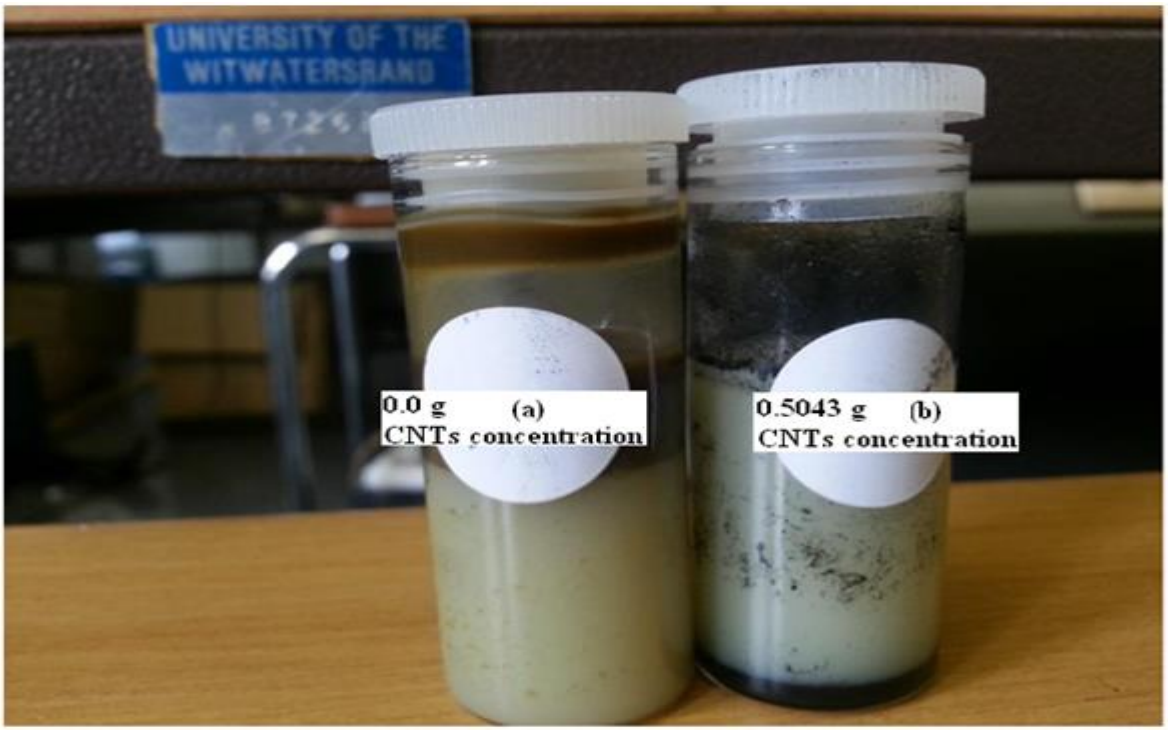

Figure 4.21: Picture of (a) initial solution of oil waste-water and (b) oily wastewater containing 0.5 g of raw MWCNTS for pre-treatment by flocculation

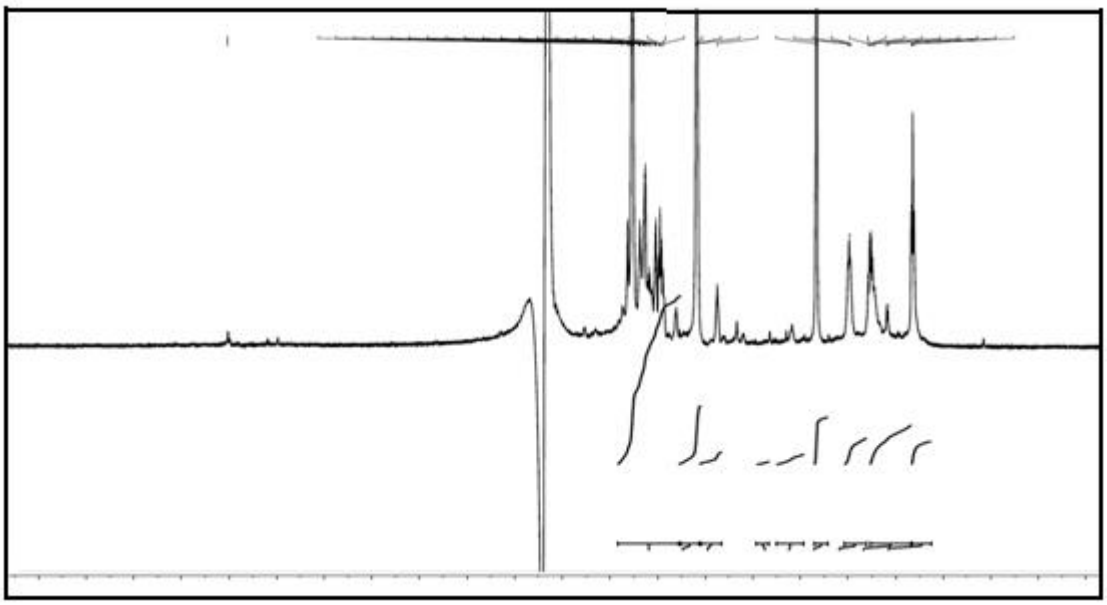

Figure 4.22: H NMR spectra of the emulsion after the pre-treatment (coagulation and flocculation) with 0.5 grams of raw MWCNTs

This experiment was designed to investigate the role of raw MWCNTs as heterogeneous coagulant and flocculent for oil wastewater pre-treatment. It is widely agreed that particles smaller than 10^{-7} m form stable colloids and their separation from wastewater is very difficult [3]. It is also well known that coagulation and flocculation are the standard techniques in the wastewater industry for removal of colloidal particles [3]. The mechanisms of coagulation and flocculation are based on destabilisation of the structure of colloidal particles, which subsequently allows their aggregation and separation from the solution [4].

Figures 4.14 (a); 4.17 (a); 4.19 (a) and 4.21 (a) show the initial oil wastewater sample as provided by Oil skip. Figures 4.14 (b); 4.17(b); 4.19 (b) and 4.21 (b) show the oily waste water containing 0.2, 0.3, 0.4 and 0.5 grams of raw MWCNTs, respectively (for pre-treatment before membrane filtration). An observation with natural eyes proves that colloidal particles, impurities and other compounds have been removed with addition of MWCNTs which acted as coagulant and flocculant. The natural observation could also show the change of colour after pre-treatment, especially for the amount of 0.4 grams of raw MWCNTS which gave the best result.
Figures 4.16, 4.18, 4.20 and 4.22 show the H NMR spectra of the oily waste water emulsion pre-treated with 0.2, 0.3, 0.4 and 0.5 grams of raw MWCNTs, respectively.

It has been observed that raw MWCNTs can be used as heterogeneous coagulants and/or flocculants in the pre-treatment of the oily wastewater [3]. The H NMR spectra show that despite the lack of information about the composition of the oil wastewater the pre-treatment with raw MWCNTs has removed certain compounds. The comparison at the H NMR spectra of the initial emulsion of oily wastewater (Figure 4.15) with the H NMR spectra recorded after pre-treatment (Figure 4.15), easily detected that several undesirable and unknown compounds have been removed with coagulation and flocculation by raw MWCNTs. The H NMR spectra of the emulsion after the pre-treatment (coagulation and flocculation) with 0.4 g of raw MWCNTs shows the best results compared to the others. This means that the amount of 0.4 grams of MWCNTS shows the best and appreciable pre-treatment since the spectra reveals an optimal removal of undesirable components compared to the initial spectra.

4.4. Membrane permeation test

4.4.1 Influence of MWCNTs on the membrane performance (pure water flux)

To investigate the influence of the MWCNTs on the membrane performance the cross-flow system was used at room temperature (25 °C ± 5 °C). The effect of weight fraction of MWCNTs on the membrane performance was studied. The MWCNTs/PSF membranes containing 0.1 to 0.6 wt% MWCNTs were prepared using the phase inversion method [5]. The pure polymeric membrane without MWCNTs was also prepared using the same technique [5].

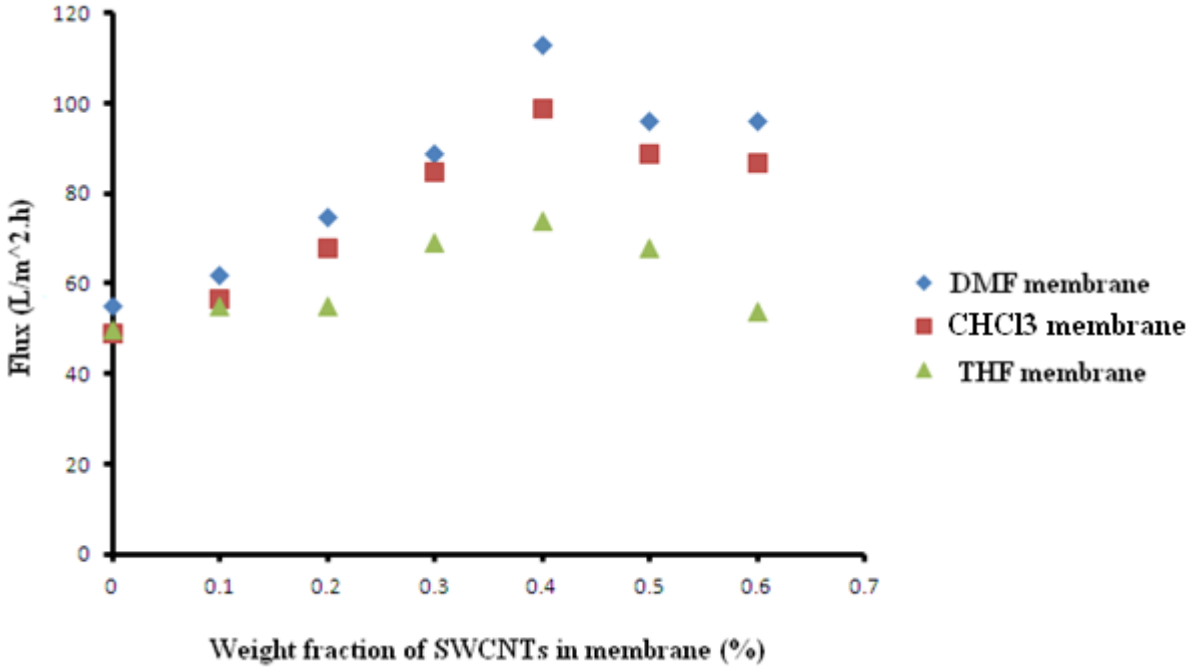

Figure 4.23: Variation of the pure water flux with MWCNTs composition at different membrane solvents

Figure 4.23 shows the flux calculated using equation 1 for different % MWCNTs loadings (at constant pressure of 2 bar) using a cross flow filtration module at room temperature. It has been found that the water flux of the DMF, $CHCl_3$ and THF blended membranes increases with addition of functionalized MWCNTs. In the case of the DMF membrane incorporated with functionalized MWCNTs, the water flux reaches appreciable values especially, for the 0.4 wt% of MWCNTs which gives the highest water flux of 113 L/m^2.h. However, a

decrease of flux was observed for concentration of MWCNTs above 0.4 wt% for the three different membranes due to the increasing density of functionalized MWCNTs; this causes the steric hindrance between the functionalized CNTs to agglomerate inside the polymer matrix during the phase inversion [5]. The increase in water flux is usually found with increase in surface pore size and increased hydrophilicity of the membranes.The higher water flux of the DMF blended membrane might be due to increased surface pore size and the right dispersion of MWCNTs in the PSF membrane matrix, which controls the pore size and alters the pore structure of the PSF layer allowing for greater flux across the membrane. The flux increases to a maximum loading for 0.4 wt% MWCNTs for the DMF membrane, but decreases at greater amounts of MWCNT. This can be explained by the large Van der Waals forces experienced between the MWCNTs and the membrane matrix when the density of the MWCNTs is high in the membrane structure [6]. The high density causes an increase in viscosity of the casting solution [6]. Finally, 0.4 wt% CNTs has been retained as the optimum concentration of the functionalized MWCNTs in PSF membrane which showed the best results for the three different types of (DMF, $CHCl_3$ and THF) blended membranes which were produced and tested.

4.4.2 Influence of pressure (driving force) on the membrane performance

The water fluxes of pure polymeric and blended membranes were measured at room temperature (25°C ± 5 °C) and at different transmembrane pressure with a constant concentration of MWCNTs (0.4 wt. %) retained as the optimum MWCNTs concentration from the previous experiments.

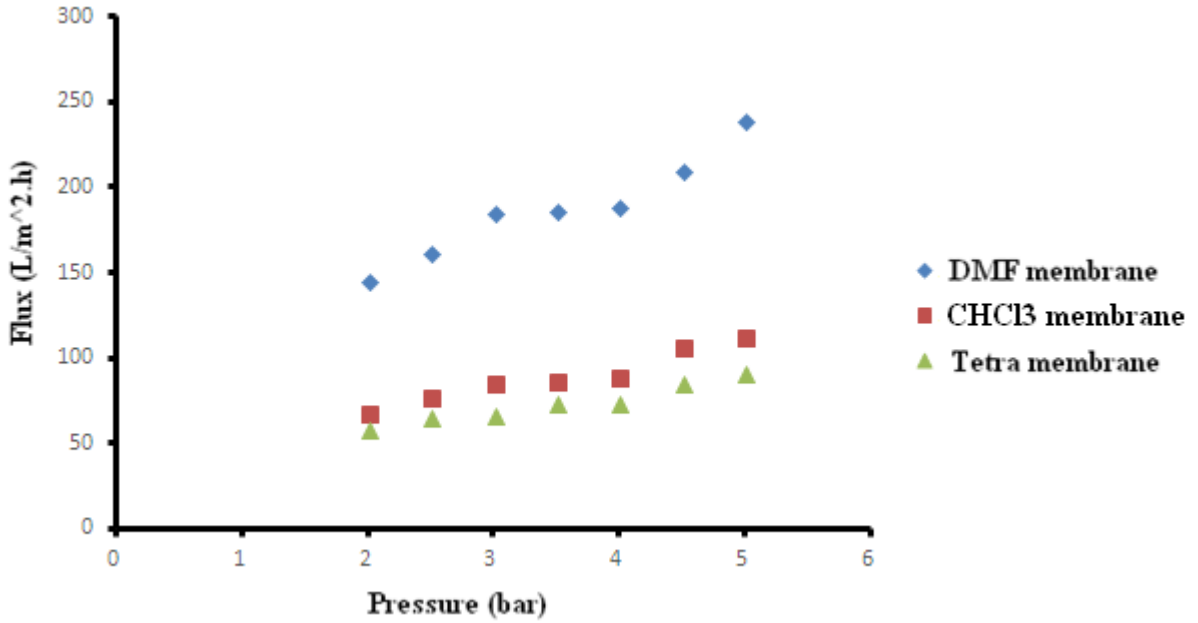

(a)

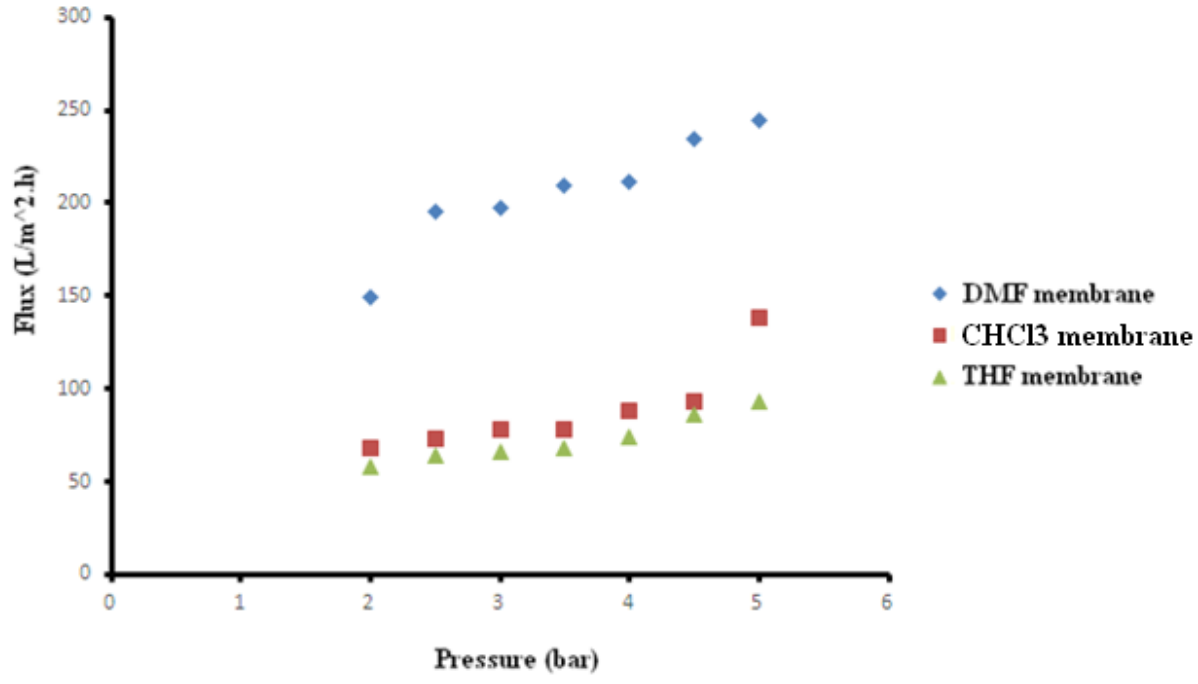

(b)

Figure 4.24. **(a, b):** Variation of the pure water flux with pressure at a constant MWCNTs loading.

Figure 4.24 (a, b) show the flux calculation using Equation 1 for different pressures and constant % MWCNT loading of 0.4 retained as the suitable concentration of MWCNTs in PSF membrane for ultrafiltration using a cross flow module at room temperature. The flux

through the membrane increases with an increase in pressure; however flattening behaviour has been observed between 3 and 4 bar for each blended membrane which might be due to fouling inside the pores or on the top surface of the membranes. DMF blended membrane gives the best water flux which might be due to the hydrophilicity and porosity of the DMF blended membrane, since a better dispersion of MWCNTs in DMF solvent across the PSF matrix was observed. The pressure 5 bar gives appreciable results for each blended PSF membrane. The decrease in flux may be predicted after the pressure of 5.5 bar because of the fouling and concentration polarization.

The permeate flux was found to increase with an increase of pressure, and flux declines during the initial stages of filtration for all the membranes and then increased continuously (the increase ranging from 3 to 5 bar). The reason that the pressure between retentate and permeate played the role of an effective driving force (and the increased pressure) could overcome the resistance, hence compelling more solution to filter through the membrane and resulting in a higher permeate flux [7].

4.4.3 Influence of filtration time on membrane performance

The water fluxes of pure polymeric and blended membranes were measured at room temperature (25 °C ± 5 °C) and at different filtration time with a constant concentration of MWCNTs (0.4 wt. %) and pressure (4.5 bar) .

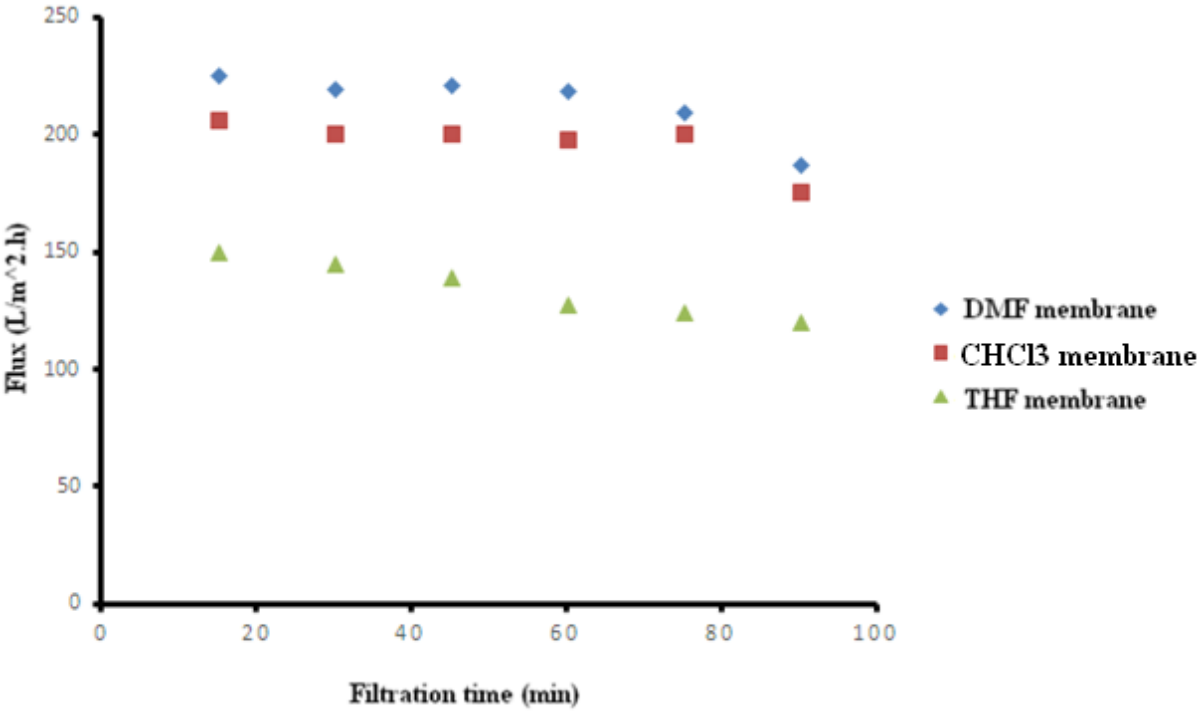

(a)

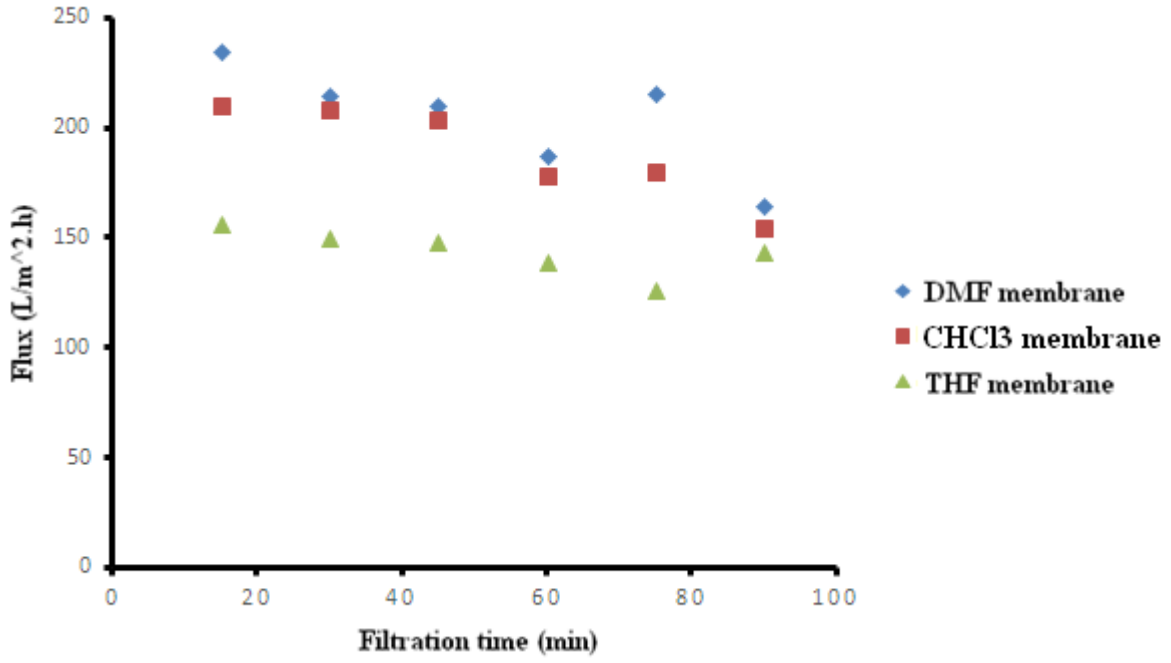

(b)

Figures 4.25 (a, b): Two different graphs showing the variation of the pure water flux with filtration time at a constant MWCNTs loading.

Figure 4.26: Picture of the final permeate obtained after pre-treatment and filtration using the optimum conditions detailed above.

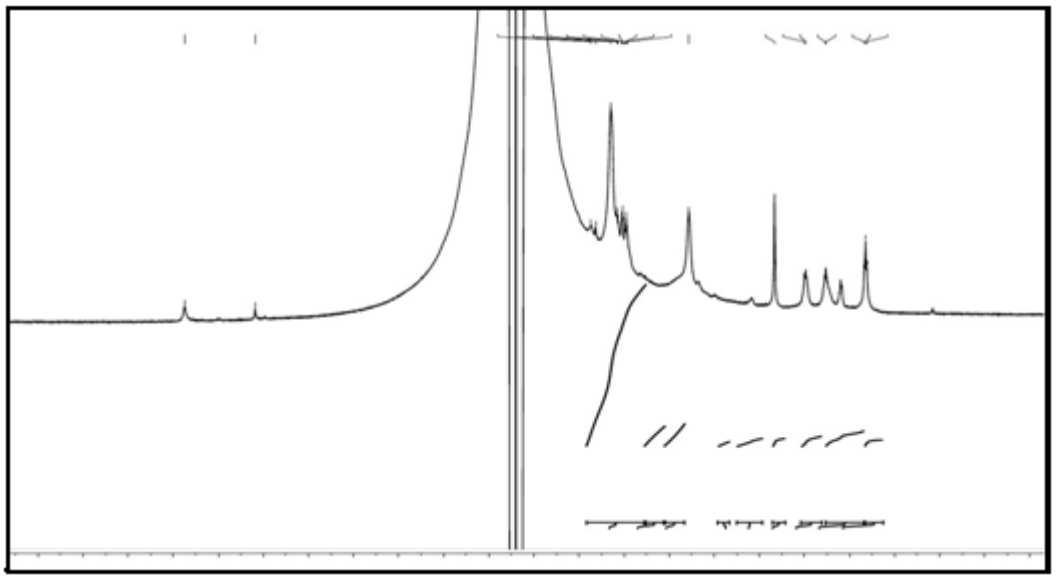

Figure 4.27: H NMR spectra of the permeate obtained after pre-treatment and filtration using the optimum conditions retained above

Figures 4.25 (a, b) show the variation of the flux with filtration time at a constant % MWCNT loading of 0.4 and pressure of 4.5 bar (which were retained from the previous experiments) as optimum parameters for membrane ultrafiltration using a cross flow module at room temperature. The plots show the permeate flux over time during fouling of the pure polymeric and blended membranes with oil droplets. The different membranes give an appreciable flux for the filtration time from 15 min. The greatest fraction of flux decline was observed after the first 45 min of introducing the feed solution. This flux reduction can be attributed to the adsorption of oil droplets on the surface of the membranes upon initial introduction of the solution (concentration polarization) [8]. This could also be explained by the fact that the feed solution was more than the critical micelle concentration (CMC) [9], could form a large number of micelles, not only more and more sodium dodecyl sulphate micelles (SDS) deposited on the membrane surface and then assembled into cake formation, but also the existence of surfactant monomer (these monomers appear to form smaller aggregations, called pre-micelles), and some of monomers could be rejected by the gel layer whereas the rest of them would probably get through the pores or be absorbed by the pores. Therefore the permeate flux was lower than the others. With the initial feed concentration, in

the first 15 min, the permeate flux decreased quickly. This behaviour may be attributed to concentration polarization, namely, solution of micelles deposited quickly on the membrane surface and blocked the membrane pores in a short time [9]. Furthermore, the retentate stream was recycled to the feed tank, and the feed concentration increased gradually so that membrane fouling assembled into cake formation (along the time) [10]. As a result, the permeate flux decreased more and more slowly and tended to be constant. However, appreciable results were observed from the DMF membrane comparison to $CHCl_3$ and THF membrane, due to the good dissolution of MWCNTs in the DMF solvent, which reduced fouling and concentration polarization, and controlled the membrane pore sizes. Finally, the filtration time of 45 minutes was retained as the optimum filtration time for this research.

4.4.4 Effects of forward flushing and backwashing on permeate flux

The cleaning interval between two successive filtration cycles is a very important parameter [11]. As can be seen from Figure 4.25 **(**a), permeate flux decreased quickly at first, and then tended to be stable after 15 min filtration. Therefore, to save on the cost of operation, the filtration time should be fixed at 15 min and the cleaning cycle to 10 min. Forward flushing tests were performed with the permeate valve closed in order to avoid permeation and to obtain a high cross flow velocity with lower pressures. The results are shown in Figures 4.25 (a, b) and 4.26 (a, b). This graph which shows that as flushing time increases, the flushing effect of the three different membranes (DMF, $CHCl_3$ and THF) gets better and better. Meanwhile, with the experiment progressing permeate flux reduced gradually until it levelled off. Without forward flushing, the flux was about 145, 67 and 58 L/m^2.h after 1 h; with forward flushing, the flux increased, about 225, 210 and 150 L/m^2.h for DMF, CHCl3 and THF, respectively. This behaviour can be explained by the fact that forward flushing can eliminate the deposition of foulants on the membrane surface due to concentration polarization [8]. It forward flushing time is too short; it is not able to flush foulants on the membrane surface completely. From the point of view of energy and water savings, forward flushing for 80 s is more appropriate [11].

This is because of the reason that during the forward flushing process, the permeate valve closed, then there is no convective transport, the fouling on the membrane surface was swept loosely and some SDS monomers were not washed away which can go through pores or adsorbed by the membrane internally. However, internal fouling in the pores cannot be swept away by forward flushing, which resulted in the phenomenon that forward flushing has no capacity to clear them. The process of backwashing pushes washing water (tap water)

through the membrane to remove the internal fouling present in the membrane pores [7]. The permeation is forced in the reverse direction through the membrane, so the foulants on the membrane surface can be lifted off and be suspended by tangential flow [7]. Figures 4.25 (a, b) show the comparison of permeate flux is a function of time when operated in the presence and absence of backwashing. When backwashing was performed, the observed permeate flux increased significantly compared to without backwashing.

4.5 References

1. Jianying S., Markus Flury, James B., Richard L.,(2008). Comparison of different methods to measure contact angles of soil colloids. Journal of colloid and interface science, 328,299-307.
2. Lian Y.,Tai S., Chun C., Zhen H., Santi K.,(2005). Fundamental understanding of nano-sized zeolite distribution in the formation of the mixed matrix single and dual –layer asymmetric hollow fiber membranes.
3. Simate G.S., Iyuke S.E., Ndlovu S., Heydenrych M., (2012). The heterogeneous coagulation and flocculation of brewery of brewery wastewater using varbon nanotubes. Water Research 46 (4), 1185-1197.
4. Xiaolei Qu, Pedro J., Alvarez, Qilin L.,(2013). applications of nanotechnology in water and wastewater treatment. water Research, 47, 3931-3946.
5. Shi Q., Liguang W., Xuejie P., Huanlin C., Congjie G.,(2009). Preparation and properties of functionalized carbon nanotube/PSf blend ultrafiltration membranes. Journal of Membrane Science, 324, 165-172.
6. Choi J., Jegal J., Kim N.,(2006). Fabrication and characterization of multi-walled carbon nanotubes/polymer blend membranes. Journal of Membrane science, 69, 152-160.

7. Jinhui H., Liuxia L., Guangming Z.,(2014). Influence feed concentration and transmembrane pressure on membrane fouling and effect of hydraulic flushing on the performance of ultrafiltration.Desalination,335, 1-8.

8. Zhao Y., Wu K., Wang Z., Zhao L., Li S., (2000). Fouling and cleaning of membrane. Journal of Environmemtal Sciences.12, 241-251.

9. Vinder A., Simonic M., Novak Z., (2014). Influence of surfactants on the removal of AOX using micellar – enhanced ultrafiltration. Journal of Membrane Research. 1, 205-212.

10. Persson K., Milson J.,(1991). Fouling resistance models in MF and UF. Desalination, 80, 123.

11. Ning m., jing X., Dequiag C., Xi S., (2015). Comparison of filtration performances between membrane and non-membrane filters. International symposium on computers and informatics (ISCI 2015).

Chapter 5 Conclusions and Recommendations

5.1 Conclusions

The main aim of this study was to assess the effect of functionalized MWCNTs on a PSF membrane and to characterize the system using TEM, SEM, tensile strength test, hydrophilicity (contact angle test), H NMR and the cross-flow filtration system. MWCNTs were synthesized using the CVD process at the temperature range: 800 °C - 900 °C. The CNTs were produced by passing acetylene and argon (which are carrier gases) through a furnace with ferrocene acting as both a carbon source and a catalyst. The MWCNTs were purified and functionalized by acid treatment in order to remove any impurities from the catalyst and to also introduce acid functional groups (e.g. carboxyl groups) onto the surface of the MWCNTs for the improvement of their dispersion in organic solvents (and in resultant membranes). The degree of functionalization was successfully confirmed by Raman spectroscopy. Composite membranes containing PSF and MWCNTs were successfully prepared by the phase inversion method. Three different solvents (DMF, $CHCl_3$ and THF) were used to dissolve separately the PSF, followed by adding different concentrations of MWCNTs (0.1, 0.2, 0.3, 0.4, 0.5 and 0.6 wt %) to improve the properties of the polymeric membranes. The ultrasonicator was used to improve the homogeneity of the solution. The mixture was then cast on a glass support and submerged in a bath of water (phase immersion) to allow evaporation of solvent. Finally the membranes were placed in an oven at 100 °C for 30 min to remove the absorbed water. Characterization of the MWCNTs by TEM was used to measure basic parameters (nanotube diameter etc) and Raman spectroscopy was used to confirm any defects present in the functionalized MWCNTs.

Characterization of the MWCNT/PSF membrane surfaces and cross - sections using SEM revealed that there is no pronounced difference in the morphology of the cross-sections of all the MWCNT/PSF membranes produced (with different solvents). All have finger-like structures with various pore sizes. Furthermore, as the amount of MWCNTs increases, the surface of the MWCNTs/PSF membrane becomes rougher and the pores of the cross-section become larger. The MWCNT/PSF membrane with 0.4 wt% MWCNTs has the roughest surface and the largest pore size. For membranes containing more than 0.4 wt% MWCNTs, the surfaces become smoother and the pore sizes of the cross-section become smaller due to the to the increasing density of functionalized MWCNTs and van der Waals forces. This causes the steric hindrance between the functionalized MWCNTs to agglomerate inside the polymer matrix during the phase inversion. The contact angle and mechanical analyses

demonstrated that blending MWCNTs even at low wt% to the pure PES membrane could increase both the hydrophilicity and the mechanical properties of the polymeric membranes.

Raw MWCNTs were used for pre-treatment of the oily wastewater emulsion. The pre-treatment test was carried out by dispersing raw MWCNTs in oil – water emulsion. A constant amount of the oil-water emulsion with solid particles and impurities (15ml) was added in six different sample tubes. Different concentrations of raw MWCNTs: 0.0, 0.1, 0.2, 0.3, 0.4 and 0.5 g were added in each respective tube. After mixture improvement with an ultrasonicator, the sample tubes were then left for 21 days. The result of pre-treatment shows that raw MWCNTs can lead to coagulation and flocculation of solid particles contained in the emulsion. The amount of 0.4 g of MWCNTs gives the best result for both appearance (Figure 4.19) and H NMR spectra (Figure 4.20) which leads to retain 0.4 g 15 ml as the optimum composition of raw MWCNTs and oily wastewater respectively, for coagulation and flocculation.

The MWCNT/PES membranes performance was also tested for any improvements in pure water flux. Improved performances were observed with addition of different fractions of MWCNTs on the polymeric membranes produced with different solvents (DMF, $CHCl_3$ and THF). An appreciable 48.6 % increase in water flux was observed with 0.4 wt% of MWCNTs to PES membrane produced with DMF as solvent. At values above 0.4 wt% MWCNTs the water flux decreased. The increase in permeability of the membrane was related to the hydrophilicity and adsorption effects of MWCNTs. However, increased viscosity of the casting solution at higher MWCNT loading (>0.4wt %), retarded the exchange between solvent and non-solvent during the phase inversion process, smoother membrane surfaces and smaller pores appearing. Hence, water flux was severely limited. At a relatively higher ratio, more MWCNT agglomeration resulted in the formation of gaps, which are large enough for water molecules to pass through. Eventually, water flux increased while the rejection decreased to some extent. Therefore, if a right amount of MWCNTs is added, the permeation flux of the MWCNTs/polymer membranes can be improved and the selectivity can be simultaneously well maintained.

After comparison of the initial oily wastewater solution (Fig.4.14) and the final permeate (Fig. 4.26); it was confirmed that MWCNTs/polymer membrane did treat the oily wastewater. The final H NMR spectra (Fig.4.15) also reveals an optimal removal of undesirable components compared to the initial spectra. It can be concluded that

functionalized MWCNTs modified PSF membranes improve the mechanical and chemical properties of the polymeric membrane. However, there is a certain amount of MWCNTs to use for blending. DMF has been retained as the best solvent compared to $CHCL_3$ and THF because it decreased the intertube interactions leading to a better dispersion of MWCNTs in the matrix of the PSF membrane.

5.2 Recommendations

It has been revealed that raw MWCNTs can be used for pre-treatment of oily wastewater emulsion before the membrane separation process. It will be necessary to study the improvement of this process by using several concentrations of raw MWCNTS for oil wastewater pre-treatment in order to confirm and verify the optimum conditions and parameters for this process.

The cross - flow filtration module used in this work contains a pump with limited range of pressure. For future work, it would be appropriate to use a large pump with large range of pressures to test the efficiency of the membrane.

Appendix A

Determination of MWCNT diameter

After observation of the SEM image, it has been found that the scale bar of 200 nm corresponds to 15 nm. Choosing any chain of MWCNTs, the diameter is approximately determined by using a ruler. From the image represented in Figure 5.1, it has been shown that 5 nm is the MWCNTs diameter.

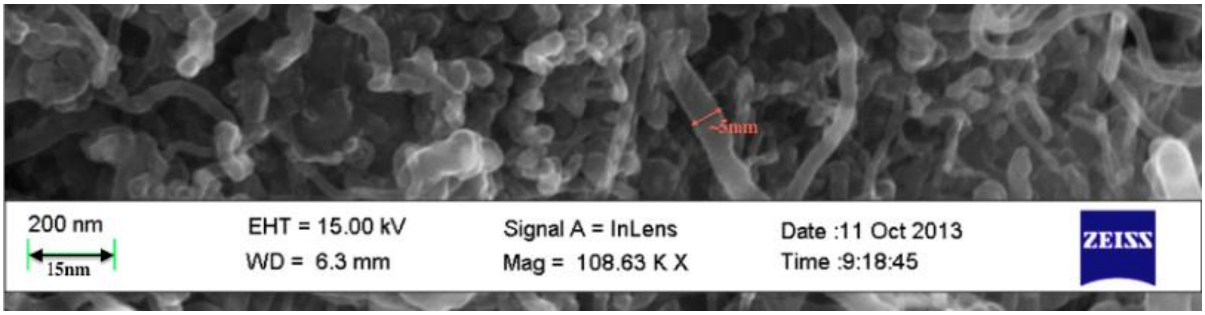

Figure 5.1: SEM image of the MWCTs

In this figure we trying to determine the average diameter of the MWCNTs

The average diameter of the MWCNTs is then determined as:

$$\text{Wall Diameter} = \frac{5 \text{ mm}}{15 \text{ mm}} . 200 \text{ nm}$$

$$\text{Wall Diameter} = 66.67 \text{ nm}$$

Calculation of the $I_{D/G}$ ratio

It has been found that before functionalization of the MWCNTs, the D band is detected at a wavelength of 1342.5 cm^{-1} and intensity of 268.752 The G band is detected at 1587cm^{-1} and the intensity of 265.692

$I_{D/G} = 1.012$

Table A: Intensity ratio calculation for the unfunctionalized and functionalized MWCNTs

Unfunctionlazed MWCNTs		**Functionalized MWCNTS**	
D band	G band	D band	G band
1342.5	1587	1340.50	1572.50
268.752	265.752	33.670	30.258
1.012		**1.113**	

From the table above: % $increase = \frac{1.113-1.012}{1.012} \times 100$

= 9.98 %

Determination of the permeate flux of the membrane

The permeate flux of the membrane was calculated using the equation A1:

$$F = \frac{\mathrm{V}}{\mathrm{A} \times \mathrm{t}} \quad \text{(A1)}$$

Where

V = volume of permeate collected (ml)

A = specific area of the membrane (cm^2) and

t = time required to obtain the permeate across the membrane (min)

Table B: Table representing of the membrane flux calculations.

Membrane area	45 cm^2				
Concentration of MWCNTS WT %	0.0	0.2	0.4	0.5	0.6
Time (min)	10	10	10	10	10
Volume of permeate Cm^3	6.5	5.03	21.5	12.0	7.0
Flux (ml/cm^2.min)	0.014	0.011	0.047	0.02	0.015